Modelling the Marine Carbonate Pump and its Implications on the Atmospheric CO_2 Concentration

Dissertation
zur
Erlangung des Grades eines
Doktors der Naturwissenschaften
- Dr. rer. nat. -

dem Fachbereich Physik der
Universität Bremen
vorgelegt von

Heiko Jansen
aus Bremen

Juni 2001

1. Gutachter: Prof. Dr. Dirk Olbers
2. Gutachter: Prof. Dr. Dieter Wolf-Gladrow

Abstract

The marine carbonate pump includes the production of calcium carbonate, $CaCO_3$, by marine organisms and its subsequent transport to depth. The balance between carbonate production in surface waters and dissolution and accumulation in sediments influences the surface water CO_2 concentration and thus the ocean's capacity to take up atmospheric CO_2.

As most parts of the oceanic water column are supersaturated with respect to calcium carbonate, it is to be expected that dissolution of biogenic carbonates takes place at the seafloor. However, observations point to loss of calcium carbonate particles in the water column. Three models are developed to investigate on calcium carbonate dissolution in the oceanic water column. Model results yield that dissolution in zooplankton guts contributes a significant portion of the proposed carbonate loss. Physico-chemical dissolution of individually settling $CaCO_3$ particles is seen to be of minor importance and to be restricted to the Equatorial and North Pacific Ocean. Dissolution fueled by the respiration of organic matter in marine snow aggregates is very sensitive to the size and settling velocity of the aggregate, which determines the boundary layer thickness and the stability of an undersaturated microenvironment. The constraints set by field data yield that the chemical gradients between the aggregate and the bulk seawater are too small to enable significant carbonate dissolution. Thus, it is concluded that dissolution facilitated by respiration processes in marine snow aggregates does not contribute to the observed loss of calcite column in the water column.

Furthermore, the role of the carbonate pump in regulating atmospheric pCO_2 on glacial to interglacial timescales is investigated. To this end, a model of calcium carbonate dissolution and accumulation in the marine sediments is developed. The model is used to determine the contribution of the marine carbonate pump on the observed glacial to interglacial shift in atmospheric pCO_2. Increased glacial production of organic carbon yields increased carbonate dissolution in the sediments, explaining a $\sim 30-50\,\mu$atm lower pCO_2 at the Last Glacial Maximum $\sim$ 20,000 years before present, which accounts to approximately half the observed shift. The organic matter production change, however, has to be accompanied by a deepening of the remineralization depth. This result is independent of the amount of calcium carbonate dissolved in the water column. A glacial pCO_2 reduction is seen to be consistent with increased $CaCO_3$ production (raising surface ocean pCO_2) as long as the organic matter production is enhanced, which compensates this effect by intensifying $CaCO_3$ dissolution at depth.

Contents

Overview of the Thesis

The modelling work in the present thesis focuses on two parts of the oceanic carbonate pump: Dissolution of calcium carbonate in the water column and dissolution of calcium carbonate in the sediments. The first part is important as a precursor to the sediments: It determines how much calcium carbonate reaches the seafloor.

As calcium carbonate producing pelagic organisms such as coccolithophorids, foraminifera and pteropods settle through the water column, they may or may not dissolve, depending on the saturation state of the bulk seawater with respect to calcite or aragonite. From a geochemical viewpoint it is of interest whether dissolution can start already while the particle is sinking through the water column or only after reaching the sediments. The partitioning of this process influences the timescales on which the oceanic carbonate system equilibrates and is thus relevant for e.g. glacial-interglacial transitions. The timescale at which processes in the water column influence the atmosphere are much shorter than the timescales that come into play with the sediments. Furthermore, the ratio of organic carbon to calcium carbonate reaching the seafloor influences the amount of calcium carbonate that is dissolved in the pore waters [*Emerson and Bender*, 1981; *Milliman et al.*, 1999]. This in turn has consequences for the ocean's uptake capacity for atmospheric CO_2 [*Archer and Maier-Reimer*, 1994]. The time a settling particle spents in undersaturated waters before arriving at the seafloor is very short compared to the calcite dissolution timescale. Thus, it is expected that the major part of carbonate dissolution takes place in the sediments. However, observations point to $CaCO_3$ loss in the water column. *Milliman et al.* [1999] estimate as much as 60-80% of the produced calcium carbonate to be dissolved in the upper 500-1000 m of the ocean. In this depth range, ocean waters are supersaturated with respect to both calcite and aragonite. The mechanisms underlying the proposed loss of calcium carbonate are not understood yet.

Thus, the key questions adressed in the present thesis are

- Can the estimated dissolution of calcium carbonate in the water column be explained by biologically mediated mechanisms ?

- How much of the observed glacial to interglacial shift in atmospheric pCO_2 is attributable to changes in the marine carbonate pump ?

- Can the observations of increased glacial *p*H and lysocline depth be reconciled by a decoupling of the lysocline from the saturation horizon ?

In chapter 2, two models are developed that investigate calcium carbonate dissolution in the water column. The first one simulates settling particles that are subject to dissolution after crossing the saturation horizon. The second one models the export of particles in aggregates, where the respiration of organic matter may fuel carbonate dissolution while settling. A third scenario for carbonate dissolution in the water column is investigated in chapter 3. A model of zooplankton guts has been developed. Coccolithophorids are grazed by zooplankton and their calcareous parts may be subject to dissolution in the rather acid guts.
Chapter 4 adresses the other two key questions. A conceptual model of calcium carbonate relevant processes in the sediments is presented. Glacial scenarios of productivity changes are investigated with respect to their ability to decouple the lysocline from the saturation horizon and the resulting glacial atmospheric CO_2 concentration.

Chapter 1

Introduction

1.1 The global carbon cycle

In this section, an overview of the global carbon cycle is given. This includes the processes focused at in the present thesis. The global carbon cycle consists of the geochemical reservoirs that store carbon and the pathways that transport carbon between them. Fig. 1.1 presents a schematic overview of the reservoirs and processes which make up the carbon cycle. Time scales of the processes span many orders of magnitude, ranging from days (e.g., assimilation/respiration of carbon by marine biota and by the continental vegetation) to hundreds of millennia and more (e.g., volcanism, sea-floor alteration).

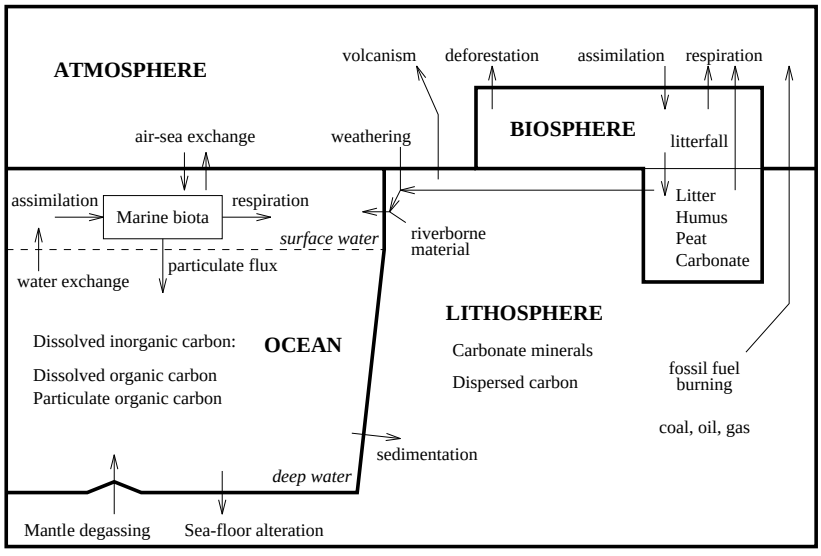

Figure 1.1: The global cycle of carbon: reservoirs and processes. Adapted from *Holmen* [1992]; Fig. courtesy of *Munhoven* [1997].

The present thesis focuses on the oceanic part of the carbon cycle. Processes in the ocean is play a key role within the global carbon cycle. The oceanic reservoir is by far the largest of the three

reservoirs active on time scales of say less than one million years, i.e. the atmosphere, the biosphere and the ocean. Currently the atmosphere contains $\sim$ 750 Gt C as carbon dioxide. The terrestrial biosphere stores $\sim$ 2000 Gt C, whereas the ocean's global carbon content is $\sim$ 40,000 Gt C, an order of magnitude larger than that of the atmosphere and the terrestrial biosphere taken together. The fluxes per year between the reservoirs are on the order of 5-10% of the contents (considering for the ocean the surface content only). All carbon content values and fluxes taken from *Siegenthaler and Sarmiento* [1993]. Ultimately, it is the oceanic carbon system which determines CO_2 levels in the atmosphere.

Before describing the oceanic reservoir of carbon, a short description of the oceanic environment itself is of need. Many features of the distribution and cycling of carbon compounds in the ocean are strongly dependent on the ocean circulation patterns.

In general, the oceanic water column is characterized by a well-pronounced vertical stratification, strongly inhibiting vertical water movements. It can be divided into three zones, primarily based on the density distribution, itself governed by temperature and salinity distributions: the surface ocean, the pycnocline and the deep ocean [*Wright and Colling*, 1995].

- The *surface ocean*, averaging about 100 m in thickness, contains the least dense water. It is well mixed by the action of winds and waves. Furthermore, the surface ocean is relatively warm, except at high latitudes (the average surface ocean temperature is $\sim 15^{\circ}$C). As the surface ocean is light penetrated, this also is the zone of biological production.

- The *pycnocline* lies beneath the surface ocean. It extends to a typical depth of about 1,000 m. Water density rapidly increases with depth. This density increase is most often associated with temperature decrease, and the pycnocline often coincides with the *thermocline*, the zone where temperature quickly declines from the surface values to the top temperature of the underlying deep-water zone. Here, most of the organic compounds produced in the surface ocean are remineralized into their inorganic constituents.

- The *deep ocean*, which contains the most dense water, extends from a depth of 1,000 m to the bottom. Temperatures gently decline from about $4-5^{\circ}$C at the top to $0-3^{\circ}$C at the bottom. Neither temperature nor salinity are affected by seasonal variations. This zone is characterized by the absence of vertical gradients in the chemical composition.

The large-scale overturning of the oceans is driven by the *thermohaline* circulation, the density-driven ventilation of the deep waters. An idealized overview of the water movement by the thermohaline circulation in the oceans is presented in Fig. 1.2 [*after Schmitz*, 1995] , a modification of Broecker's *Great Ocean Conveyor Belt* [*Broecker*, 1991]

Water that is dense enough to sink from the surface to the bottom of the ocean forms at present only in the cold high-latitude regions of the North Atlantic and around the Antarctic continent [*Broecker and Peng*, 1982; *Broecker*, 1991; *Marshall and Schott*, 1999]. The mechanisms for the required densification are cooling by winds and salinity increases due to sea ice formation (the latter being, however, of secondary importance) during the winter season.

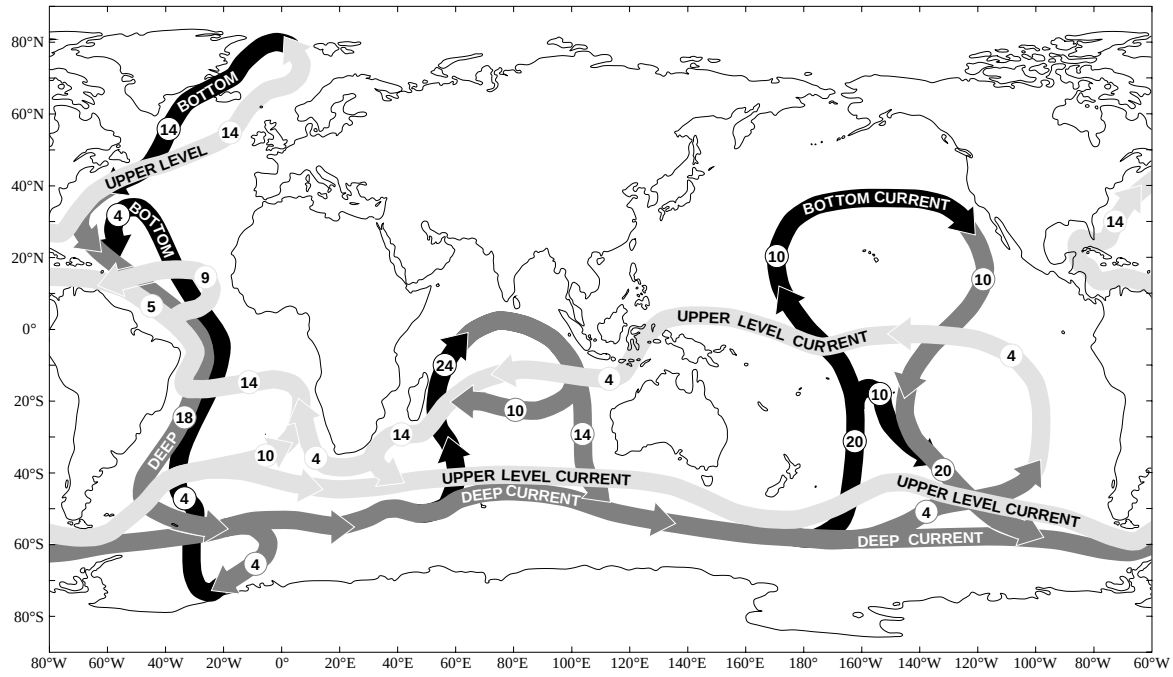

Figure 1.2: Three-layer thermohaline conveyor belt circulation (courtesy of *Munhoven* [1997]; adapted from [*Schmitz*, 1995]). The grey arrows represent the flow pathways of water near the bottom (black), in the deep (dark grey) and in the upper water column (light grey). Changing grey tones along pathways indicate water mass conversion. The circled numbers are estimates for the water transport in sverdrups (1 sverdrup = 1 Sv = $10^6\,\mathrm{m}^3/\mathrm{s}$).

In the North Atlantic (more precisely, in the Labrador, Greenland and Norwegian Seas), cooling of the already very salty surface water during winter time leads to the formation of North Atlantic Deep Water. It then flows to the south through the western basin of the Atlantic Ocean to the tip of South America, where it gets entrained by the eastward flowing Antarctic Circumpolar Current (ACC). It finally enters the deep Indian and Pacific basins. Further areas of deep water formation are the Weddel Sea in the ACC and the Mediterranean Seas [*Marshall and Schott*, 1999]. The formation of bottom and deep waters is compensated by a return flow of water to the surface. This return flow is not confined to restricted areas as is the deep water formation. Major upwelling areas exist at the western coasts of Africa, South and North America. Deep water masses get progressively older starting in the North Atlantic until they reach the deep North Pacific Ocean. This feature is reflected in the distribution of carbon species, as will be discussed later in this chapter.

1.1.1 The CO_2 system in seawater

Four major pools of carbon can be distinguished in the ocean. These are, by decreasing size [*Siegenthaler and Sarmiento*, 1993], the *dissolved inorganic carbon* or *total carbonate concentration*, $\sum \mathrm{CO}_2$ (sometimes denoted by DIC, $\sim$ 40,000 Gt C), the dissolved organic carbon (DOC, $\sim$ 700 Gt C) and

the and the particulate organic carbon ($\sim$ 3 Gt C). Within the atmosphere, CO_2 is chemically rather inert and its budget is controlled by the exchange with the terrestrial biosphere and the ocean. In aqueous media, the situation is very different. Upon dissolution, CO_2 is hydrated to $[H_2CO_3]$, leading to the formation of bicarbonate and carbonate ions. The dissolved inorganic carbon is defined as [*Millero*, 1995]

$$\sum CO_2 = [CO_{2(aq)}] + [HCO_3^-] + [CO_3^{2-}]. \tag{1.1}$$

$[H_2CO_3]$ only exists in trace amounts and is conveniently included with CO_2 as $[CO_{2(aq)}]$. The relative amounts of these three different species depend on the *p*H buffer capacity of the ocean. This buffer capacity is generally expressed in terms of *total* or *titration alkalinity*, TA, which is a measure of the acid neutralization capacity of a solution. TA used to be expressed in proton equivalents per unit mass. The unit recently changed to mol per kg, the same as $\sum CO_2$. In this work, the so-called *carbonate alkalinity* is used. Here, TA, which contains small contributions by a number of compounds, is approximated by:

$$TA = [HCO_3^-] + 2\,[CO_3^{2-}]. \tag{1.2}$$

If the relevant thermodynamic equilibrium constants for carbonate and borate equilibria (and the dissociation constant for water in seawater) are known, one can calculate the individual concentrations of $CO_{2(aq)}$, HCO_3^- and CO_3^{2-} from $\sum CO_2$ and TA. In the present thesis, the dissociation constants given by *DOE* [1994] and by *Millero* [1995] have been used. For quantitative calculations, borate has to be taken into account. The dissociation equilibria are

$$\begin{aligned} CO_{2(aq)} + H_2O &\rightleftharpoons HCO_3^- + H^+, \\ HCO_3^- &\rightleftharpoons CO_3^{2-} + H^+, \\ H_2O &\rightleftharpoons OH^- + H^+, \\ H_2O + B(OH)_3 &\rightleftharpoons B(OH)_4^- + H^+. \end{aligned} \tag{1.3}$$

As can be seen by the presence of H^+ ions in Eq. (1.3), the equilibrium between the individual carbonate species determines *p*H. In the ocean, the majority of dissolved inorganic carbon is present as HCO_3^-, so sea water generally is slightly alkaline, with a *p*H around 8.1-8.3 [*Wright and Colling*, 1995] (cf. Fig. 1.3).

The general distributions of $\sum CO_2$ and TA in the world oceans are known since the *Geochemical Ocean Sections* (GEOSECS) expeditions from 1972 to 1977. Starting in the early 1990's, more extensive measurements have been made in the *World Ocean Circulation Experiment* (WOCE) and other initiatives, however, these data are not yet available as a unified global data set. Thus, GEOSECS data are used in this study.

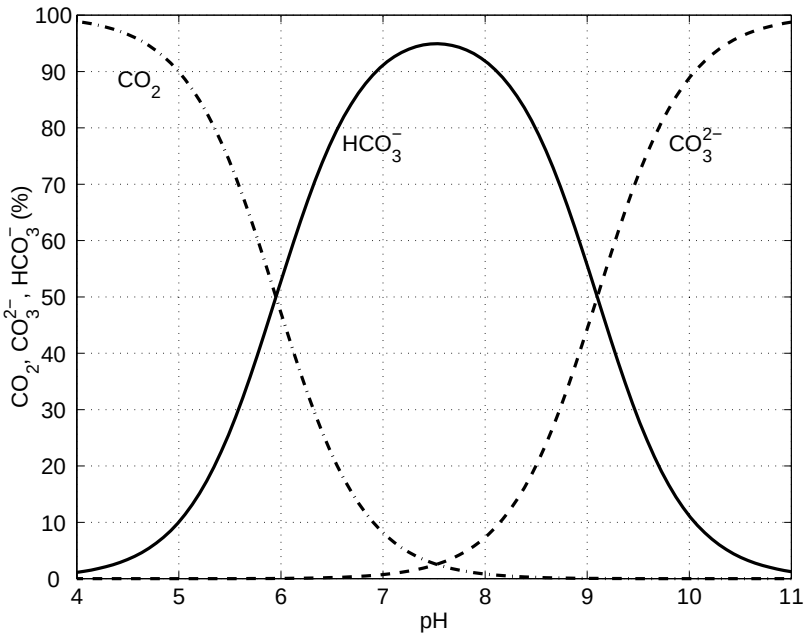

Figure 1.3: Distribution of carbonate species in percent at T = 15°C and S=35.

Fig. 1.4 shows average distributions of both quantities throughout the ocean basins. Two large-scale gradients can be distinguished for both $\sum CO_2$ and TA:

- an overall surface-to-deep sea gradient with maxima at $\sim$ 1000 m depth ($\sum CO_2$) and $\sim$ 2500 m depth (TA).

- within the deep sea, a gradient along the pathway of deep water transport, from the North through the South Atlantic to the Antarctic Circumpolar waters, and from there, continuing through the South to both the North Indian Ocean and the North Pacific Ocean.

Both are maintained by the interplay between the air-sea exchange of CO_2, biologically mediated fluxes from the surface to the deep waters and the large-scale water circulation in the World oceans. Carbon and alkalinity taken up by marine organisms at the surface are released to solution at depth during remineralization. Here they are collected all along the pathway of water transport between the deep parts of the ocean basins, leading to the observed gradual enrichment.

1.1.2 The oceanic carbon pumps

The oceanic carbon pumps include two biological pumps, which are characterized by the production and transport to depth of either organic matter (usually referred to as the *organic carbon pump* or *soft tissue pump*) or calcium carbonate (usually referred to as the *carbonate pump*). As will be discussed in detail below, the main features of the carbon pumps are

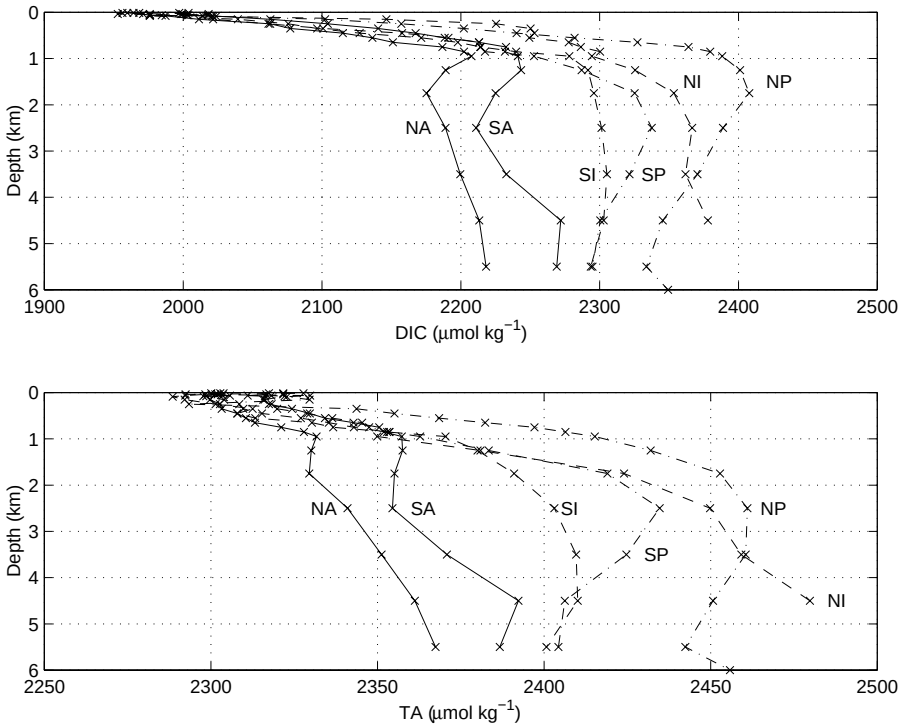

Figure 1.4: Average distributions of $\sum CO_2$ (Top) and TA (Bottom) normalized to the mean world ocean salinity of 34.78 psu. Shown are the North and South Atlantic (NA, SA), the North and South Indian (NI, SI) and the North and South Pacific (NP, SP). Drawn from data of [*Takahashi et al.*, 1981].

- The *organic carbon pump* decreases surface water pCO_2 and is thus favourable for oceanic uptake of atmospheric CO_2. The *carbonate pump* raises surface water pCO_2 and diminishes the ocean's ability to take up atmospheric CO_2.

- Nearly all organic carbon is remineralized in the water column, whereas a considerable amount of calcium carbonate accumulates in the sediments.

In the euphotic zone, which is restricted to the uppermost 100–200 m, organic matter (*particulate organic carbon*, POC) is produced by phytoplankton during photosynthesis. During this process, dissolved inorganic carbon and nutrients (essentially phosphate and nitrate) are taken up and oxygen is released. The stoichiometry can be described by the following idealized chemical equation [*Redfield et al.*, 1963]:

$$106CO_2 + 16NO_3^- + H_2PO_4^- + 17H_3O^+ + 105H_2O \longrightarrow (CH_2O)_{106}(NH_3)_{16}(H_3PO_4) + 138O_2. \tag{1.4}$$

The characteristic C : N : P : O_2 ratios of 106:16:1:-138 in this equation are known as *Redfield ratios*. Their exact values are still a subject of debate (cf. Table 1.1).

Redfield ratios		Reference
$r_{O/C}$	$r_{C/N}$	
1.30	6.6	Redfield et al. [1963]
-	4.8-5.4	Copin-Montegut and Copin-Montegut [1983]
1.45	8.4	Anderson and Sarmiento [1994]
1.36	9.4	Shaffer [1996] [a]
1.25	8.3	Hupe and Karstensen [2000]
-	5-15	Körtzinger et al. [2001]

Table 1.1: Redfield ratios field and model ([a]) data. The measurements of *Körtzinger et al.* [2001] display high variability between bloom (low $r_{C/N}$) and non-bloom (high $r_{C/N}$) situations.

Besides organic matter, some marine organisms also produce carbonate material for their skeletons and shells, referred to as *particulate inorganic carbon* (PIC). Most of this is calcium carbonate as calcite and aragonite, two forms of $CaCO_3$ which exhibit a different crystal structure. Calcite is produced by coccolithophorids, a class of phytoplankton and foraminifera, which are zooplankton. Aragonite is formed by corals and the zooplankton class of pteropods (Fig. 1.5).

Calcite and aragonite differ in the geometry of the mineral structure and have different solubility properties. $CaCO_3$ production can be described by [*Holligan and Robertson*, 1996]

$$2HCO_3^- + Ca^{2+} \longrightarrow CaCO_3 + CO_2 + H_2O. \tag{1.5}$$

The production of organic matter and of calcium carbonate have different effects on the seawater's carbonate system. Let ΔC_{org} and ΔC_{CaCO_3} (mol) be the amount of organic carbon and dissolved calcium carbonate produced or remineralized / dissolved in one kg solution, respectively. Then, the change in dissolved inorganic carbon (DIC) and total alkalinity (TA) is given by (assuming that nitrate is the nitrogen source)

$$\begin{aligned} \Delta DIC &= -\Delta C_{org} - \Delta C_{CaCO_3}, \\ \Delta TA &= \frac{1}{r_{C/N}} \Delta C_{org} - 2\,\Delta C_{CaCO_3}, \end{aligned} \tag{1.6}$$

where $r_{C/N}$ is the Redfield ratio of C and N in organic carbon (Table 1.1). The build up of organic carbon diminishes DIC and it slightly increases TA, due to the nitrate uptake [*Brewer and Goldman*, 1976; *Goldman and Brewer*, 1980]. The production of calcium carbonate decreases DIC and TA in a ratio of 1:2, as two moles of the charged species HCO_3^- are consumed and one mole CO_2 is released for each mole $CaCO_3$ produced. The changed concentrations of DIC and TA determine a new equilibrium between the carbonate species according to Eq. (1.3), thus not all CO_2 molecules released by calcium carbonate production remain in the water as dissolved CO_2, some are converted to CO_3^{2-} or HCO_3^- ions. In the case of remineralization / dissolution, reactions (1.4) and (1.5) are reversed. Thus, at the surface ocean, the production of C_{org} decreases pCO_2, while the production

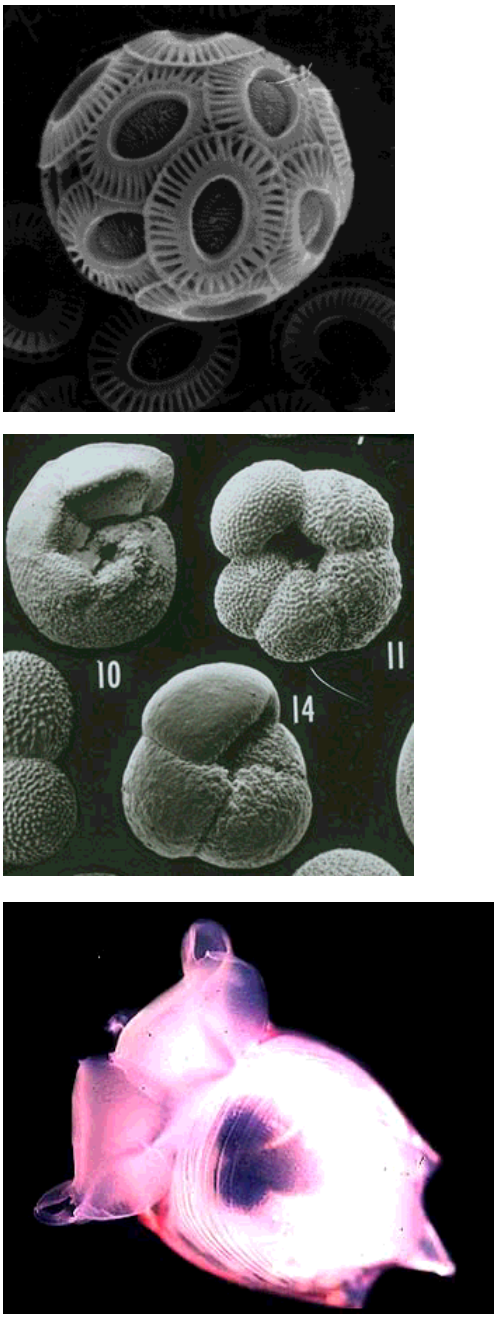

Figure 1.5: Calcium carbonate producing organisms. From top to bottom: Coccolithophorid, foraminifera (both calcite), and pteropod (aragonite). Note that the graphs are not to scale. Pteropods and foraminifera are approximately the same size and much bigger than coccolithophorids. The coccolithophorid picture is taken from http://www.soc.soton.ac.uk/SUDO/RES/tt/eh/, the foraminifera image is found at http://www-class.unl.edu/geol109/classifi.htm, and the pteropod picture is taken from http://life.bio.sunysb.edu/marinebio/plankton.html.

of carbonate increases it. The remineralization of organic carbon at depth releases CO_2 and the dissolution of $CaCO_3$ consumes CO_2.

The POC:PIC production ratio is not uniform throughout the oceans. In high-productivity areas, diatoms, which produce opaline shells, tend to dominate carbonate-walled organisms, thus leading to increased ratios. Estimates for POC:PIC ratios in the export production (the fraction of production that leaves the euphotic zone) are in a range from 3.5 : 1 to 7.5 : 1 [*Shaffer*, 1993]. The global mean ratio is given by 5 : 1 [*Li et al.*, 1969].

In the intermediate and deep waters below, the exported organic matter is rapidly oxidized through microbial activity and by the organic metabolism of bathypelagic fauna. In the open ocean, about 80% of the exported POC is remineralized before reaching a depth of 1,000 m [*Suess*, 1980; *Martin et al.*, 1987]. During remineralization in the water column, oxygen is taken up, while the carbon and the nutrients fixed in the organic matter are released to their dissolved inorganic form at depth from where they may return to the euphotic layer through upwelling and diffusive mixing. As a consequence, only a very small fraction of the exported POC reaches the sediments at the sea-floor where remineralization continues.

Together with the organic export production, the hard remains of calcifying organisms sink out of the euphotic zone. While the fate of organic export production largely depends on microbial activity in the water column, that of carbonate depends on the saturation state of seawater with respect to carbonate minerals. The *degree of saturation* of seawater with respect to calcite (Ω_{Calc}) and that with respect to aragonite (Ω_{Arag}) are defined by

$$\Omega_{Calc} = \frac{[Ca^{2+}]\,[CO_3^{2-}]}{K_{Calc}} \quad \text{and} \quad \Omega_{Ara} = \frac{[Ca^{2+}]\,[CO_3^{2-}]}{K_{Ara}} \tag{1.7}$$

respectively, where K_{Calc}, K_{Arag} $(mol^2\,kg^{-2})$ are the solubility products of calcite and aragonite in seawater, which differ due to the different crystal structures of the molecules. The *Aragonite* and *Calcite Saturation Horizons* (ASH and CSH) are defined as the depths where the respective degree of saturation equals unity. Waters where $\Omega_{Calc} < 1$ are undersaturated with respect to calcite, those where $\Omega_{Calc} > 1$ are supersaturated (analogous for aragonite). In the oceans, the concentration of Ca^{2+} is only very weakly affected by the precipitation and dissolution of carbonate minerals, and it can be considered as quasi-conservative (deviations from strict conservation are less than 0.5%). Variations of Ω_{Calc} and Ω_{Arag} are thus related to deviations of CO_3^{2-} from the respective carbonate ion concentrations at saturation (also referred to as *critical carbonate saturations*) defined by

$$[CO_3^{2-}]_{Calc\ sat} = \frac{K_{Calc}}{[Ca^{2+}]} \quad \text{and} \quad [CO_3^{2-}]_{Ara\ sat} = \frac{K_{Ara}}{[Ca^{2+}]} \tag{1.8}$$

The solubility products of calcite and aragonite depend on pressure and, to a minor extent, on temperature. Thus, the critical carbonate ion concentrations increase with increasing depth, as is illustrated in Fig. 1.6. At given pressure and temperature, $K_{Arag} > K_{Calc}$, which results in $[CO_3^{2-}]_{Arag\ sat} > [CO_3^{2-}]_{Calc\ sat}$ at a given depth. Thus, aragonite is more easily dissolved than calcite.

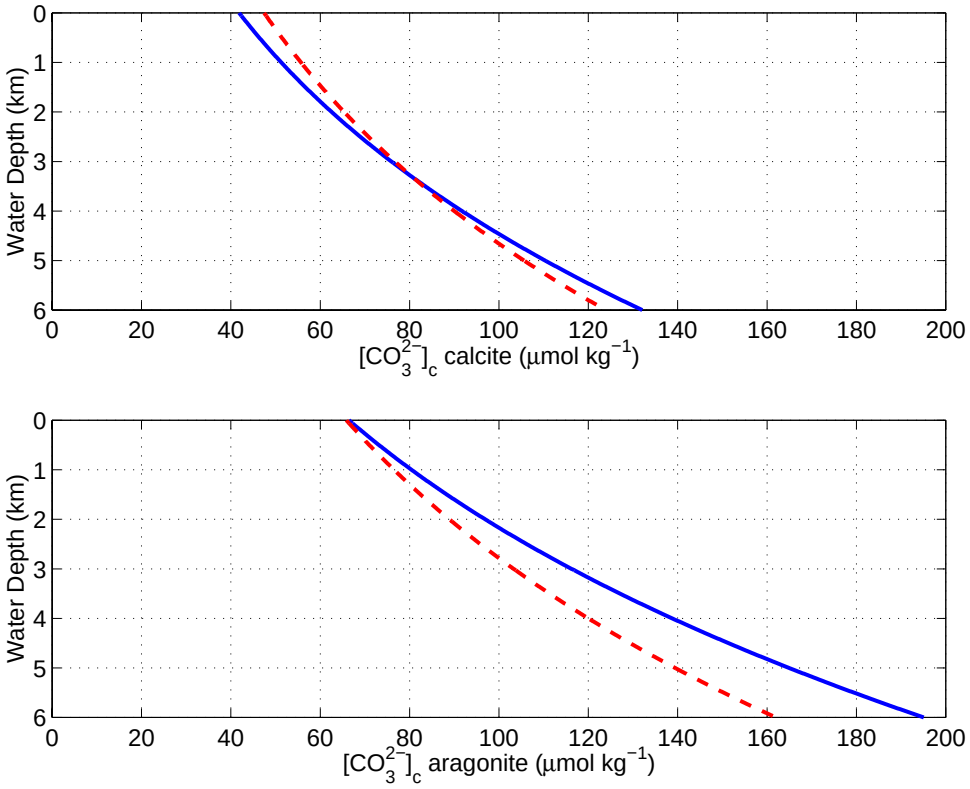

Figure 1.6: Critical carbonate ion concentration versus depth. Values for calcite in the top graph and for aragonite in the bottom graph. Solid lines are calculated according to *Millero* [1995] (used in chapters 3 and 4), broken lines show the *Broecker and Takahashi* [1978] parameterization (used in chapter 2).

Fig. 1.7 shows the distributions of CO_3^{2-} throughout the oceans that are calculated from the GEOSECS data on $\sum CO_2$ and TA distributions [*Takahashi et al.*, 1981]. The distribution of $[CO_3^{2-}]$ follows that of $\sum CO_2$ and TA depicted in Fig. 1.4, as these quantities are related by Eq. (1.1),(1.2) and (1.3). For pH$>$ 8, $[CO_3^{2-}] \approx TA - \sum CO_2$. The deep water masses get progressively older from the North Atlantic towards the North Pacific. Thus, they contain increasingly more CO_2 released by the remineralization of organic matter. The distributions of CO_2 and CO_3^{2-} are inverse to each other (cf. Fig. 1.3). Therefore, the North Atlantic is the most saturated ocean basin, while the North Pacific is the least saturated ocean basin with respect to calcium carbonate.

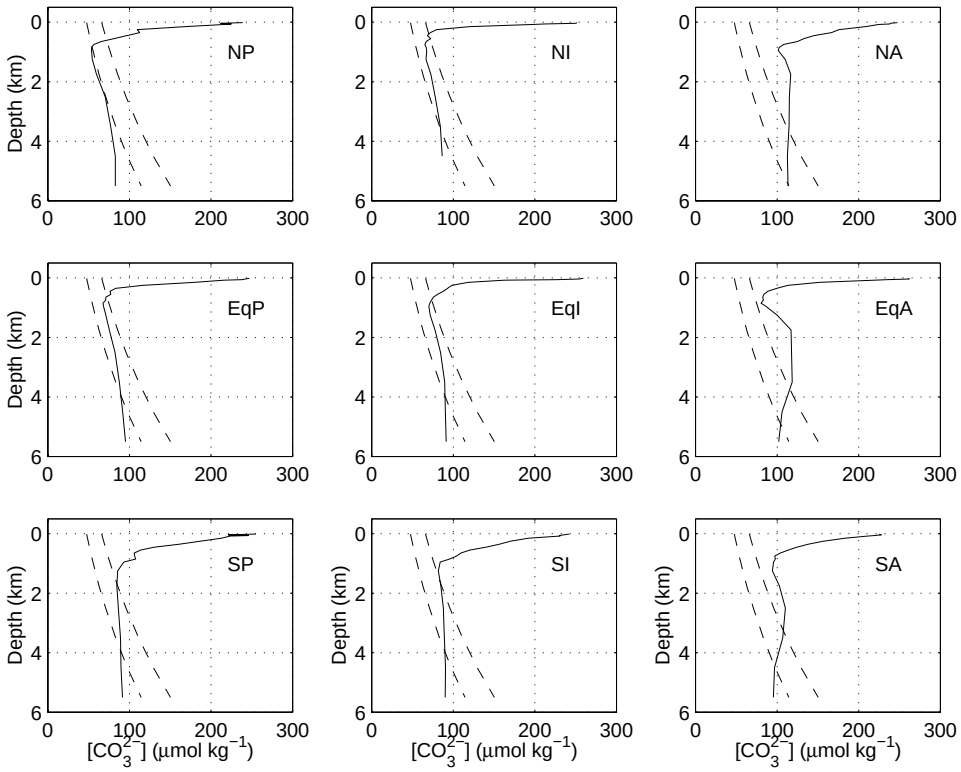

Figure 1.7: Profiles of $CaCO_3$ (solid lines) in different ocean basins (Notation as in Fig. 1.4). The dashed lines denote the critical carbonate concentration for calcite (lower values) and aragonite (upper values). The crossing of the in-situ carbonate concentration with the critical concentration is the respective saturation horizon.

The solubility of both aragonite and calcite increases with depth: Surface and intermediate waters are supersaturated with respect to these minerals, the deep parts of the oceans are undersaturated. When reaching the seafloor, the inorganic detritus will dissolve if the sediment is bathed in undersaturated waters. Different characteristic depth horizons can be identified. See Fig. 1.8 for a schematic illustration.

- *Lysocline*. At this depth, dissolution effects on carbonate shells are first seen in the sediments. Different lysoclines can be defined, depending on whether particular microfossils are used as indicators (e.g., pteropod lysocline, foraminiferal lysocline, . . .), or particular minerals (aragonite lysocline, calcite lysocline).

- *Compensation Depth*. This is the depth where sedimentation and dissolution fluxes balance each other in the sediments. Again, *Aragonite* and *Calcite Compensation Depths*, ACD and CCD, are distinguished. The CCD is often identified with the depth where the fraction of $CaCO_3$ in the surface sediment has fallen to a given threshold value, typically 0–20%, depending on the authors [*Broecker and Peng*, 1982; *Morse and McKenzie*, 1990].

- *Saturation Horizon (SH)*. The calcite saturation horizon (CSH) is defined a the depth in the water column where the carbonate concentration at saturation, $[CO_3^{2-}]_{\text{Calc sat}}$, equals the in-situ carbonate concentration. Below this depth, waters are undersaturated with respect to calcite. The aragonite saturation horizon (ASH) is defined analogue (cf. Fig. 1.7). If not specified, the term saturation horizon (SH) will henceforth refer to the calcite saturation horizon.

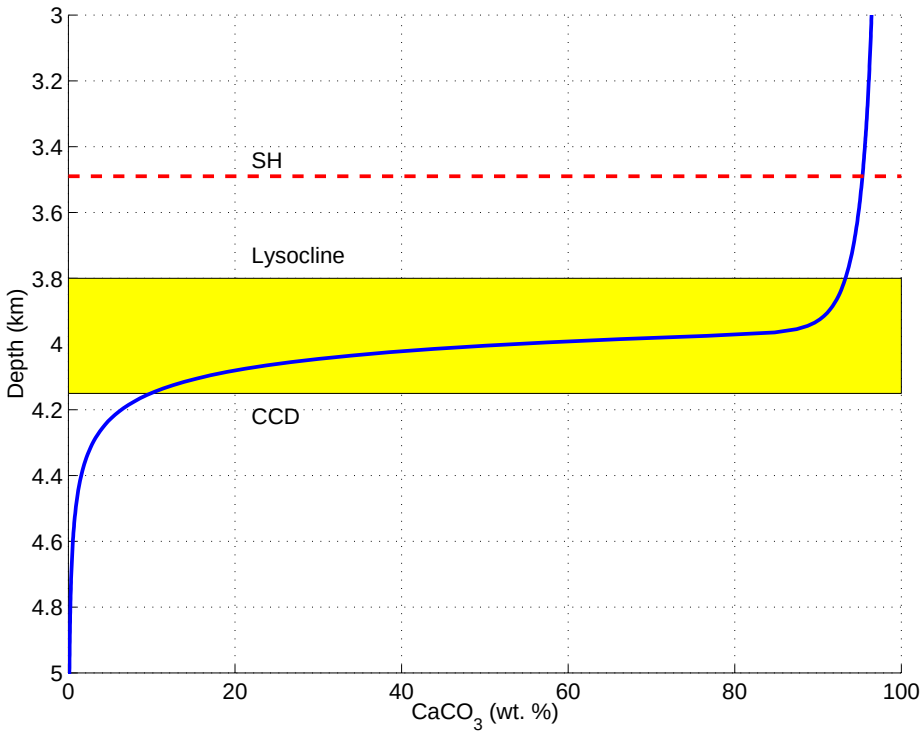

Figure 1.8: Carbonate concentration (weight %) in sediment versus depth. The lysocline is the depth where dissolution becomes visible and generally lies below the saturation horizon. The CCD marks the depth where carbonate concentration falls below a certain threshold, here chosen as 10%.

The location of the lysocline is connected, but not strictly tied to, the location of the SH. In the case of infinitely fast dissolution kinetics, the lysocline would fall together with the SH, as all carbonate shells falling below the SH would instantly dissolve. As this is not the case, there is a separation between the lysocline and the SH. The lysocline is generally located deeper than the saturation horizon at a point where undersaturation becomes strong enough to make dissolution visible (cf. to Appendix A for a discussion on carbonate dissolution kinetics). In areas of high production, the lysocline may be considerably depressed with respect to the SH, because the rain rate of carbonate particles exceeds their dissolution rate close to the SH. It is important to note that the lysocline is not the depth where the onset of dissolution is located but the depth where dissolution at first becomes visible. The lysocline might also be shallower than the SH if significant amounts of organic matter enter the sediments. In this case, the CO_2 released by respiration of the organic carbon decreases $[CO_3^{2-}]$ in the porewaters of the sediment, creating an environment undersaturated with respect to calcium carbonate. Thus, $CaCO_3$ is dissolved at a depth that is above the SH.

As is visible in Fig. 1.7, most parts of the oceanic water column are supersaturated with respect to calcium carbonate. The figure indicates differences between ocean basins; the Atlantic Ocean is the most saturated part of the global ocean, while the Pacific Ocean is least saturated, with decreasing saturation towards the north. This pattern follows the pattern of DIC and TA concentrations displayed in Fig. 1.4. The time a settling particle spents in undersaturated waters before arriving at the seafloor is very short compared to the time it spents in the sediment. Thus, it is expected that the major part of carbonate dissolution takes place in the sediments. However, observations point to $CaCO_3$ loss in the water column. *Milliman et al.* [1999] estimate as much as 60-80% of the produced calcium carbonate to be dissolved in the upper 500-1000 m of the ocean. In this depth range, ocean waters are supersaturated with respect to both calcite and aragonite. The mechanisms underlying the observed loss of calcium carbonate are not understood yet. The present thesis investigates some proposed processes with regard to their ability to explain the proposed loss of $CaCO_3$ in the water column.

1.2 Glacial - Interglacial changes in the global carbon cycle

About 18–21 kyr ago, the Earth was at the Last Glacial Maximum (LGM). This period corresponds with the maximal ice extent and is well defined in the ice core records (cf. Fig. 1.9). It is the peak of the latest of a number of glaciations that took place over the past million years, alternating with much shorter warm periods (interglacials) at intervals of about 100 kyr. The Earth's surface conditions at LGM were considerably different from today's. Huge ice-sheets, possibly up to several kilometers thick, covered large parts of the Northern Hemisphere continents. As a consequence, sea level was 120–130 m lower than presently [*Fairbanks*, 1989]. Sea surface temperatures were on average about $2-5\,\mathrm{K}$ lower than today [*McIntyre et al.*, 1981; *Rostek et al.*, 1993; *Bard*, 1999; *Elderfield and Ganssen*, 2000].

1.2.1 Ice-Core Records

The analysis of air trapped in the ice is the most reliable source of information on the evolution of the atmospheric CO_2 content over the glacial-interglacial cycles. The Vostok ice-core provided the first record of the atmospheric CO_2 content over a whole glacial-interglacial climate oscillation [*Barnola et al.*, 1987]. It was already known from previous ice-core studies that CO_2 was 25–30% less abundant in the LGM than in the Holocene atmosphere [*Neftel et al.*, 1982]. The Vostok CO_2 record was nevertheless the first to unveil the close relationship between atmospheric CO_2 levels and climate, indicated by the correlation to the temperature evolution reconstructed from the deuterium profile along the same core [*Jouzel et al.*, 1987]. Both records are represented in Fig. 1.9 together with that of methane (CH_4) [*Chappelaz et al.*, 1990]. Atmospheric CO_2 oscillates between extreme levels of $\sim 280\,\mu$atm (full interglacials) and $\sim 200\,\mu$atm (glacials). The records have recently been extended back to 420 kyr BP [*Petit et al.*, 1999]. CO_2 shows four cycles oscillating between amazingly regular glacial and interglacial pCO_2 levels.

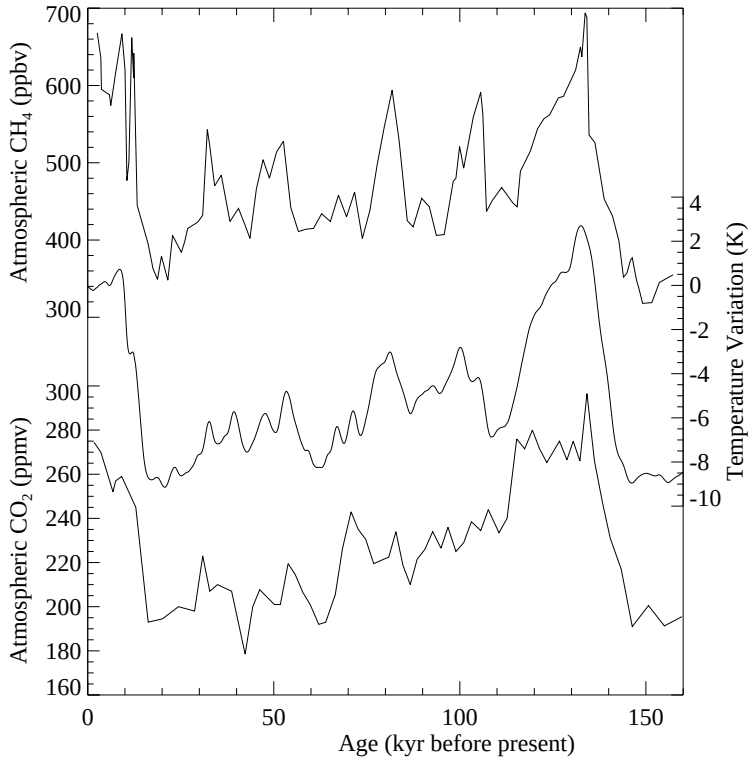

Figure 1.9: Vostok ice-core records of (top) CH_4 [*Chappelaz et al.*, 1990], (middle) temperature [*Jouzel et al.*, 1987] and (bottom) CO_2 [*Barnola et al.*, 1987] for the past 160,000 years.

1.2.2 Calcium carbonate compensation

Geological records suggest that the Atlantic lysocline was 0.3 - 1 km shallower during the last glacial [*Crowley*, 1983; *Curry and Lohmann*, 1986], while it was 0.8 km deeper in the Pacific Ocean [*Farrell and Prell*, 1989]. The reasons for the observed fluctuations are not fully understood. On long time scales, a process called *carbonate compensation* [*Broecker and Peng*, 1982] is thought to regulate the location of the lysocline. The position adjusts such that

$$CO_3^{2-} \text{ river influx} + CaCO_3 \text{ dissolution} = CaCO_3 \text{ production}, \tag{1.9}$$

i.e. the carbonate production is balanced by the river influx of dissolved constituents and re-dissolution of produced carbonates (the Ca^{2+} concentration is not significantly perturbed by carbonate production, as pointed out in the previous section). Presently, biogenic carbonate is build at approximately 4 times the rate at which the dissolved constituents are delivered to the oceans [*Li et al.*, 1969]. Thus, out of 4 moles $CaCO_3$ produced, 3 moles are expected to dissolve at depth, while 1 mole may accumulate on the seafloor. If the lysocline is located in a shallow depth, large areas of the seafloor are susceptible to dissolution and the majority of carbonates are re-dissolved. When the lysocline deepens, less and less calcium carbonate is dissolved.

Imagine the lysocline is in a location where Eq. (1.9) is out of balance, say the production is less than the dissolution plus river influx. Then, river influx is too large, which, however, does not react directly to the oceanic production balance. Thus, too much carbonate is dissolved at depth. The released CO_3^{2-} increases bottom water $[CO_3^{2-}]$, which deepens the saturation horizon. Accordingly, dissolution rate in the sediments diminishes and the lysocline deepens. This process continues until the lysocline is so deep that Eq. (1.9) balances again. The equilibration time scale for this process is on the order of 10,000 years [*Archer et al.*, 2000]. However, the marine carbonate system probably never actually reaches the ideal balance but is either in a state of too much or too less production [*Milliman*, 1993].

1.2.3 Boron Isotopes and Paleo-pH

The Bjerrum plot (Fig. 1.3) shows that seawater *p*H is a key parameter of the carbonate chemistry. Paleo-*p*H records should therefore provide very useful constraints on the evolution of carbonate chemistry with time. One potential tracer of seawater *p*H is the boron isotopic composition of marine carbonate. Calcareous organisms incorporate trace amounts of boron when building up their shells. There are two stable isotopes of boron, ^{10}B and ^{11}B, which respectively make up about 20% and 80% of the total boron in seawater [*Hemming and Hanson*, 1992]. There are also two dominant species of boron in seawater: $B(OH)_3$ and $B(OH)_4^-$. The partitioning between them is *p*H-dependent, according to

$$B(OH)_3 + 2\ H_2O \rightleftharpoons B(OH)_4^- + H_3O^+. \tag{1.10}$$

Kakihana et al. [1977] have shown that $B(OH)_3$ is enriched in ^{11}B with respect to $B(OH)_4^-$ by about $20\,{}^0/_{00}$. The isotopic composition of the two species thus also depends on *p*H. *Hemming and Hanson*

[1992] find that modern marine carbonates have a boron isotopic composition very close to that of $B(OH)_4^-$ in seawater. The isotopic composition of boron incorporated in calcite has been established as a reliable proxy for *p*H [*Hemming et al.*, 1995; *Sanyal et al.*, 1996; *Sanyal and Bijma*, 1999; *Sanyal et al.*, 2000]. δ^{11}B analysis of sediment cores suggest that the glacial deep ocean *p*H was approximately 0.3 units higher than today, as is illustrated in Fig. 1.10 [*Sanyal et al.*, 1995; *Sanyal et al.*, 1997; *Palmer et al.*, 1998].

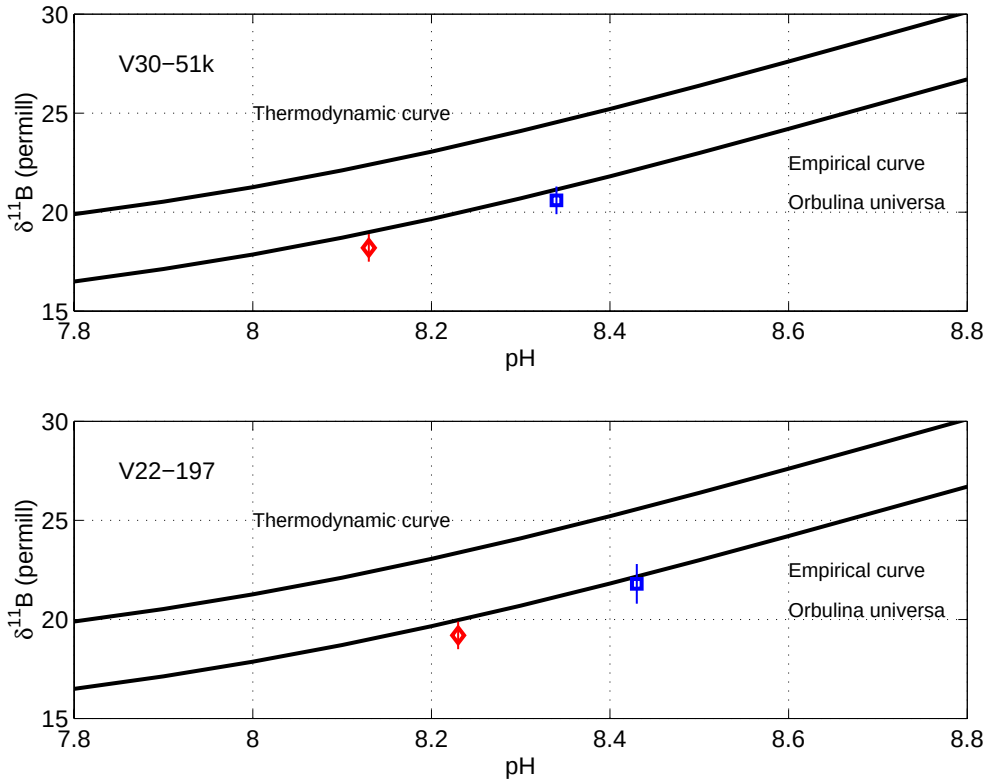

Figure 1.10: Boron isotopic composition of the foraminifera *Orbulina universa* from the Holocene and the last glacial period obtained from cores V30-51k (19°52′N, 19°55′W, 3409m) and V22-197 (14°10′N, 18°35′W, 3167m) in the northwest African upwelling zone. Diamonds: Holocene values, squares: Last Glacial Maximum values. Data taken from *Sanyal and Bijma* [1999]. The empirical curve for *Orbulina universa* is based on culture experiments [*Sanyal et al.*, 1996], it has a constant offset to the thermodynamic curve due to vital effects (3.4 permil).

This variation of *p*H in the deep sea corresponds to an increase of the CO_3^{2-} ion concentration of the order of $100\,\mu\mathrm{mol\,kg^{-1}}$. This would be equivalent to a deepening of the calcite saturation horizon of several kilometers, in strong disagreement with the observations of glacial lysocline depths. Reconciling this difference is one aim of the present thesis.

Chapter 2

Dissolution of carbonate particles settling in the water column

This chapter deals with the dissolution of biogenic carbonate particles while they are settling through the water column. Two scenarios are investigated. A given particle can either sink isolated and be dissolved when entering depths that are undersaturated with respect to aragonite or calcite, respectively. Alternatively, the particle can be contained, together with other particles and material, in an aggregate. In the latter case, respiration of organic matter may create a chemical microenvironment in the aggregate stimulating dissolution in oversaturated waters.

The first section of the chapter outlines a simple model simulating inorganic dissolution during particle settling. A sensitivity analysis is given to provide insight into critical parameters and the model is applied to oceanic settings utilizing GEOSECS data. Section 2.2 considers the possibility of respiration driven dissolution. Literature data on settling velocities are discussed in Appendix B.

Modelling work concerning water column dissolution of calcium carbonate shells is limited. *Pond et al.* [1971] formulated a model for settling foraminifera and concluded that they have the potential of being dissolved before reaching the seafloor. *Honjo* [1977] elaborates on modelling, observational and experimental work, pointing out that no major dissolution of biogenic carbonates takes place in the water column. *Byrne et al.* [1984] model water column dissolution of aragonite in the Pacific Ocean and state that the dissolution of settling pteropod shells should be identified with alkalinity maxima as observed by *Fiadeiro* [1980].

2.1 A model of physico-chemical dissolution

2.1.1 Model description

The water column dissolution model considers a biogenic particle comprised of either calcite or aragonite, settling through the water column. As the particle enters undersaturated waters, it experiences dissolution. A simple approach in one spatial dimension is followed. The chemistry of the bulk seawater is given as forcing data. The amount of calcite or aragonite dissolved at a certain depth is the only prognostic variable. Dissolution of biogenic carbonates in the water column depends on

(1) the dissolution rate of each mineral phase, (2) the surface area in contact with water, (3) the residence time of the particles in undersaturated waters and (4) the magnitude of undersaturation. Let *C(t)* (mol) be the calcite or aragonite content at time *t* (days). The kinetics may be formulated as [*Archer*, 1996]

$$\frac{\mathrm{dC(t)}}{\mathrm{dt}} = \begin{cases} 0 & \text{if } [CO_3^{2-}] \geq [CO_3^{2-}]_c, \\ -\kappa \left(1 - \dfrac{[CO_3^{2-}]}{[CO_3^{2-}]_c}\right)^{\eta} C(t) & \text{if } [CO_3^{2-}] < [CO_3^{2-}]_c. \end{cases} \tag{2.1}$$

where κ denotes the dissolution rate constant (d^{-1}) and η the dissolution rate order. $[CO_3^{2-}]$ is the in-situ carbonate ion concentration (μmol kg^{-1}) and $[CO_3^{2-}]_c$ is the carbonate ion concentration at saturation. The latter is a function of depth (pressure; the weak dependence on temperature is neglected) and is dependent on the crystal structure, namely calcite (foraminifera and coccolithophorids) or aragonite (pteropods):

$$[CO_3^{2-}]_c(z) = \begin{cases} 90\ \exp(0.16[z-4]), & \text{calcite} \\ 120\ \exp(0.15[z-4]), & \text{aragonite} \end{cases} \tag{2.2}$$

where *z* is depth (km), as proposed by *Broecker and Takahashi* [1978] (Fig. 1.6). This parameterization is preferred over the more recent calculations by *Millero* [1995], since it conveniently can be included into the model's equations and small differences can be ignored given the uncertainties in several other model parameters.

As a first approximation, and for use in the sensitivity experiments, bulk $[CO_3^{2-}]$ is assumed to be constant and independent of depth. This is a valid simplification as the in-situ $[CO_3^{2-}]$ is virtually constant for depths greater than 2000 m and shallower waters are generally supersaturated with respect to calcium carbonate (cf. Fig. 1.7).

Let *v* ($\mathrm{m\,d}^{-1}$) be the settling velocity of the aggregate. Then, after time *t* the particle's depth is *z(t)* $= \mathrm{v\,t}$. Thus, Eq. (2.1) may be formulated as (considering calcite)

$$\frac{\mathrm{dC(t)}}{\mathrm{dt}} = \begin{cases} 0 & \text{if } t \leq t^*, \\ -\kappa \left(1 - \dfrac{[CO_3^{2-}]}{90}\ \exp[-1.6\times10^{-4}vt + 0.64]\right)^{\eta} C(t) & \text{if } t > t^*, \end{cases} \tag{2.3}$$

where

$$t^* = \frac{6250 \ln([CO_3^{2-}]/90) + 4000}{v} \tag{2.4}$$

is the time after which undersaturation is reached. An analogue formulation is derived for aragonite, using the appropriate parameterization in Eq. (2.2).

Standard model parameters are given in Table 2.1. The results of the corresponding model run are shown in Fig. 2.1. The bulk seawater concentration of 90 μmol CO_3^{2-} corresponds to a calcite saturation horizon at 4 km depth and an aragonite saturation horizon at 2 km depth. Calcite dissolution is defined here to be visible when one percent of the particle is dissolved. In the standard model run, dissolution of calcitic shells is visible $\sim$ 1 km below the saturation horizon. At 6 km

depth, $\sim$ 38% of a settling calcite particle is dissolved within the water column. The onset of aragonite dissolution lies $\sim$ 2 km below the saturation horizon, as the pteropod shells sink faster than coccolithophorids. At 6 km depth, a $\sim$ 30% of a settling aragonite particle is dissolved within the water column.

Parameter	Standard value	Range	Reference
η (c)	4.5	1-5	Hales and Emerson [1997], Keir [1980]
η (a)	4.2	1-5	Hales and Emerson [1997], Keir [1980]
κ (c)	$5\,\mathrm{d}^{-1}$	$1-7\,\mathrm{d}^{-1}$	Keir [1980]
κ (a)	$3.2\,\mathrm{d}^{-1}$	$1-7\,\mathrm{d}^{-1}$	Keir [1980]
v (c, coccolithophorids)	$10\,\mathrm{m\,d}^{-1}$	$1-100\,\mathrm{m\,d}^{-1}$	Smayda [1971], Fok-Pun and Komar [1983]
v (a, pteropods)	$300\,\mathrm{m\,d}^{-1}$	$80-1080\,\mathrm{m\,d}^{-1}$	Noji et al. [1997]
$[CO_3]_{\mathrm{bulk}}$	$90\,\mu\mathrm{mol\,kg}^{-1}$	$50-250\,\mu\mathrm{mol\,kg}^{-1}$	Takahashi et al. [1981]

Table 2.1: Parameters of the physico-chemical dissolution model. The standard bulk concentration of CO_3^{2-} corresponds to a saturation horizon at 4 km for calcite (c) and at 2 km for aragonite (a).

2.1.2 Sensitivity Studies

This section describes results obtained with sensitivity experiments. All parameters are used with standard values except the one which is varied. Sinking rates of biogenic particles determine the time the carbonate is exposed to water column dissolution. The results of numerical experiments with settling velocities varied over two orders of magnitude are displayed in Fig. 2.2. Settling velocities estimated from experimental and field work are discussed in Appendix B (Table B.1, B.2). It is noted that only for sediment depths well below the saturation horizon, significant dissolution takes place in the water column provided that the settling velocity is low.

The dissolution rate is determined by the rate constant, κ, and the order of kinetics, η, as seen in Eq. (2.1). Keir (1980) gives $3\,\mathrm{d}^{-1} < \kappa < 7\,\mathrm{d}^{-1}$ as a range for single coccoliths. The rate order of calcite dissolution kinetics is not well constrained (Table A.1), as values cited in the literature range between 1 [*Hales and Emerson*, 1997] and more than 5 [*Keir*, 1980]. The latter author reports a value of 4.5 ± 0.7 in dissolution experiments with a wide range of species as well as mixed sediment probes. *Hales and Emerson* [1997] fit $\eta = 1$ to data obtained from in-situ pore water measurements. *Svensson and Dreybrodt* [1992] find the rate order to be dependent on the magnitude of undersaturation. For saturation values smaller than 0.8, they measure a rate order of 1.5-2.2, whereas the dissolution slows down to a rate order of 4 when the medium is closer to equilibrium. The kinetics of aragonite

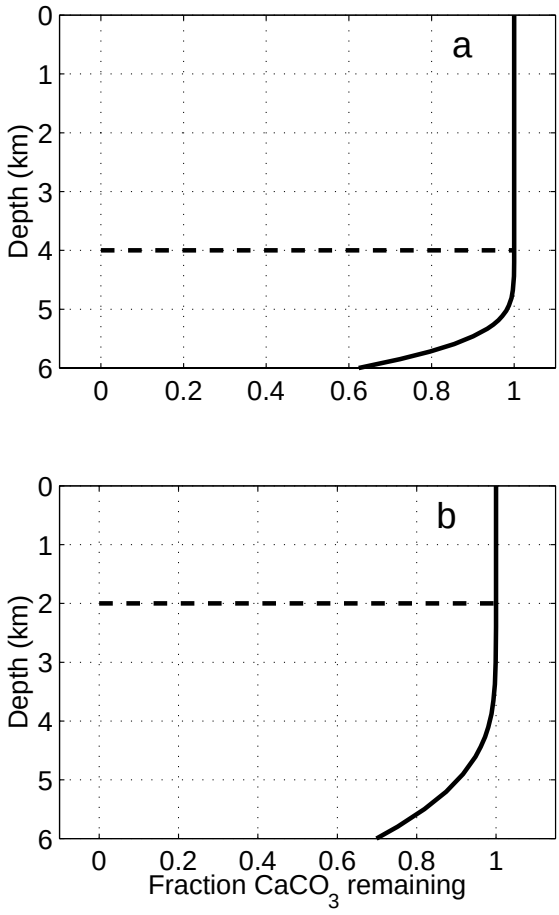

Figure 2.1: Model results using standard parameters as shown in Table 2.1 for (a) calcite and (b) aragonite shells. Shown is the fraction of calcium carbonate remaining at a certain depth. The saturation horizons are marked by straight broken lines.

dissolution are not as thoroughly investigated. However, it is generally assumed that the rate order of aragonite dissolution is a little less than that of calcite dissolution, i.e. when undersaturation is the same, aragonite dissolves more quickly [*Keir*, 1980; *Morse and Berner*, 1979].

The results of numerical experiments with dissolution rate constants $1\,\mathrm{d}^{-1} < \kappa < 7\,\mathrm{d}^{-1}$ are displayed in Fig. 2.3. When compared to other parameters, varying κ has a rather minor effect on the magnitude of dissolution. Fig. 2.4 illustrates the importance of the kinetic rate order. Varying η between 1 and 5 yields by far the largest range in model results among the sensitivity experiments. Thus, better constraints on this parameter by experimental work are most desirable.

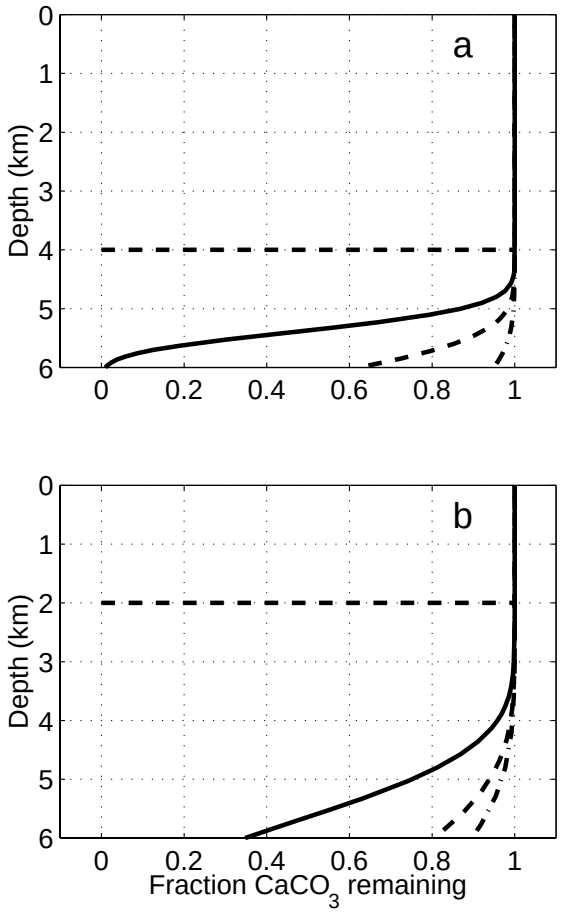

Figure 2.2: Influence of settling velocity on dissolution of (a) calcite and (b) aragonite particles. Shown is the fraction of calcium carbonate remaining at a certain depth. Standard parameter values as given in Table 2.1. Calcite shells settle with $1\,\mathrm{m\,d^{-1}}$ (solid), $10\,\mathrm{m\,d^{-1}}$ (dashed) and $100\,\mathrm{m\,d^{-1}}$ (dash-dotted), while aragonite tests sink with $100\,\mathrm{m\,d^{-1}}$ (solid), $500\,\mathrm{m\,d^{-1}}$ (dashed) and $1000\,\mathrm{m\,d^{-1}}$ (dash-dotted),

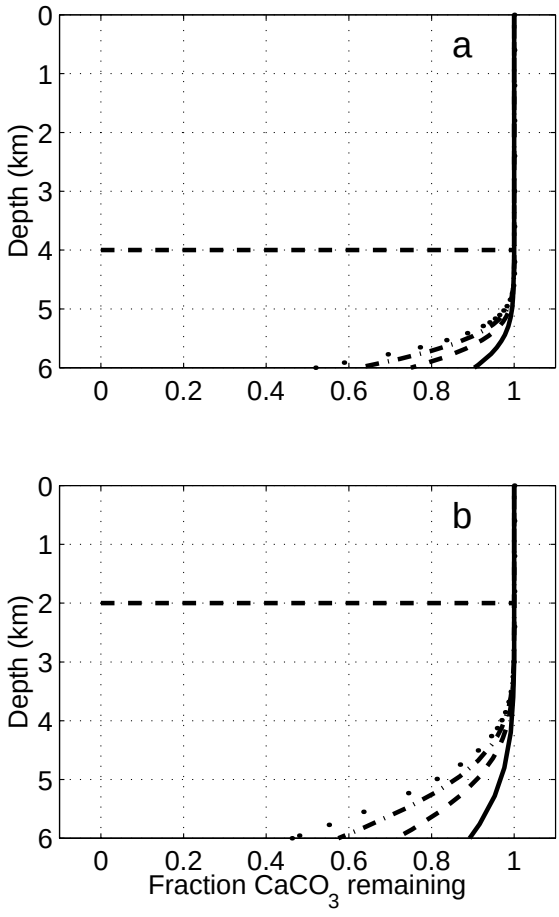

Figure 2.3: Influence of variations in the dissolution rate constant on dissolution of (a) calcite and (b) aragonite shells. Solid line: $\kappa = 1\,\mathrm{d}^{-1}$, dashed: $\kappa = 3\,\mathrm{d}^{-1}$, dash-dotted: $\kappa = 5\,\mathrm{d}^{-1}$, dotted: $\kappa = 7\,\mathrm{d}^{-1}$.

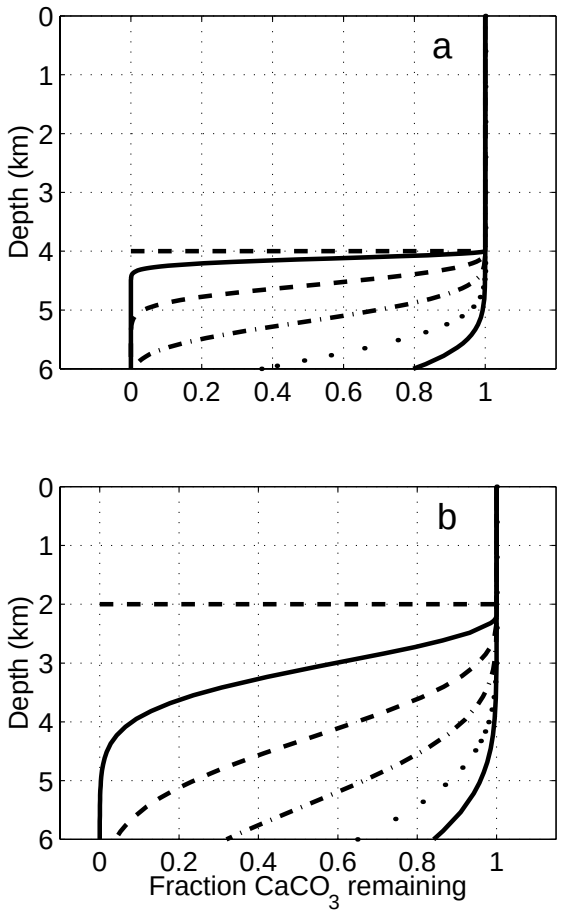

Figure 2.4: Influence of variations in the kinetic rate order on dissolution of (a) calcite and (b) aragonite shells. Solid line left: $\eta = 1$, dashed: $\eta = 2$, dash-dotted: $\eta = 3$, dotted: $\eta = 4$, solid line right: $\eta = 5$,.

2.1.3 Application to oceanic settings

Up to now, profiles with constant CO_3^{2-} bulk concentration have been used. In order to resolve the origin of the relative shallow alkalinity maximum in the Pacific Ocean, the proposed model is run with the in-situ profile of the CO_3^{2-} concentration in this region (Fig. 2.5 and 2.6). Both the Indian Ocean and the Atlantic Ocean are too oversaturated with respect to CO_3^{2-} to yield significant dissolution in the water column.

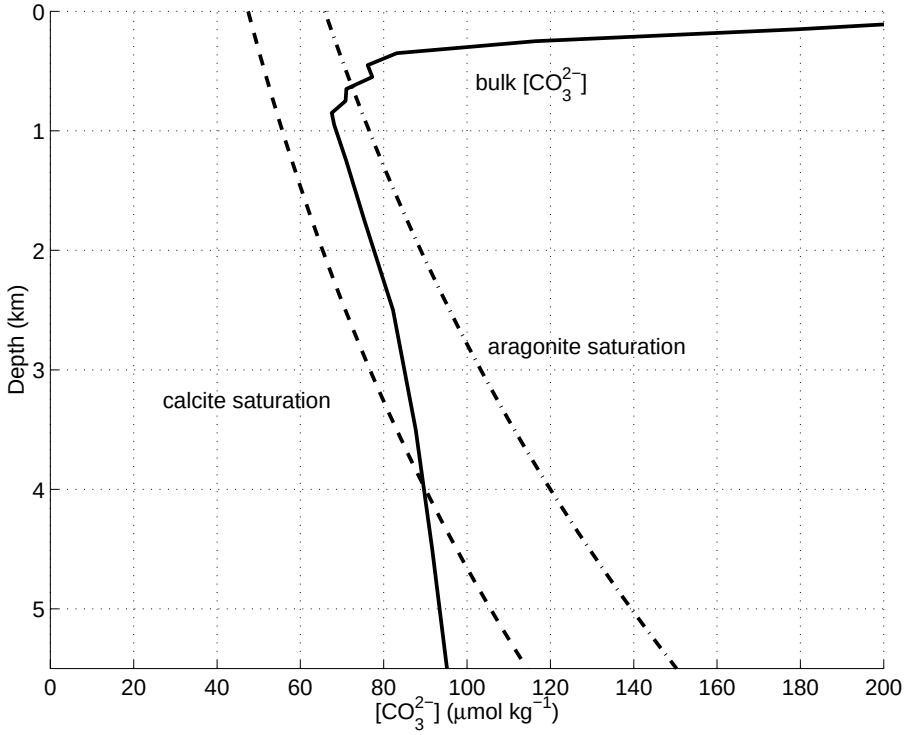

Figure 2.5: In-situ carbonate concentration and critical carbonate concentration in the Equatorial Pacific region (GEOSECS data *Takahashi et al.* [1981]). Dashed line critical carbonate concentration for calcite, dashed dotted line for aragonite. Note that the saturation horizons of the two mineral phases are separated by more than 3 km.

The model is applied to a specific oceanic setting with standard settling velocities ($10\,\mathrm{m\,d^{-1}}$ for calcite (coccolithophorids), $300\,\mathrm{m\,d^{-1}}$ for aragonite (pteropods)) and with various parameterizations for the dissolution kinetics proposed in the literature (Table 2.2).

Results for the Equatorial Pacific are illustrated in Fig. 2.7. In complete analogy, the North Pacific region is considered (Fig. 2.8). In the Equatorial Pacific region, between 15% and 100% of the initial calcite are dissolved at 6 km depth, depending on the kinetic parameterization. The onset of aragonite dissolution is seen $\sim$ 2 km below the saturation horizon. At 6 km depth, up to 65% of aragonite (pteropods) is dissolved in the water column. Aragonite dissolution kinetics are not as thoroughly investigated as calcite dissolution kinetics, so a rate order smaller than 3 cannot be excluded. Adopting the parameterization of *Hales and Emerson* [1997] to aragonite yields the onset

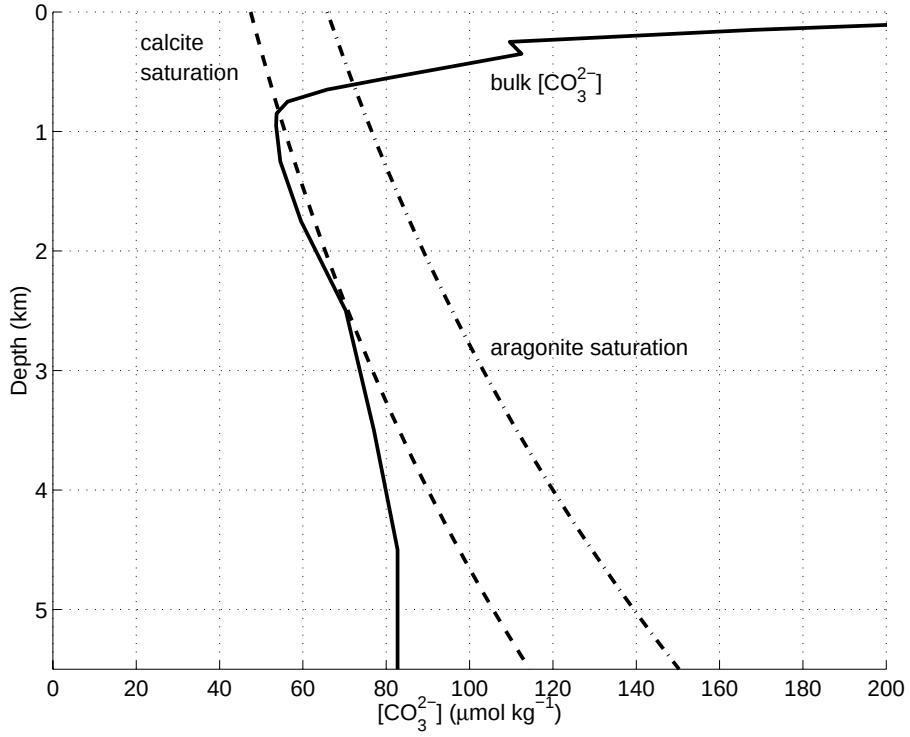

Figure 2.6: In-situ carbonate concentration and critical carbonate concentration in the North Pacific (GEOSECS data *Takahashi et al.* [1981]). Dashed line critical carbonate concentration for calcite, dashed dotted line for aragonite.

of dissolution at the saturation horizon, 20% dissolved at 2.5 km depth and 75% dissolution at 6 km depth.

The North Pacific model run shows increased dissolution mainly for calcite: Dissolution starts at ca. 800 m water depth. Between 2 km and 3 km depth, dissolution slows down due to the near-equilibrium situation (cf. Fig. 2.6). With linear kinetics, nearly all calcite is dissolved at 3 km depth. Aragonite dissolution reaches 95%. The parameterization of *Morse et al.* [1979] and of *Byrne et al.* [1984] yield almost indistinguishable results.

The drastic difference in calcite dissolution between the Equatorial and North Pacific is due to the location of the calcite saturation horizon. As can be seen in Fig. 2.5 and 2.6, the saturation horizons of calcite and aragonite are separated by approximately 3 km in the Equatorial Pacific, while they are both shallower than 1 km in the North Pacific.

$\kappa\,(\mathrm{d}^{-1})$	$\eta\,(-)$	Reference
calcite		
5	4.5	Keir [1980]
1	2.9	Walter [1985]
5	3.0	Morse [1978]
0.38	1.0	Hales and Emerson [1997]
aragonite		
3.18	4.2	Keir [1980] (pteropod shells)
13.2	4.2	Keir [1980] (synthetic aragonite)
1.1	2.93	Morse et al. [1979]
1.3	3.1	Byrne et al. [1984] (fit to model results)

Table 2.2: Parameterizations of dissolution kinetic according to Eq. (2.1).

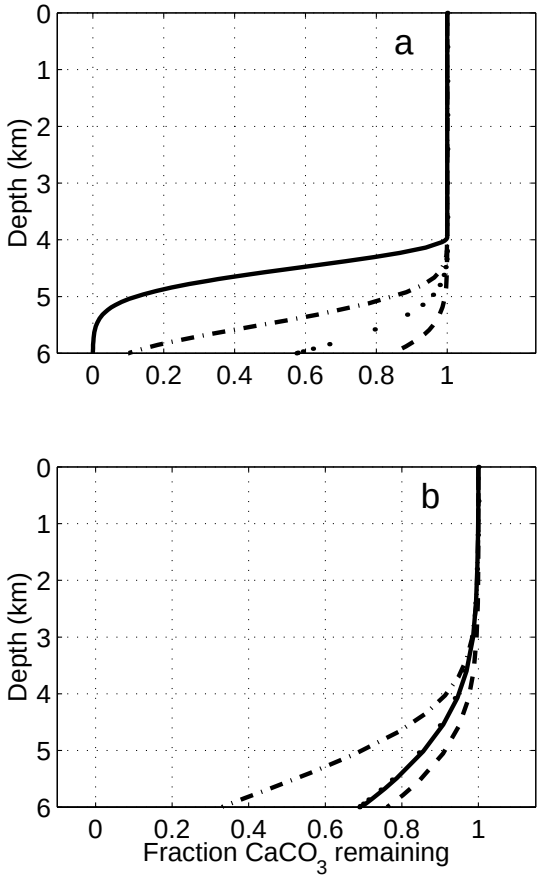

Figure 2.7: Dissolution of (a) calcite and (b) aragonite shells in the Equatorial Pacific. Parameter values as given in Table 2.2. Calcite: Solid line: $(\kappa, \eta) = (0.38, 1)$, dash-dotted: $(\kappa, \eta) = (5, 3)$, dotted: $(\kappa, \eta) = (1, 2.9)$, dashed: $(\kappa, \eta) = (5, 4.5)$. Aragonite: Solid line: $(\kappa, \eta) = (1.3, 3.1)$, dash-dotted: $(\kappa, \eta) = (13.2, 4.2)$, dotted: $(\kappa, \eta) = (1.1, 2.93)$, dashed: $(\kappa, \eta) = (3.18, 4.2)$.

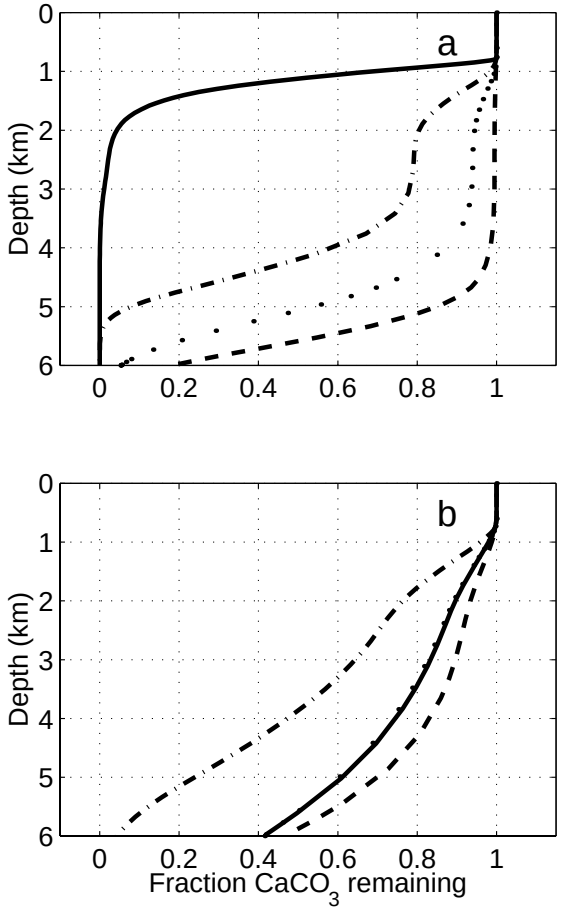

Figure 2.8: Dissolution of (a) calcite and (b) aragonite shells in the North Pacific. Parameter values as given in Table 2.2. Calcite: Solid line: $(\kappa, \eta) = (0.38, 1)$, dash-dotted: $(\kappa, \eta) = (5, 3)$, dotted: $(\kappa, \eta) = (1, 2.9)$, dashed: $(\kappa, \eta) = (5, 4.5)$. Aragonite: Solid line: $(\kappa, \eta) = (1.3, 3.1)$, dash-dotted: $(\kappa, \eta) = (13.2, 4.2)$, dotted: $(\kappa, \eta) = (1.1, 2.93)$, dashed: $(\kappa, \eta) = (3.18, 4.2)$.

2.2 A model of respiration driven dissolution

Marine snow aggregates provide an important pathway of transport of biogenic matter from the surface to the ocean interior [*Shanks and Trent*, 1980; *Alldredge and Silver*, 1988; *Alldredge and Gotschalk*, 1988; *Diercks and Asper*, 1997]. Phytoplankton, faecal pellets and organic debris collide by differential settlement and collision in shear flow, and stick together with a finite probability, forming macroaggregates sized up to the order of millimeters. As the organic matter inside a marine snow aggregate is respired, a microenvironment might form with locally enhanced CO_2 concentration, resulting in decreased CO_3^{2-} concentration. In this way, carbonate dissolution well above the saturation horizon might be possible. This section presents a model of a marine snow aggregate and the processes inside to estimate the potential of CO_2 respiration through organic matter remineralization on calcite dissolution.

2.2.1 Model description

The aggregate is modelled as an idealized porous sphere consisting of water, organic carbon and calcite. Initial data are the C_{org} content given in $\mu g\, C$, the calcite content ($\mu g\, CaCO_3$) and the porosity. The volume of the aggregate is then calculated as

$$v_a = \frac{v_c + v_{cal}}{1 - \phi}, \tag{2.5}$$

where ϕ is the porosity and v_c, v_{cal} (m^3) are the volumes of the organic carbon and calcite content, respectively, which are derived from mass via the specific densities. The standard value for the porosity is $\phi = 0.9$, following in-situ observations by *Alldredge and Gotschalk* [1988]. The settling velocity V $(m\, d^{-1})$ is calculated via the parameterization by *Alldredge and Gotschalk* [1988], who observed settling velocities of marine snow aggregates to be less than those of an equivalent spherical particle settling according to Stokes' law:

$$V = 50\, d_a^{0.26}, \tag{2.6}$$

where $d_a = 2r_a$ (mm) is the diameter of the aggregate.

The CO_2 produced by organic matter respiration is assumed to be released at the spherical surface of the aggregate. Dissolution via chemical alteration of the microenvironment requires the establishment of a stable diffusive boundary layer around the sinking particle, for which the aggregate radius and the sinking velocity are crucial. The concentration of a dissolved species (i.e. CO_2, CO_3^{2-}, NO_3^- or O_2) at the aggregate surface may be calculated using the relation [*Ploug et al.*, 1999]

$$Q = 4\,\pi\, r_a^2\, D\, \frac{C_\infty - C_a}{\delta_{eff}}, \tag{2.7}$$

where Q $(mol\, s^{-1})$ is the area-integrated flux of the dissolved species in question out of the aggregate and D $(m^2\, s^{-1})$ is the appropriate diffusion coefficient. C_∞, C_a, $(mol\, m^{-3})$ are the concentration of the species in the bulk medium and at the aggregate surface, respectively, and δ_{eff} (m) is the effective

thickness of the diffusive boundary layer. Due to shear, the latter decreases with increasing settling velocity. The relative increase of advection compared to diffusivity is described by the Sherwood number *Sh* [*Sherwood et al.*, 1975]:

$$\mathrm{Sh} = \frac{r_a}{\delta_{\mathrm{eff}}} \tag{2.8}$$

In a stagnant fluid, $Sh = 1$ and thus, $r_a = \delta_{\mathrm{eff}}$. The Sherwood number varies with both the Reynolds number *Re* and the Peclet number *Pe*:

$$\begin{aligned} \mathrm{Re} &= \frac{V\, r_a}{\nu}, \\ \mathrm{Pe} &= \frac{V\, r_a}{D}, \end{aligned} \tag{2.9}$$

where ν is the kinematic viscosity of sea water ($\sim 0.7 \times 10^{-6}\,\mathrm{m^2\,s^{-1}}$).

Parameterizations of the Sherwood number are given by *Karp-Boss et al.* [1996]:

$$\mathrm{Sh} = \begin{cases} 1 + 0.29(\mathrm{Pe})^{1/2}; & \mathrm{Re} \ll 1,\ \mathrm{Pe} < 0.01, \\ 1.014 + 0.15(\mathrm{Pe})^{1/2}; & \mathrm{Re} \ll 1,\ 0.01 < \mathrm{Pe} < 100, \\ 0.55(\mathrm{Pe})^{1/3}; & \mathrm{Re} < 1,\ \mathrm{Pe} > 100. \end{cases} \tag{2.10}$$

Solving Eq. (2.7) for C_a and using Eq. (2.8) yields

$$C_a = C_\infty - \frac{Q}{4\,\pi\, r_a\, D\, \mathrm{Sh}}. \tag{2.11}$$

Applying Eq. (2.11), one can calculate $\sum CO_2$ and alkalinity concentrations at the aggregate surface, considering the fluxes deriving from remineralization of organic matter and dissolution of carbonate. From $\sum CO_2$ and alkalinity, $[CO_3^{2-}]$ is derived via the carbonate dissociation constants from *DOE* [1994] and pressure corrections by *Culberson and Pytkowicz* [1968].

In the case of undersaturation, calcite is dissolved as described in the previous section (Eq. (2.1), Table 2.1). Organic carbon is remineralized according to first order kinetics:

$$\frac{dC_{org}}{dt} = -\lambda\, C_{org}(t), \tag{2.12}$$

where $\lambda\,(\mathrm{d^{-1}})$ is the remineralization rate constant, i.e. $1/\lambda$ gives the e-folding time. Respiration of one mole organic carbon consumes $r_{O/C}$ moles oxygen, where $r_{O/C}$ is the Redfield ratio of oxygen to carbon (cf. Table 1.1). Using Eq. (2.11) and bulk oxygen concentrations from GEOSECS data *Takahashi et al.* [1981], the maximal amount of C_{org} is calculated that may be oxidized in one time step avoiding oxygen depletion.

The numerical implementation of the model is as follows. Initial conditions are the content of calcite and organic carbon. The radius of the aggregate and initial settling velocity are computed. The time step is set to a quarter of a day. At each time step, first the Sherwood numbers are computed from the radius and settling velocity. Then, the fluxes of CO_2 and NO_3^- are derived from the remineralization of organic matter. In the case of undersaturation, the flux of CO_3^{2-} is calculated. From these fluxes and the bulk chemistry, $\sum CO_2$ and TA at the aggregate surface are

derived according to Eq. (2.11), setting the new value for calcite saturation. The radius of the aggregate is decreased according to the amount of organic matter respired and calcite dissolved in the present time step while keeping porosity constant. Then, the new settling velocity and depth is computed. This scheme is iterated until the aggregate has reached the seafloor at a prescribed depth.

2.2.2 Parameter values

The model's parameter values are given in Table 2.3. Experimentally derived parameterizations of the calcite dissolution kinetic are discussed in Appendix A. *Westrich and Berner* [1984] give a compilation of experimentally determined first-order decay constants for oxic organic matter decomposition. The e-folding time varies between 11 and 122 days with a mean of 32 days. *Walsh et al.* [1988] find an average e-folding time of 38 days in sediment traps deployed in three North Pacific stations. Experimentally, *Westrich and Berner* [1984] derive e-folding times of 15 days for oxic decomposition, this value has been used for the model runs.

Symbol	Parameter	Value	Reference
ϕ	Porosity	0.9	Alldredge and Gotschalk [1988]
	C_{org} content	$0 - 15\,\mu g\,C$	cf. Table 2.4
	Calcite content	$0 - 3\,\mu g$	Beers et al. [1986], Tyrrell and Taylor [1996]
	Density calcite	$2.7\,g\,cm^{-3}$	Young [1994]
	Density C_{org}	$1.07\,g\,cm^{-3}$	Young [1994]
κ	Calcite dissolution rate constant	$5\,d^{-1}$	Keir [1980]
η	Calcite dissolution rate order	4.5	Keir [1980]
λ	C_{org} respiration time constant	$1/15\,d^{-1}$	Westrich and Berner [1984]
$r_{O/C}$	Redfield ratio oxygen to carbon	170/117	Anderson and Sarmiento [1994]

Table 2.3: Parameter values.

The aggregate's calcite content is considered to be *E. huxleyi* cells. In a field study of two *E. huxleyi* blooms in the Gulf of Maine, *Balch et al.* [1991] find 25-100 and 100-400 coccoliths per cell, respectively. *Fernández et al.* [1993] point out that numbers are much lower in open ocean blooms, as they find 20-40 coccoliths per cell in an *E. huxleyi* bloom in the northeast Atlantic Ocean. *Tyrrell and Taylor* [1996] state that 10-50 coccoliths per cell are typical with one coccolith containing

1.7-8.3 pg calcite. *Trent* [1985] and *Beers et al.* [1986] observed coccolithophorid cell numbers per aggregate ranging between 180 and 870. Assuming 30 cells per coccolith, 5 pg calcite per coccolith and 1000 cells per aggregate yields 0.15 μg calcite ($\hat{=} 1.5 \times 10^{-3}$ μg C). There are hints that at the end of the bloom, when marine snow aggregates are formed, the coccolithophorids are more heavily plated [*Balch et al.*, 1991]. Adopting 100 cells per coccolith and 5000 cells per aggregate gives 2.5 μg calcite content at the upper end of the range.

The organic carbon content of marine snow aggregates generally ranges from 0.1 μg C to 12 μg C, but may be as high as 220 μg C (Table 2.4). The calculations presented here adopt values of $1 - 15$ μg C per aggregate. It has to be stressed that there is no functional relationship between organic carbon content and the number of cells of calcareous organisms contained in the marine snow particle.

Reference	POC	Time, Location
Alldredge [1976]	6.90	July-Aug, Gulf of California
Alldredge [1979]	3.37	July-Aug, Gulf of California
Alldredge [1979]	4.32	Oct-March, Santa Barbara Channel
Shanks and Trent [1980]	1.36	June-July, Monterey Bay
Hebel [1983]	3.21	June, Pt. Sur
Hebel [1983]	1.23	June, Monterey Bay
Prezelin and Alldredge [1983]	0.1	April, Santa Barbara Channel
Prezelin and Alldredge [1983]	0.71	July, N. E. Atlantic
Alldredge and Gotschalk [1988]	0.4-222[a]	March-July, San Pedro Basin, Santa Barbara Channel
Alldredge and Gotschalk [1989]	12.3[a]	Feb-Sep, Santa Barbara Basin, California Current
Ploug et al. [1999]	3.87-7.77	June, Catalina Island

[a] Calculated via dry weight assuming that marine snow particles are approximately 20% carbon.

Table 2.4: Organic carbon content of marine snow aggregates (μg C agg^{-1}).

2.2.3 Model runs

In order to investigate the capacity of respiration driven dissolution, a number of model runs are performed (Table 2.5).

C_{org} (μg C)	$CaCO_3$ (μg)	(κ, η) (d^{-1}, $-$)	ϕ	Ocean basin	Results
15	0.15	(5,4.5)	0.9	North Pacific	Fig. 2.9, 2.10
15	0.15	(5,3)	0.9	North Pacific	Fig. 2.11
0-15	0.15	varied	0.9	North Pacific	Table 2.6
0-15	2.5	varied	0.9	North Pacific	Table 2.7
5-15	1	(5,4.5)	0.1-0.9	Eq. and North Pacific	Fig. 2.12
10	1	(5,4.5)	0.3	North Pacific	Fig. 2.13, 2.14
15	1	(5,4.5)	0.1	Eq. Pacific	Fig. 2.15

Table 2.5: Initial conditions and parameter settings of model runs.

Fig. 2.9 and 2.10 show results of a model run with GEOSECS data of the North Pacific [*Takahashi et al.*, 1981] determining the bulk carbonate system. A marine snow aggregate is considered consisting of 15 μg C_{org} and 1000 *E. huxleyi* cells, with 0.15 μg calcite. The initial diameter (Fig. 2.10(b)) is 1.75 mm, which lies in the range of marine snow aggregates observed by *Alldredge and Gotschalk* [1988]. The settling velocity is initially 58 m d^{-1} and decreases down to 42 m d^{-1} (Fig. 2.10(a)). The Sherwood numbers decrease from 4-5 down to 2-3. This results in the diffusive boundary layer thickness ranging between 35 μm and 200 μm, which conforms to *Alldredge and Cohen* [1987], who measured chemical boundary layers hundreds of micrometer thick in marine snow aggregates in a flow tank simulating advective forces as they appear when the aggregate is settling through the water column. Respiration of the organic matter increases $[CO_2]$ at the aggregate surface over the bulk concentration ($\sim$ 52 μmol kg^{-1} at that point) by maximally 7 μmol kg^{-1} (Fig. 2.9(a)), which lowers the calcite saturation, as is visible in Fig. 2.9(c). However, due to rather fast settling velocities and slow dissolution kinetics, this does not have a significant effect on calcite dissolution. In 3 km depth, nearly all organic matter has been respired, so the amount of calcite dissolution at this depth is a good measure for dissolution attributable to respiration effects. Here, a mere 0.8% of the calcite content is dissolved, in contrast to 0.03% in the absence of organic matter remineralization.

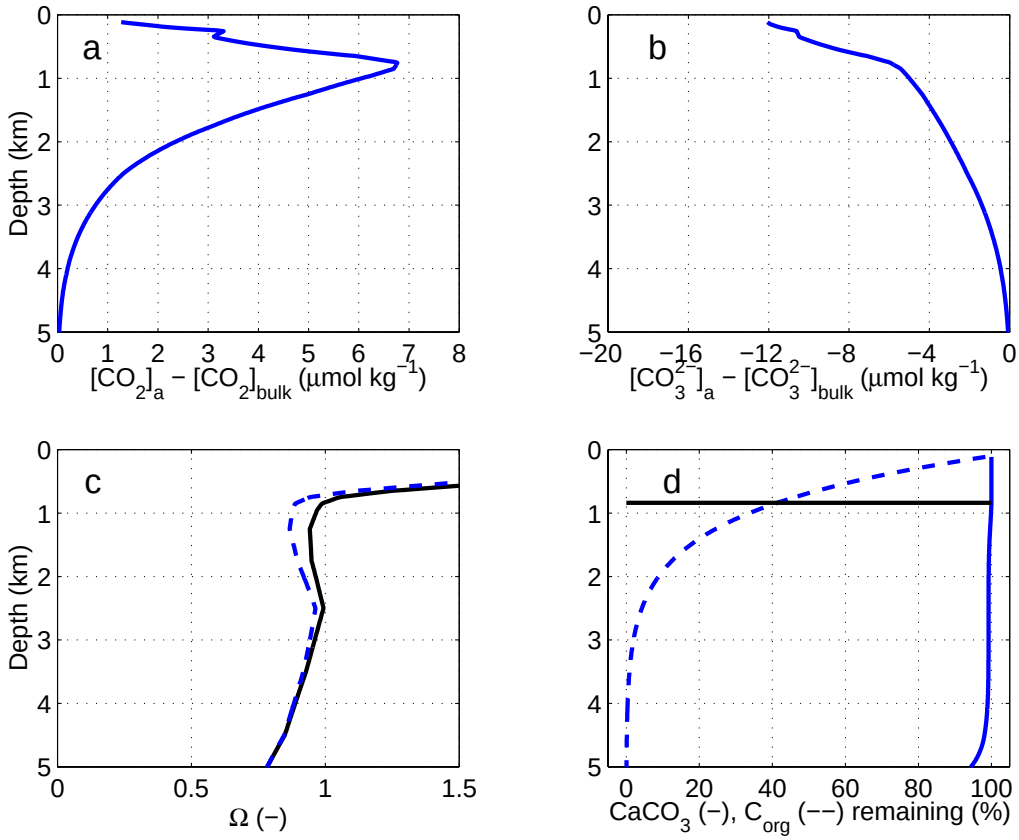

Figure 2.9: Respiration driven dissolution in the North Pacific. Aggregate of 0.15 μg calcite (1,000 *E. huxleyi* cells) and initial organic carbon content of 15 μg C_{org}. (a,b) CO_2 and CO_3^{2-} difference between aggregate surface and bulk sea water. (c) Calcite saturation (bulk value solid, aggregate value dashed) (d) C_{org} (dashed), $CaCO_3$ (solid) remaining in the aggregate. The depth of the bulk saturation horizon at ~ 0.8 km is marked by a straight line.

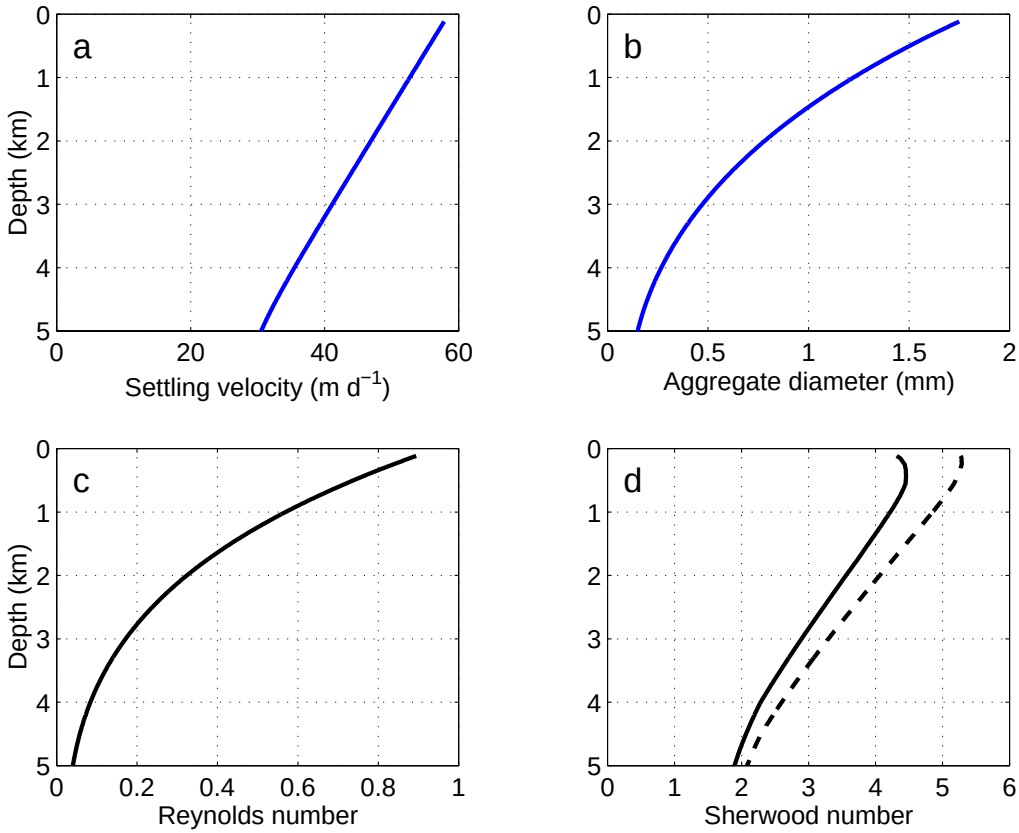

Figure 2.10: Respiration driven dissolution in the North Pacific. Aggregate of 0.15 μg calcite (1,000 *E. huxleyi* cells) and initial organic carbon content of 15 μg C_{org}. (a) Settling velocity decreases as the aggregate gets smaller due to C_{org} remineralization. (b) Aggregate diameter. (c) Reynolds number. (d) Sherwood numbers (solid line: CO_2, dashed line: CO_3^{2-}).

The model is then tested for different dissolution kinetics proposed in the literature (cf. Table 2.2 on page 30). As *Keir* [1980] is the only work specifically dealing with coccoliths (cf. Table A.1), it is assumed to be the most adequate kinetic for the present model. However, other results should not be excluded, e.g. the work of *Walter and Morse* [1985] deals with low-Mg calcite, which is attributable to coccoliths. At 3 km depth, no calcite dissolution is evident in the Equatorial Pacific, no matter what kinetic parameters are chosen. Fig. 2.11 shows the same model run as Fig. 2.9 but with dissolution kinetics proposed by *Morse* [1978] ($\kappa = 5\,\mathrm{d}^{-1}$, $\eta = 3$). In this case, 19% of the initial calcite content are dissolved in 3 km depth, compared to 3% without organic matter remineralization. Table 2.6 displays results varying the amount of organic matter in the aggregate. Inclusion of organic carbon always enhances the amount of calcite dissolved. In case (C), $\kappa = 5\,\mathrm{d}^{-1}$ and $\eta = 3$, the influence of respiration is significant. In the case of linear kinetics (D), $\kappa = 0.38\,\mathrm{d}^{-1}$ and $\eta = 1$, calcite dissolution is so fast that the addition of C_{org} has less effect on the amount of calcite dissolved. Note that with $1\,\mu\mathrm{g}\,C_{org}$, less calcite is dissolved than without addition of organic matter. This is due to the fact that C_{org}, due to its low density ($1.07\,\mathrm{g\,cm}^{-3}$) strongly increases the diameter of the aggregate and hence its sinking speed. In this case, initial settling velocity is $46\,\mathrm{m\,d}^{-1}$ with and $28\,\mathrm{m\,d}^{-1}$ without organic matter. As with linear kinetics the dissolution is so strong even in near-equilibrium situations, the settling velocity is more important than the magnitude of undersaturation.

C_{org} (μg C)	calcite dissolved (%)			
	A	B	C	D
	$(\kappa,\eta) = (5, 4.5)$	$(\kappa,\eta) = (1, 2.9)$	$(\kappa,\eta) = (5, 3)$	$(\kappa,\eta) = (0.38, 1)$
0	0.0	0.7	2.7	64.6
1	0.1	1.0	3.8	63.0
2	0.1	1.3	4.8	64.8
5	0.2	2.1	7.9	69.3
10	0.4	3.5	13.2	74.6
15	0.8	5.0	18.7	78.3

Table 2.6: Model results using different dissolution kinetics. Displayed is the fraction of calcite dissolved at 3 km depth (North Pacific) depending on the organic carbon content. *Keir* [1980]: $(\kappa,\eta) = (5, 4.5)$, *Walter* [1985]: $(\kappa,\eta) = (1, 2.9)$, *Morse* [1978]: $(\kappa,\eta) = (5, 3)$, *Hales and Emerson* [1997]: $(\kappa,\eta) = (0.38, 1)$.

Table 2.7 shows model results for the same model run as in Table 2.6 but with $2.5\,\mu$g calcite content. Note that a given dissolution rate dissolves a certain fraction of the calcite present over some time interval, not a certain amount of calcite (cf. Eq. (2.1)). In principal, when doubling the amount of calcite present, mass dissolution is expected to double, too. Only when the release of carbonate ions from dissolution significantly perturbs the carbonate system towards a more saturated state is the amount of calcite present relevant for the fraction dissolving per time interval. So incorporating

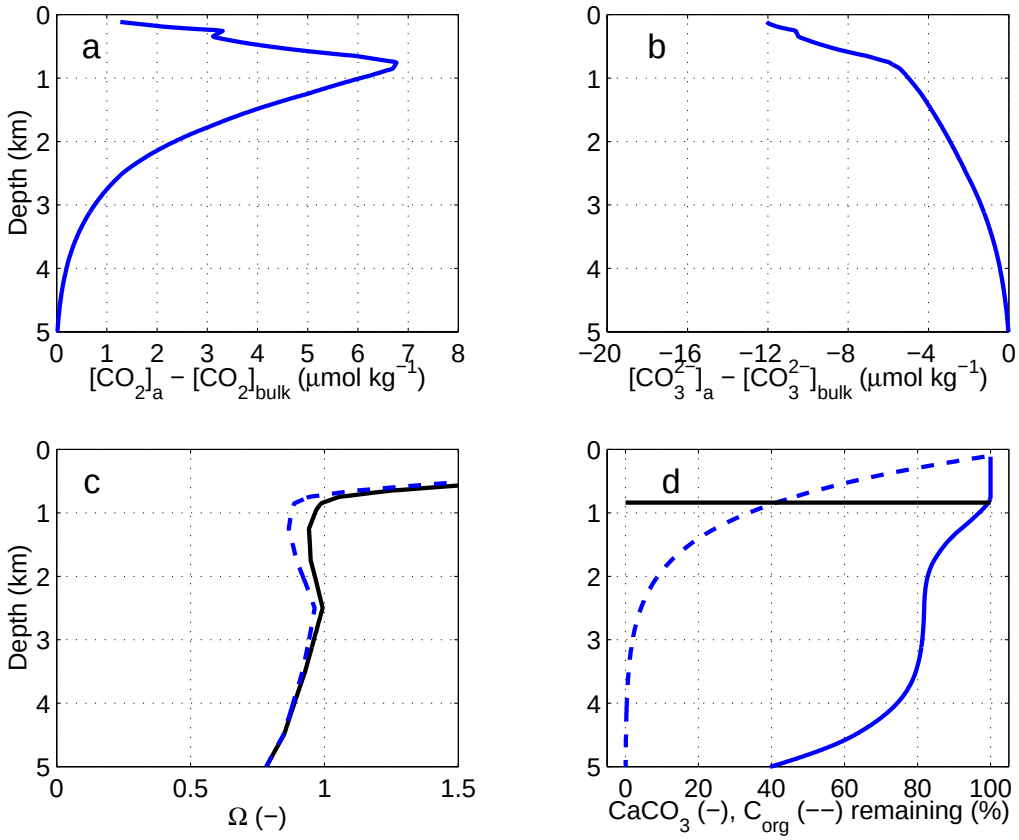

Figure 2.11: Respiration driven dissolution in the North Pacific. Aggregate of $0.15\mu g$ calcite (1,000 *E. huxleyi* cells) and initial organic carbon content of $15\,\mu g\,C$. Dissolution kinetic parameters set to ($\kappa = 5d^{-1}\,\eta = 3$). (a,b) CO_2 and CO_3^{2-} gradient between aggregate surface and bulk sea water. (c) Calcite saturation (bulk value solid, aggregate value dashed) (d) C_{org} (solid), $CaCO_3$ (dashed, without organic matter remineralization dash-dotted) remaining in the aggregate. The depth of the bulk saturation horizon at $\sim 0.8\,km$ is marked with a straight line.

more calcite into the aggregate should not lead to less dissolution fractionwise simply because there is more calcite present but because more calcite should make the aggregate larger and settle faster. However, the fraction dissolved in 3 km depth does not differ significantly from the model results displayed in Table 2.6 except for linear kinetics. This is due to the fact that calcite, with its large density ($2.7\,g\,cm^{-3}$) does not influence the radius and hence the settling velocity of the aggregate significantly. This might be a drawback of the model formulation. However, other estimates on marine snow settling velocities (Table B.3) conform to the settling velocities calculated by the present model, though they are a bit higher, as most aggregates investigated are between 1 mm and 10 mm in diameter, and the aggregate sizes modelled here are on the lower end of this range. The marine snow particles investigated by *Alldredge and Gotschalk* [1988] to derive the formulation (2.6) partly contained diatoms or faecal pellets, which are comparable in density with calcite.

C_{org} (μmol C)	calcite dissolved (%) A $(\kappa,\eta)=(5,4.5)$	B $(\kappa,\eta)=(1,2.9)$	C $(\kappa,\eta)=(5,3)$	D $(\kappa,\eta)=(0.38,1)$
0	0.02	0.6	2.0	47.9
1	0.05	0.9	3.3	55.9
2	0.08	1.2	4.4	59.8
5	0.2	2.0	7.5	66.8
10	0.4	3.4	12.8	73.2
15	0.8	4.9	18.2	77.3

Table 2.7: Model results using different dissolution kinetics. Same model run as displayed in Table 2.6 but with 2.5 μg calcite.

It is now investigated what parameter variations would yield an aggregate that exhibits significant calcite dissolution. The main reason for the low effectiveness of respiration driven dissolution is the porosity of the aggregate. High porosities lead to large diameters. Given a constant flux of e.g. CO_2, the concentration gradient between the aggregate surface and the bulk medium decreases with increasing radius. Thus, larger diameters at constant source strength Q are unfavourable for creating locally undersaturated chemical environments. To overcome these disadvantages with respect to calcite dissolution, the aggregate has to be loaded with large amounts of organic matter, which in turn increases the radius drastically due to the low density of C_{org}. This makes the aggregate settling faster, according to Eq. (2.6). The effect of a high settling velocity is twofold. It reduces the time the aggregate spents in undersaturation, and it decreases the thickness of the boundary layer, which in turn decreases the concentration gradient as can be seen from Eq. (2.8)-(2.11). In order to quantify these relationships, the model is run with variable porosity. Results are illustrated in Fig. 2.12. Respiration driven dissolution is significant in the North Pacific provided $\phi \leq 0.4$ and in the Equatorial Pacific when $\phi \leq 0.2$. However, these results may be overestimations since the settling velocity parameterization (Eq. (2.6)) has been derived with aggregates having porosity $\phi \geq 0.9$. Aggregates with smaller porosity are expected to settle faster because the density increases with decreasing porosity. Stokes' law is not valid for the model's parameter range in Fig. 2.12 since its application leads to Reynolds numbers larger than one.

A specific model run with $\phi = 0.3$ and 10 μg C organic carbon is shown in Fig. 2.13. Between 1 km and 2 km depth, 30% of the calcite content are dissolved due to organic matter respiration. Then, the organic matter has vanished, and calcite dissolution ceases until at $\sim$ 4.5 km depth, bulk undersaturation is strong enough to trigger some more dissolution. The gradients in $[CO_2]$ and $[CO_3^{2-}]$ (Fig. 2.13(a,b)) are much larger than with porosity 0.9 (compare Fig. 2.9). The kink at 1 km is due to reduced organic matter remineralization as a consequence of oxygen deficiency, which is illustrated in Fig. 2.14. Decreasing the porosity reduces the diffusive fluxes and the aggregate diameter, which enhances the oxygen concentration gradient. Oxygen deficiency appears with 5, 10 and 15 μg C_{org}

when $\phi \leq 0.3$, 0.5, and 0.625, respectively. Fig. 2.15 shows model results with $\phi = 0.1$ and 15 μg C organic carbon in the Eq. Pacific. With such a low porosity and large amount of organich carbon, significant dissolution of calcium carbonate above the saturation horizon is possible.

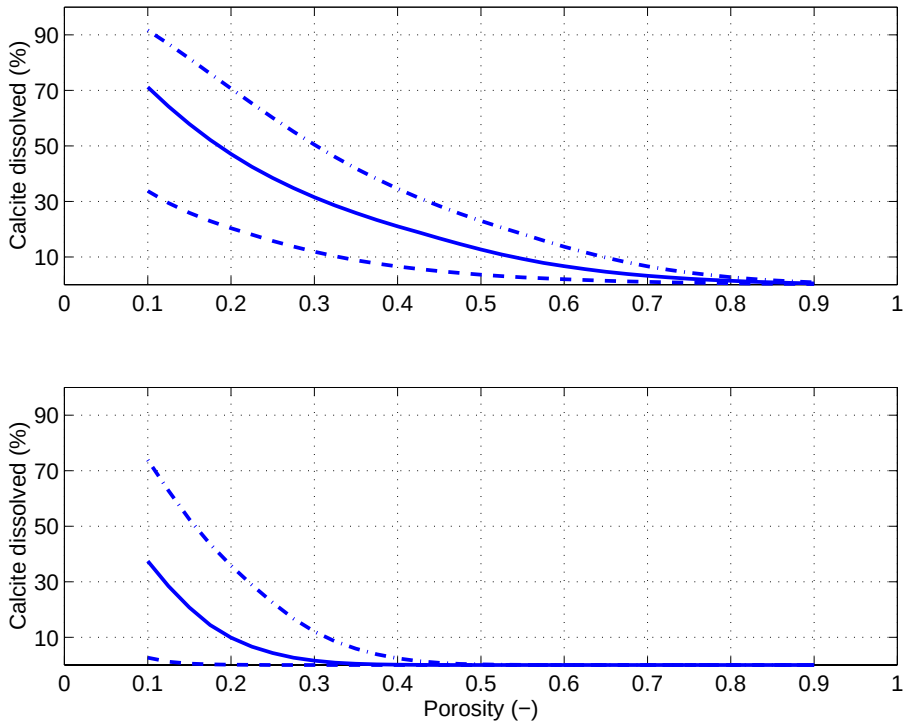

Figure 2.12: Dependency of respiration driven dissolution at 3 km depth on the porosity of the aggregate. North Pacific (top) and Equatorial Pacific (bottom) setting. Organic carbon content is 5 μg C (dashed line), 10 μg C (solid line) and 15 μg C (dash-dotted line).

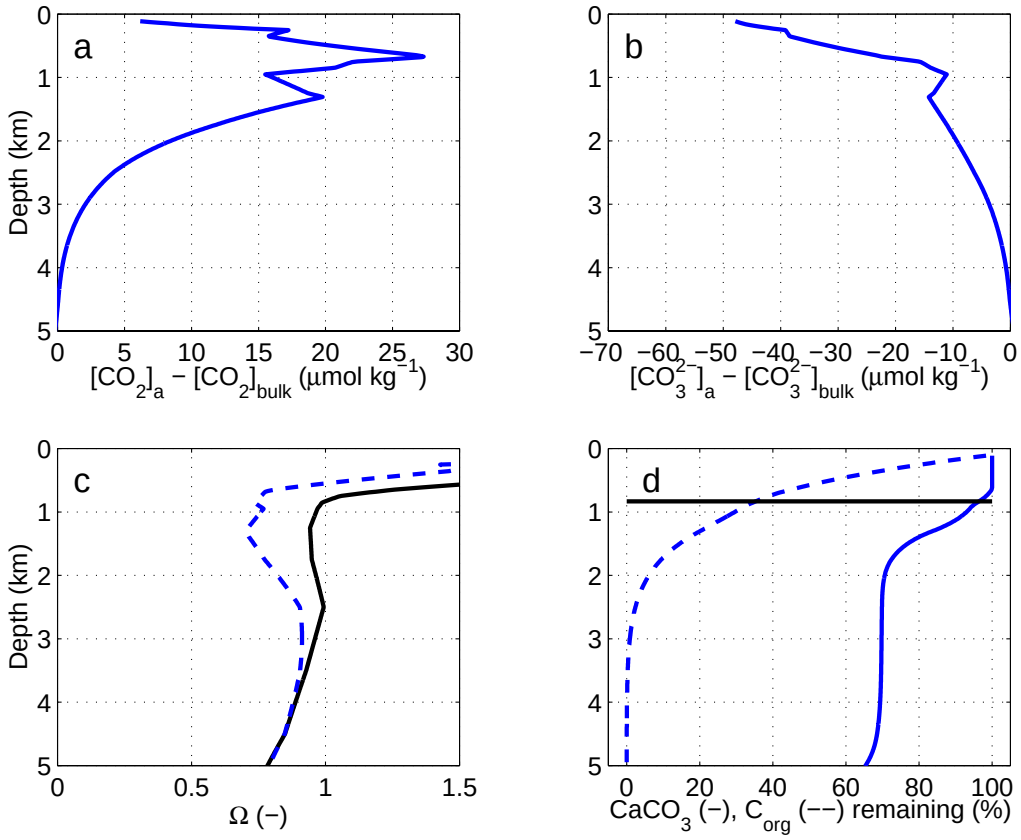

Figure 2.13: Respiration driven dissolution in the North Pacific. Aggregate of 1 μg calcite and initial organic carbon content of 10 μg C. Porosity is set to $\phi = 0.3$. (a,b) CO_2 and CO_3^{2-} gradient between aggregate surface and bulk sea water. (c) Calcite saturation (bulk value solid, aggregate value dashed) (d) C_{org} (solid), $CaCO_3$ (dashed, without organic matter remineralization dash-dotted) remaining in the aggregate. The depth of the bulk saturation horizon at ~ 0.8 km is marked with a straight line.

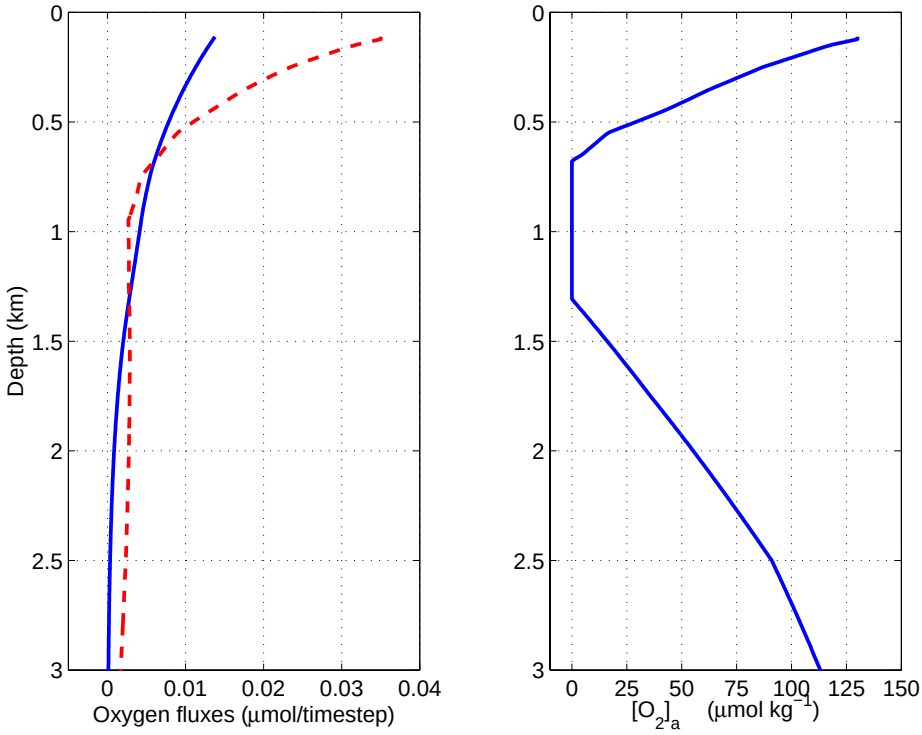

Figure 2.14: Left: Oxygen remineralization flux (solid) and maximal flux possible to prevent oxygen deficiency. Around 1 km depth, the remineralization flux is reduced. Right: Oxygen concentration at the aggregate surface.

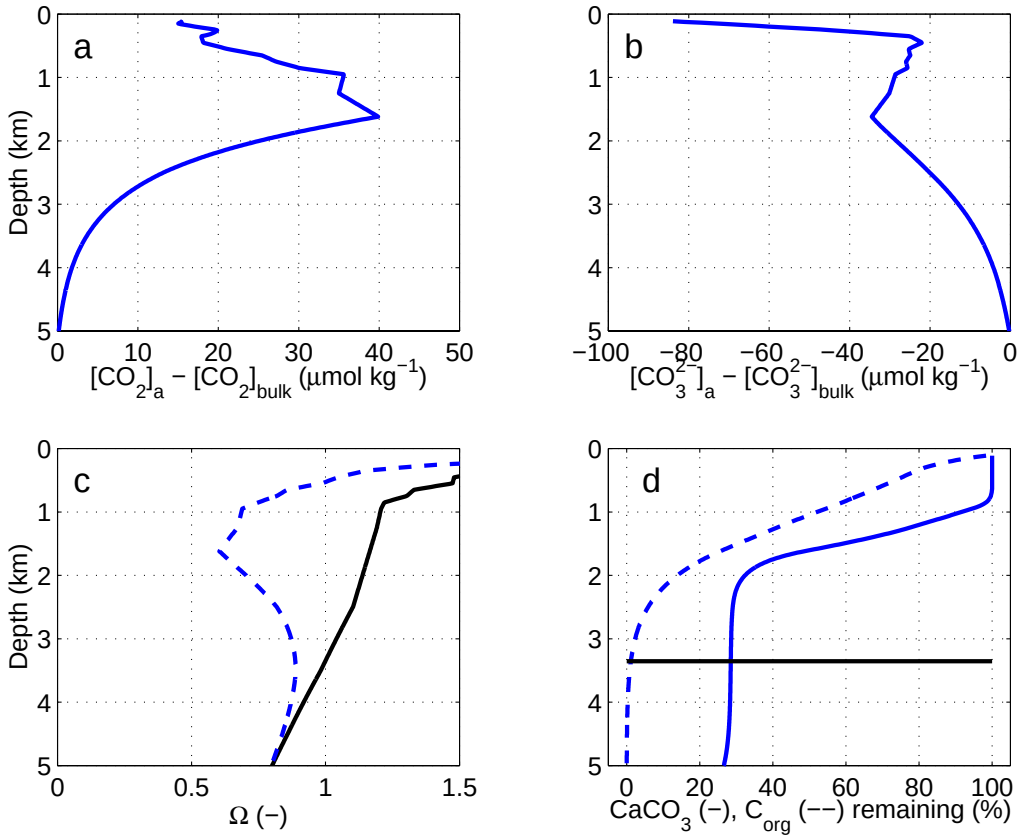

Figure 2.15: Respiration driven dissolution in the Equatorial Pacific. Aggregate of 1 μg calcite and initial organic carbon content of 15 μg C. Porosity is set to $\phi = 0.1$ (a,b) CO_2 and CO_3^{2-} gradient between aggregate surface and bulk sea water. (c) Calcite saturation (bulk value solid, aggregate value dashed) (d) C_{org} (solid), $CaCO_3$ (dashed, without organic matter remineralization dash-dotted) remaining in the aggregate. The depth of the bulk saturation horizon at ~ 0.8 km is marked with a straight line.

Chapter 3

Carbonate dissolution in zooplankton guts

Another process that may contribute to the proposed loss of calcium carbonate in the water column is the dissolution of $CaCO_3$ in zooplankton guts. The guts of e.g. copepods can be sufficiently acidic to cause carbonate dissolution. Calanoid copepods (Fig. 3.1) are present in all marine environments and usually make up 70% by mass or more of all net-collected zooplankton [*Lalli and Parsons*, 1993, page 88]. Evidence for copepod grazing on *Emiliania huxleyi* is given by *Van der Wal et al.* [1995], who observed large amounts of coccoliths in copepod faecal pellets. In a recent study of Arabian Sea copepods, thin sections of the guts of 17 specimens of the genus Spinocalanus contained 10-30% coccoliths [*M. Gowing*, pers. comm., 2000].

Figure 3.1: Calanoid copepod, approximately 2 mm in length. The picture is taken from http://www.pbrc.hawaii.edu/ petra/aetideopsis.html.

It has been proposed that copepods are able to regulate gut *p*H to enhance enzymatic activity [*Mayzaud and Mayzaud*, 1981]. The optimal *p*H for a variety of copepod digestive enzymes ranges from 4 to 9 [*Mayzaud*, 1986]. With decreasing *p*H the carbonate system is increasingly undersaturated with respect to calcite. *Pond et al.* [1995] measured *p*H values in guts of starved individuals of *Calanus helgolandicus* between 6.9 and 7.2, whereas the gut *p*H of copepods of the same species feeding on coccolithophorids ranged from 8.0 to 8.2. To the author's knowledge, no other measurements on copepod gut *p*H are available.

Modelling work on carbonate dissolution in zooplankton guts has hitherto not been persued. Field work has provided contrary evidence for carbonate dissolution in zooplankton guts, as faecal pellets contain unbroken coccoliths which show no sign of dissolution [*Honjo and Roman*, 1978; *Bathmann et al.*, 1987]. *Van der Wal et al.* [1995], however, in a study of an *E. huxleyi* bloom between the Shetland Islands and Norway, found copepod faecal pellets that almost exclusively contained fragmented coccoliths.

3.1 Model description

The proposed model assumes the copepod gut to be one box with influx and efflux. It features $CaCO_3$ content (C, μmol) and alkalinity (A, μmol kg^{-1}) as independent variables. The model is in line with *Penry and Jumars* [1986] and *Jumars and Penry* [1989], who propose to view guts as chemical reactors. In their classification, the model considers a continuous-flow, stirred tank reactor (CSTR), which incorporates constant flow of material through the gut and complete mixing within it. *p*H is set to a fixed value, and together with alkalinity determines the carbonate system [*Millero*, 1995], i.e. dissolved inorganic carbon ($\sum CO_2$) and $[CO_3^{2-}]$, the latter being ultimately responsible for the saturation state with respect to calcite. For this, the dissociation constants given by *DOE* [1994] have been used. The model's equations are as follows.

$$\begin{aligned} \frac{dC(t)}{dt} &= I - (f(t) + K)\, C(t), \\ \frac{dA(t)}{dt} &= K\, A_{bulk} - K\, A(t) + 2\, \frac{f(t)\, C(t)}{10^3 V(t)}, \end{aligned} \tag{3.1}$$

where $I\,(\mu\text{mol C min}^{-1})$ denotes the ingestion rate of calcite, $K\,(\text{min}^{-1})$ is the gut clearance rate and $f(t)\,(\text{min}^{-1})$ is the fraction of carbonate dissolving per minute at time t. The alkalinity of bulk seawater is denoted by A_{bulk}. The gut volume is denoted by $V(t)\,(\text{m}^3)$, where the effective volume is considered, i.e. total gut volume minus particulate contents. Dissolution of $CaCO_3$ depends on the possible undersaturation with respect to calcite in the gut via

$$f(t) = \begin{cases} \kappa\, (1 - \Omega(t))^{\eta} & \text{if } \Omega(t) < 1, \\ 0 & \text{if } \Omega(t) \geq 1, \end{cases} \tag{3.2}$$

where $\kappa\,(\text{min}^{-1})$ is the dissolution rate constant and η is the dissolution rate order. The saturation state is given by the quotient of $[CO_3^{2-}]$ in the gut and the critical carbonate concentration, $[CO_3^{2-}]_c$,

the latter being depth dependent due to pressure effects:

$$\Omega(t) = \frac{[CO_3^{2-}](t)}{[CO_3^{2-}]_c}. \tag{3.3}$$

Standard values for the parameters are given in Table 3.1.

Parameter (Symbol)	Range	Standard Value	Reference
Ingestion rate C_{org}	$0 - 50\,\mu g\,C\,d^{-1}$	$5\,\mu g\,C\,d^{-1}$	Båmstedt et al. [1999]
Ingestion rate $CaCO_3$ (I)	$0 - 5\,\mu g\,C\,d^{-1}$	$0.5\,\mu g\,C\,d^{-1}$	Nejstgaard et al. [1994] Huskin et al. [2000]
Gut passage time (K^{-1})	$12 - 85$ min	30 min	Irigoien [1998], Dam and Peterson [1988]
Gut volume (V)	$1 - 8\times10^{-9}$ l [a]	7×10^{-9} l	Harris [1994]
$CaCO_3$ dissolution rate constant (κ)	$3 - 7\,d^{-1}$	$5\,d^{-1}$	Keir [1980]
$CaCO_3$ dissolution rate order (η)	1-5	4.5	Keir [1980]
Critical carbonate concentration ($[CO_3^{2-}]_c$)		42.7 μmol kg^{-1} [b]	Millero [1995]
Bulk sea water DIC		2000 μmol kg^{-1} [c]	Takahashi et al. [1981]
Bulk sea water alkalinity		2300 μmol kg^{-1} [c]	Takahashi et al. [1981]

[a] calculated from faecal pellet volume data.
Gut volume $\sim$ 5 times faecal pellet volume [*U. Bathman*, pers. comm., 1999].
[b] Surface ocean value (100 m depth).
[c] North Atlantic value at 100 m depth.

Table 3.1: Parameters of the zooplankton gut model.

As observations of ingestion rates of organic carbon are much more abundant than uptake rates for calcite particles, a certain fraction of C_{org} uptake is assumed to be calcite ingestion. In feeding experiments, *Harris* [1994] has observed that the uptake of $CaCO_3$ amounts to 35-40% of organic carbon ingested. A lower value of 10% is considered, reflecting that in the field the food supply is very heterogeneous and copepods take up more organic carbon via non-calcareous phytoplankton than in culture experiments where they are deliberately fed with coccolithophorids. The calculated ingestion rates of calcite conform to those found by *Huskin et al.* [2000] (considering *Calanus helgolandicus*), they report an ingestion rate of 0.2 μg calcite C ind.$^{-1}$ d^{-1}. In a mesocosm study, *Nejstgaard et al.* [1994] analyzed grazing of *Calanus finmarchicus* on an *E. huxleyi* bloom. In the pre-bloom situation with low prey concentrations, they calculated an uptake of 0.26 μg calcite C ind.$^{-1}$ d^{-1}, which increased to 3 μg calcite C ind.$^{-1}$ d^{-1} during the bloom.

3.2 Model runs

The first approach is to assume constant grazing with a gut passage time of 30 min [*Irigoien*, 1998]. Standard parameters (Table 3.1) are considered and *p*H is varied from 5 to 8. The fraction of calcite dissolved is calculated as the difference between uptake and egestion. Calculations yield no dissolution for *p*H $\geq$ 7.5. The maximal amount of $CaCO_3$ dissolved is $\sim 6\%$ at *p*H 5. Thus, with the approach of constant grazing, no significant dissolution is evident. This may be explained by the short gut passage time compared to the rather slow dissolution kinetics (Fig. 3.2). Due to the very small volume of the gut, dissolution of $CaCO_3$ massively perturbs the carbonate system, removing any undersaturation very fast, which works against significant dissolution. This effect is not considered in Fig. 3.2, thus it illustrates an ideal upper limit of the amount of calcite that may be dissolved in 30 min.

Next, the effect of alternating grazing and non-grazing is tested. In this scenario, ingested calcite may be also dissolved during the longer non-grazing interval, when the calcite stock is not replenished. Various combinations of grazing / non-grazing cycles are tested, considering short gut passage times during grazing (K_g^{-1} = 30 min) and long passage times during non-grazing intervals (K_n^{-1} = min {length of non-grazing time, 4 hours}). *Atkinson et al.* [1996] have observed gut passage times of up to 4 hours for diurnally migrating copepods. Fig. 3.3 shows a 24 h period of a model run alternating 140 min grazing with 30 min non-grazing. At the beginning of a grazing cycle, the calcite stock inside the gut increases strongly. Dissolution sets in, raising the saturation state as well. At the end of a grazing cycle, uptake of calcite and loss due to dissolution and egestion is almost in balance, so the standing stock is nearly constant. As grazing stops, calcite is egested rapidly, dissolution rate decreases and so does the saturation.

The results of model runs varying *p*H and ingestion rate with a 30 / 120 min grazing / non-grazing cycle are given in Table 3.2. The uptake rates of $CaCO_3$ cover the range given by *Harris* [1994, Table 3]. The fraction of calcite dissolved is calculated as the difference between uptake and egestion during one grazing / non-grazing cycle.

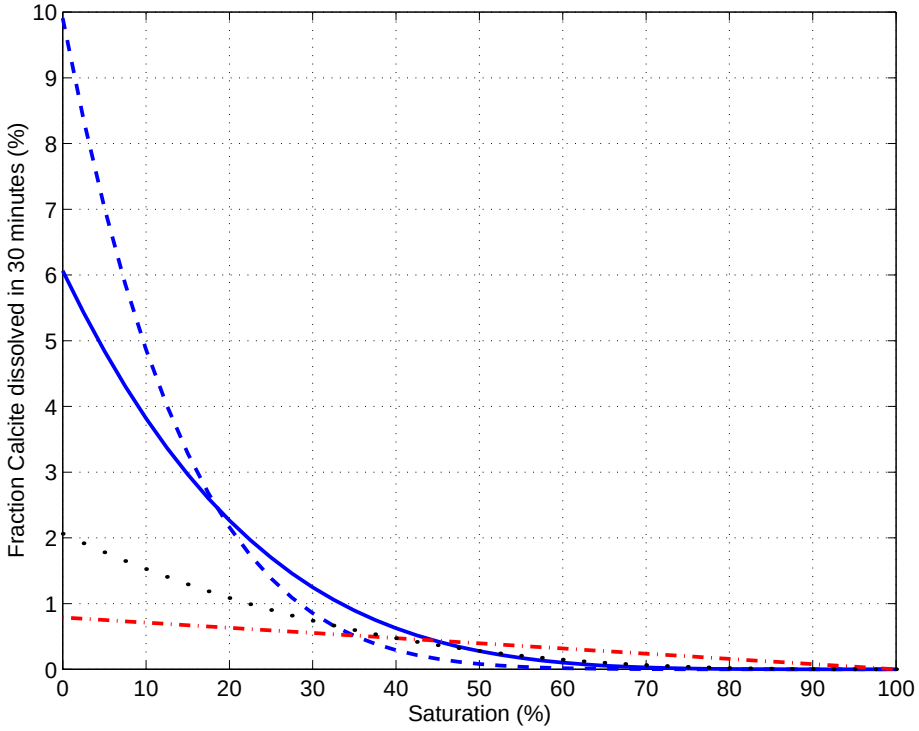

Figure 3.2: $CaCO_3$ dissolution potential assuming a gut passage time of 30 min and various dissolution kinetics: $\mathrm{dC/dt} = -\kappa(1-\Omega)^{\eta}$, Solid: $\kappa = 3\,\mathrm{d}^{-1}$, $\eta = 4.5$ [*Keir*, 1980] (lower bound for coccolithophorids), dashed: $\kappa = 7\,\mathrm{d}^{-1}$, $\eta = 4.5$ [*Keir*, 1980] (upper bound for coccolithophorids), dotted: $\kappa = 1\,\mathrm{d}^{-1}$, $\eta = 2.9$ [*Walter and Morse*, 1985], dashdotted: $\kappa = 0.38\,\mathrm{d}^{-1}$, $\eta = 1.0$ [*Hales and Emerson*, 1997]

With low ingestion rate, a moderate amount of up to $\sim 19\%$ of the ingested calcite may be dissolved inside the gut. Obviously, dissolution efficiency increases with decreasing *p*H. Also, as *p*H is lowered, the influence of the ingestion rate diminishes. Table 3.3 shows results at *p*H 6 and *p*H 5 when the non-grazing time is increased. The length of the non-grazing cycle mainly determines the fraction of calcite dissolved, as it sets the time the carbonate particles are subject to dissolution inside the gut. For very long non-grazing periods of 12 hours, the maximal dissolution efficiency of 29% is reached.

The impact of varying grazing and non-grazing interval lengths up to 4 hours at *p*H 5 and *p*H 6 is shown in Fig. 3.4. At *p*H 5, dissolution of up to 23% of the ingested $CaCO_3$ is possible. This much higher value as compared to the constant grazing scenario can be explained by long gut passage times during non-grazing, i.e. the coccoliths are subjected to dissolution for a prolonged time during which no additional calcite is taken up.

Long non-grazing times are not unusual as food availability in the field is very heterogeneous. Use of new in situ methods has shown that patch sizes of zooplankton and zooplankton food are highly variable in space [*Greene et al.*, 1998; *Gallager et al.*, 1996; *Norrbin et al.*, 1996; *Davis et al.*, 1996].

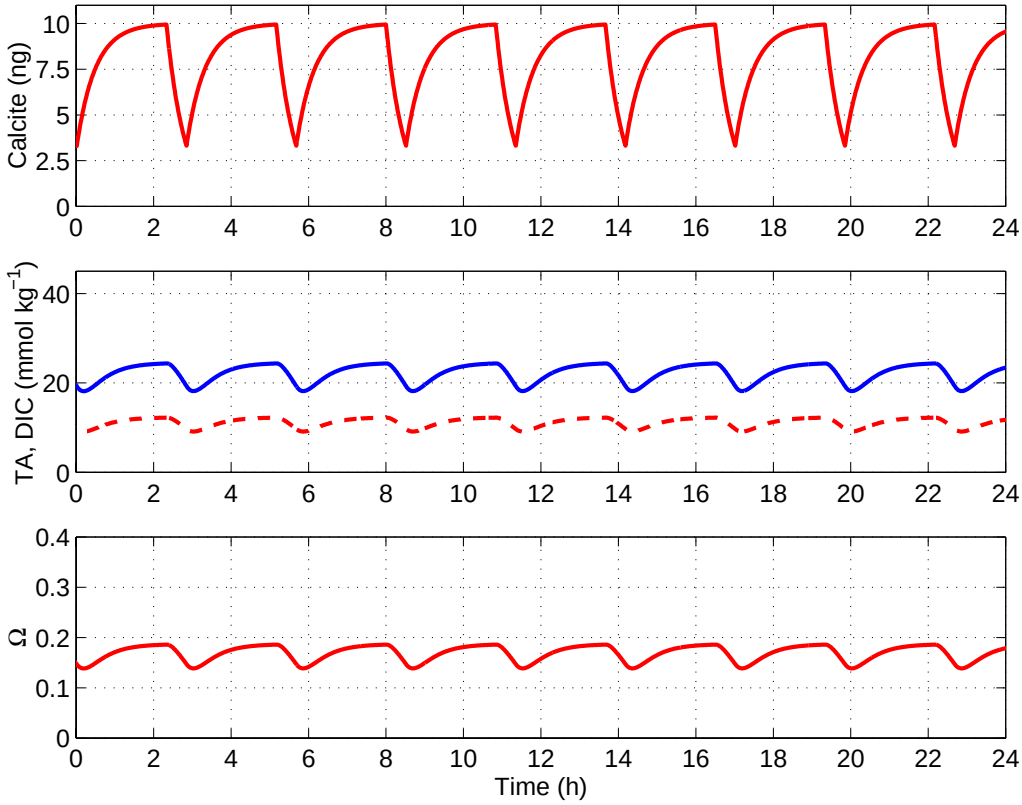

Figure 3.3: Alternating grazing / non-grazing modes. *p*H is set to 6, and the length of one grazing and one non-grazing cycle is 140 and 30 minutes, respectively. Top: Calcite standing stock in gut; middle: Dissolved inorganic carbon (solid) and alkalinity (dashed); bottom: Saturation state.

Furthermore, some zooplankton undergo diurnal migration which might result in zero food intake for several hours [*Dagg et al.*, 1989; *Atkinson et al.*, 1996]. Even in the presence of a coccolithophorid bloom, it makes sense for the copepod not to graze constantly. First, after a short time its digestive tract is filled; continuing to graze would reduce the effectivity of digesting the food. Second, a bloom site is rather a dangerous place for the copepod to be, as blooms also attract predators. Thus, it would be more favourable to move somewhere else to digest. Microcinematographic studies [*Rosenberg*, 1980; *Cowles and Strickler*, 1983] have shown that copepods alternate brief bouts of slow swimming and feeding with intervals during which swimming and feeding ceases. There is also evidence that copepods reduce or interrupt their grazing up to a few hours in response to previous feeding success [*Mackas and Burns*, 1986].

Adopting the measurements of *Pond et al.* [1995], who find high *p*H values during grazing and low *p*H values in starved individuals, slightly lowers the amount of calcite dissolution. Model runs with *p*H 8 during grazing and *p*H 6 or 5 in non-grazing intervals both give significant dissolution. However, a combination of *p*H 8 and *p*H 7 as found by *Pond et al.* [1995] in *Calanus helgolandicus*, yields merely 1.3% dissolution of the ingested calcite.

$CaCO_3$ uptake	$CaCO_3$ loss (%)			
$\mu g\,C\,d^{-1}$	pH 4	pH 5	pH 6	pH 7
0.5	19.4	17.3	8.5	0.9
1.0	19.2	15.5	5.9	0.6
1.5	18.9	14.1	4.6	0.4
2.0	18.7	13.0	3.8	0.3
2.5	18.4	12.0	3.2	0.3

Table 3.2: Results of model runs using a 30/120 min grazing / non-grazing cycle. The dissolved fraction depends heavily on the pH value.

Copepods are commonly observed to undergo diurnal vertical migration, from the top of the surface mixed layer at night to depth during daytime, crossing up to 100 m depth difference [*Mauchline*, 1998]. *Atkinson et al.* [1996] investigated a zooplankton community in the Polar Frontal Zone and found that all nine copepod species restricted grazing to the 8 hour nighttime period. Thus, model runs have been performed with various grazing / non-grazing interval lengths for a period of 8 hours, following a starvation interval of 16 hours.

An example is shown in Fig. 3.5: At the end of the nighttime period, a grazing cycle is just finished, so calcite standing stock is at its maximum value. It then decreases to zero during the day, since daytime length (16 h) is significantly longer than gut passage time (4 h). However, as the gut evacuation rate is lower than during night time, where gut passage time is 30 min throughout, initially a lot of calcite is dissolved rather than excreted, producing a spike in DIC and TA at daybreak. Note that this extra dissolution is the key difference to the model run where grazing is not restricted to the nighttime period (Fig. 3.3). Results are given in Table 3.4 and Fig. 3.6.

Due to the long daytime non-grazing interval, the dissolution efficiency is a bit higher than in the model runs where feeding is not restricted to the nighttime period. The maximum dissolution at *p*H 5 is $\sim 27\%$, compared to $\sim 23\%$ with 24 h grazing. *Penry and Frost* [1990] have suggested that egestion might be modelled better as a discontinuous process. An appropriate formulation in the model does not significantly change the results. The maximum dissolution at *p*H 5 is $\sim 28\%$, compared to $\sim 27\%$ with continuous egestion.

N − G ↓	G=30	G=60	G=90
30	5.2	4.7	4.4
	8.7	8.5	8.4
60	6.6	5.4	4.9
	12.0	10.4	9.8
120	8.5	6.4	5.6
	17.3	13.6	12.0
240	10.8	7.6	6.4
	24.9	18.4	15.3
360	12.6	8.7	7.2
	26.9	19.9	16.4
480	13.9	9.4	7.7
	27.9	20.6	17.0
600	14.8	10.0	8.1
	28.4	21.0	17.3
720	15.4	10.4	8.3
	28.7	21.2	17.4

Table 3.3: Fraction of calcite dissolved (%) as a function of grazing interval length (G, min) and non-grazing interval length (N-G, min). Standard parameter values used with *p*H 6 (top value in each cell) and *p*H 5 (bottom value). Gut passage time is 30 min during grazing and maximal 4 hours during non-grazing.

N − G ↓	G=60	G=120	G=180	G=240
30	5.8	5.3	5.1	5.0
	10.6	10.1	10.2	10.1
60	6.3	5.6	5.1	5.2
	11.6	11.3	9.8	10.6
90	7.5	6.1	5.4	5.4
	14.8	12.5	10.8	11.0
120	7.7	6.1	5.5	5.5
	15.4	12.1	11.5	11.5

Table 3.4: Fraction of calcite dissolved (%) as a function of grazing interval length (G, min) and non-grazing interval length (N-G, min). Feeding is restricted to the 8 hour night time period. Standard parameter values used with *p*H 6 (top value in each cell) and *p*H 5 (bottom value). Gut passage time is 30 min during grazing and the length of the non-grazing cycle otherwise.

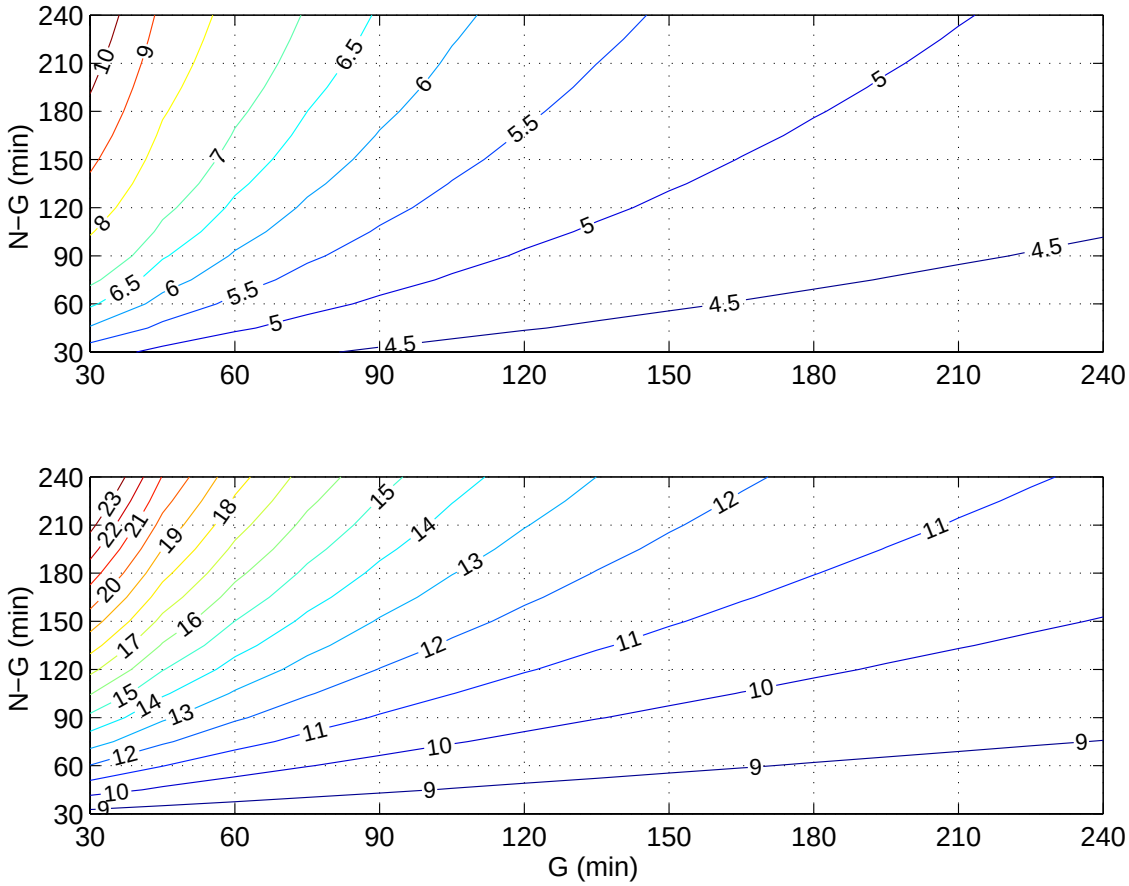

Figure 3.4: Fraction of ingested calcite dissolved (%) as a function of grazing (G) and non-grazing (N-G) interval length. Constant pH with (top) pH 6, (bottom) pH 5.

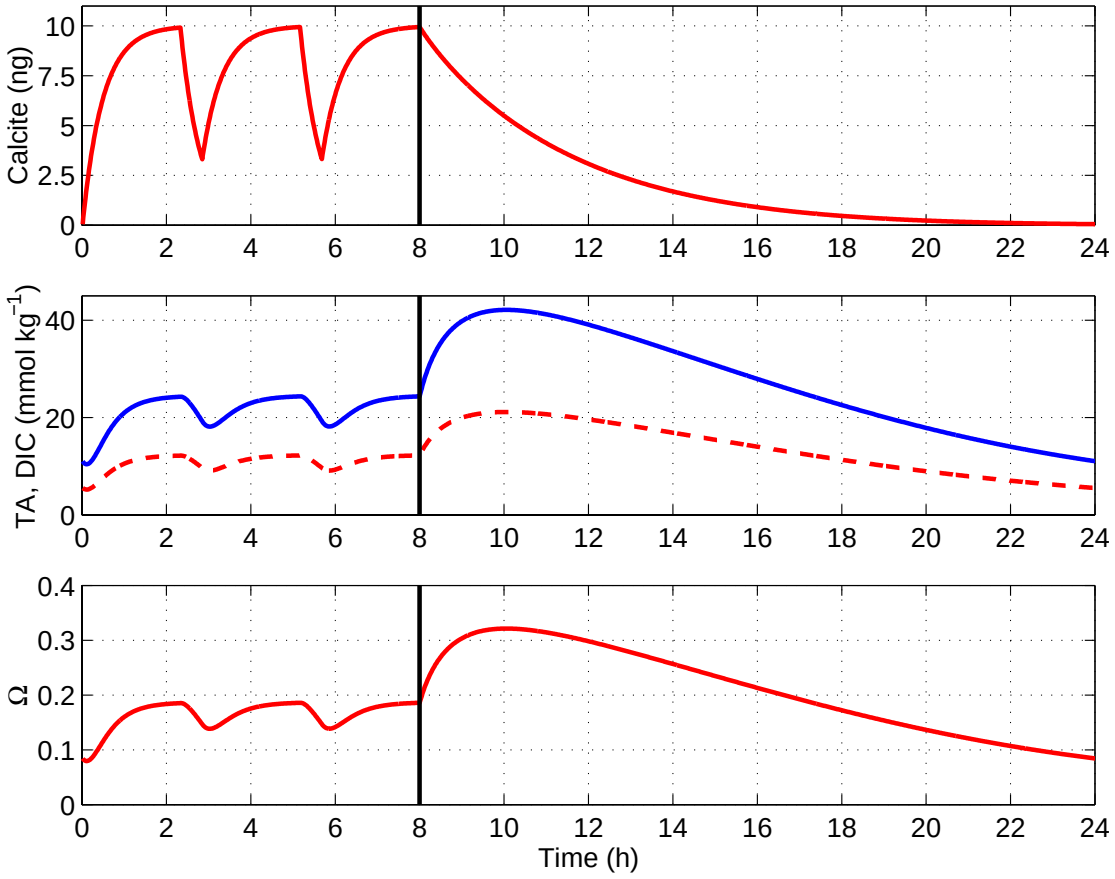

Figure 3.5: Alternating grazing / non-grazing modes restricted to the 8 hour nighttime period, followed by 16 hours starvation. *p*H is set to 6, and the length of one grazing and one non-grazing cycle is 140 and 30 minutes, respectively. Top: Calcite standing stock in gut; middle: Dissolved inorganic carbon (solid) and alkalinity (dashed); bottom: Saturation state.

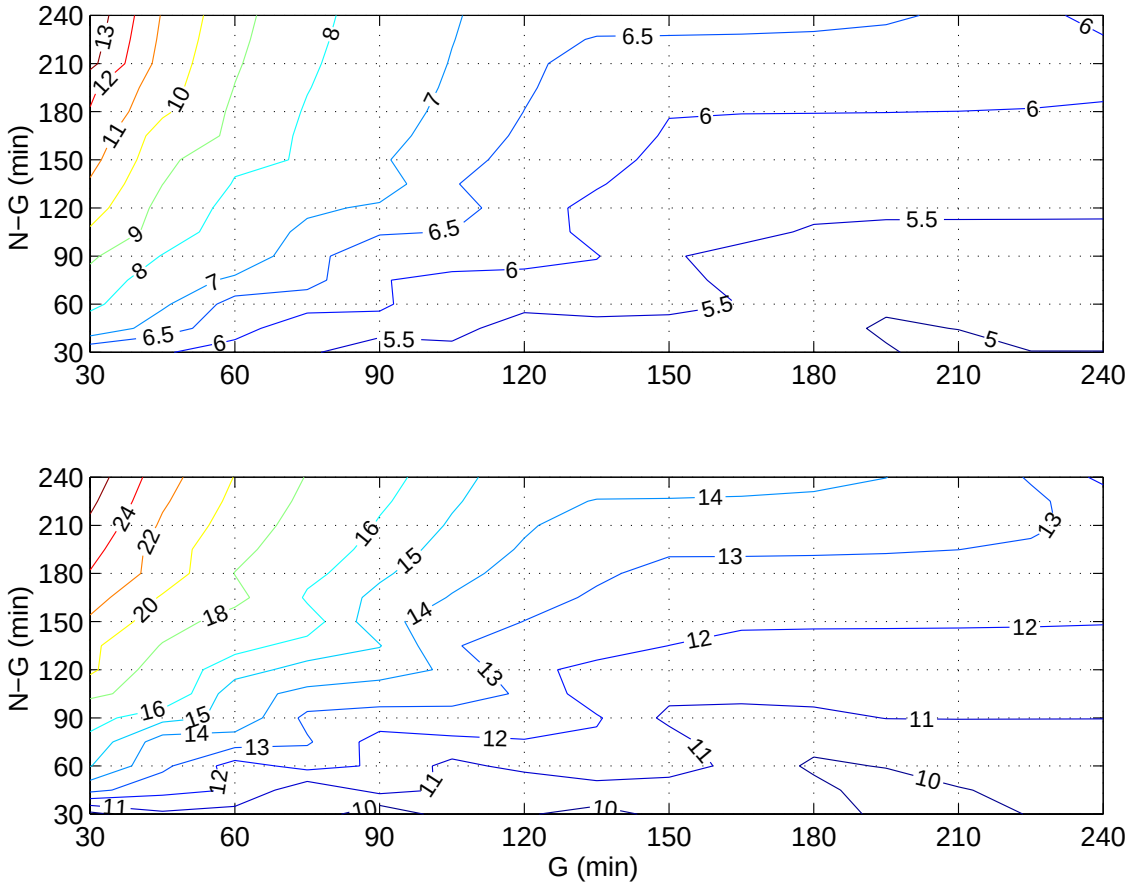

Figure 3.6: Fraction of ingested calcite dissolved (%) as a function of grazing (G) and non-grazing (N-G) interval length. Feeding restricted to the 8 hour nighttime period. Constant pH with (top) pH 6, (bottom) pH 5.

3.2.1 Critical parameters

The most critical parameter is the gut *p*H, determining the saturation state and thus dissolution rate. The next critical variable is the gut passage time K^{-1}, as it sets the time available for carbonate dissolution. It is thought to depend both on temperature and food supply. *Irigoien* [1998] and *Dam and Peterson* [1988] give values between 15 and 50 min for a temperature range between 5 and 25 °C. The volume of the gut is critical in that it determines how strongly concentrations of dissolved substances are changed by dissolution of some amount of calcite. With a smaller gut, dissolution of calcite drives the gut chemical system into supersaturation more easily, working against continued dissolution. The dissolution rate order of calcite is not well constrained, as modelled and experimentally derived values range between 1 [*Hales and Emerson*, 1997] and 5 [*Keir*, 1980]. Fig. 3.2 shows the amount of biogenic carbonate that can become dissolved in 30 minutes as the rate order is varied. Even under the most favourable circumstances (low saturation and fast dissolution kinetics), not more than 10% of the ingested calcite can be expected to dissolve. This calculation presents an upper limit for carbonate dissolution, as effects on saturation by released CO_3^{2-} are not considered in this exercise, but are taken into account in the model. On the other hand, prolonged gut passage times are likely during non-grazing intervals [*Atkinson*, 1996; *Irigoien*, 1998], enhancing the potential of $CaCO_3$ dissolution in zooplankton guts. Thus, when alternating grazing and non-grazing, the length of the non-grazing cycle is the critical parameter.

3.2.2 Contribution to calcite water column dissolution

In order to estimate how much of the observed calcite dissolution in the water column is attributable to the mechanism proposed here, the community grazing pressure of a copepod such as *Calanus* on coccolithophorid blooms has to be considered. The grazing pressure is defined as the fraction of either standing stock or daily primary production of a coccolithophorid bloom grazed by the copepod community. If not mentioned otherwise, grazing pressure is related to standing stock. Though numerous studies have been made on copepod grazing pressure on diatom or flagellate dominated blooms [*Bautista et al.*, 1992; *Bautista and Harris*, 1992; *Thibault et al.*, 1999], to the author's knowledge, no field work on copepod community grazing of coccolithophorids is available. Thus, estimates of *Calanus* standing stock together with measured ingestion rates are used to obtain an estimation of the grazing pressure. *Head et al.* [1998] investigated a bloom of *E. huxleyi* in the northern North Sea. The observed concentrations of *Calanus finmarchicus* and *E. huxleyi* were 428 ind. m^{-3} and 2.24×10^9 cells m^{-3}, respectively, where one coccolithophorid cell contained on average 12 pg C calcium carbonate and 90 pg C organic carbon. Assuming an ingestion rate of 10 μg C ind.$^{-1}$ d^{-1} of organic carbon leads to a community grazing pressure of 2.1% d^{-1}. This number is comparable to observed grazing pressures on diatom blooms, which range up to 10% with a mean of 3-5% [*Bautista et al.*, 1992; *Bautista and Harris*, 1992; *Thibault et al.*, 1999]. Considering 15% of the ingested calcite to be dissolved during gut passage, *Calanus* grazing thus may remove less than 1% of the calcite standing stock per day. Hence, this mechanism appears unable to contribute significantly to

water column dissolution during a bloom. In a post-bloom situation, however, the grazing pressure is likely to be considerably higher, if one considers that microzooplankton exert the largest grazing pressure on coccolithophorid blooms and copepods come in at a later stage and feed on the microzooplankton. *Burkill et al.* [1993] report grazing pressure of microzooplankton between 39% and 115% of the phytoplankton production during a summer bloom in the northeastern Atlantic Ocean, which was in the large size fraction dominated by diatoms and coccolithophorids [*Joint et al.*, 1993], compared to 1-2% grazing pressure of copepods. There is evidence that microzooplankton are grazed by copepods [*Sherr et al.*, 1986], so coccoliths may eventually end up in copepod guts. It is not to be expected that they dissolve in microzooplankton guts, as their guts are too small in volume, which works against dissolution by reaching supersaturation even with very small amounts of calcite dissolved. *Slagstad et al.* [1999] report annual mesozooplankton grazing pressures on primary production in the Bering Sea Shelf and the Northern Norwegian Shelf between 16 and 41%, which are mediated via microzooplankton. Recently, *Hansen et al.* [2000] have observed a copepod grazing pressure of 100% on the primary production in a mesocosm experiment. Furthermore, with decreasing food availability, the importance of faecal pellet reingestion ('coprophagy', [*Frankenberg and Smith*, 1967; *Bathmann et al.*, 1987; *Lampitt et al.*, 1990]) rises. A pellet may be recycled 5-10 times through a copepod gut [*Noji and Estep*, 1991]. In this way, even low dissolution fractions add up to significant amounts. If a faecal pellet loses 5% of its calcite content during gut passage, it has lost 23% and 41% of its carbonate after 5 and 10 gut passages, respectively. Dissolution of 10% of the calcite in one gut passage corresponds to 65% loss after 10 gut passages. Thus, for a post-bloom situation, the following calculation can be made. With 20% calcite dissolving during gut passage, 70% of the ingested calcite is lost after 5 passages. Assuming a grazing pressure of 20% yields 14% of the calcite standing stock being removed in this way. This corresponds to 23% of the calcite loss observed by *Milliman et al.* [1999].

Chapter 4

Sedimentary carbonate dissolution

This chapter focuses on calcium carbonate related processes in the sediment. The aim is to quantify estimates on the ocean sediment's role in changing the atmospheric carbon dioxide concentration on glacial-interglacial timescales. Furthermore, it is investigated whether the mismatch between observed changes in lysocline depth and changes in deep water *p*H derived from proxies can be reconciled by a decoupling of the lysocline from the saturation horizon (SH).

As discussed in the introduction, both the production of $CaCO_3$ and the subsequent accumulation or dissolution in the sediments influence the ocean's capacity to take up CO_2 from the atmosphere. Carbonate production raises surface ocean pCO_2, diminishing the amount of atmospheric CO_2 that can be dissolved in the ocean. The divide between calcium carbonate accumulation and dissolution in the sediments, the lysocline, is related to the position of the SH, which is set by the CO_3^{2-} concentration. Due to ocean circulation, the deep water $[CO_3^{2-}]$ influences surface water $[CO_3^{2-}]$ and thus, the carbonate system being in equilibrium, surface ocean pCO_2 as well.

Carbonate cycles in the Pleistocene record from the equatorial Pacific were first described by Arrhenius in 1952 (see, e.g., *Arrhenius* [1988]), even before *Emiliani* [1955] published his pioneering work on oxygen isotopes. The reconstruction of the carbonate content of sediments from the equatorial Pacific between 4,000 and 5,000 m depth for the last 800 kyr by *Farrel and Prell* [1989] shows that the location of the 80% $CaCO_3$ content level has undergone cyclic shifts of the order of 600 m. This indicates a deepening of the calcite saturation horizon by a similar amount, and thus an increase of the deep-sea CO_3^{2-} concentrations during glacials, compared to interglacials. Similar cycles have been observed in the Atlantic, but they are opposite to those in the Pacific [*Crowley*, 1983]. These out-of-phase responses of the Atlantic and Pacific are probably the result of ocean circulation changes [*Crowley*, 1985]. Thus, geological records suggest that the Atlantic lysocline was 0.3 - 1 km shallower during the last glacial [*Crowley*, 1983; *Curry and Lohmann*, 1986], while it was 0.8 km deeper in the Pacific Ocean [*Farrell and Prell*, 1989]. The value given by Farrell and Prell, however, might be an artefact, as they investigated a rather small region at the equator only, and the lysocline might not have changed in position that much at all [*David Archer*, pers.comm., 2000]. *Broecker et al.* [1991] indicate a net global average deepening of about 600 m during glacial times.

The boron isotope derived estimates of increased *p*H at the LGM call for a saturation horizon that was deepened considerably more than 600 m, which would mean that the lysocline was decoupled from the SH. Thus, significant dissolution of $CaCO_3$ above the SH must have taken place in glacial times. This is illustrated in Fig. 4.1. First, consider the lysocline to be at 4 km depth, coupled to the saturation horizon marked by SH_c.Increased glacial deep water *p*H leads to increased $[CO_3^{2-}]$ (dashed line), which depresses the SH to SH_d. If the lysocline is tied to the SH, it would deepen by 1 km, contradicting the observations. $CaCO_3$ dissolution above the saturation horizon would result in less deepening of the lysocline, decoupling it from the SH. In Fig. 4.1, the lysocline stays fixed for illustrative purposes. Here, the carbonate ion concentration in the decoupled case is approximately 25 μmol kg^{-1} higher than in the coupled scenario (dashed curve), depressing surface water pCO_2 by 29 μatm [*Broecker et al.*, 1991], since increased $[CO_3^{2-}]$ leads to reduced $[CO_2]$.

A possible mechanism to decouple the lysocline from the SH is carbonate dissolution driven by respiration processes of the benthic community in the upper 10 cm of sediment porewaters as observed by e.g. *Hales and Emerson* [1996]. Respiration of organic carbon in pore waters releases CO_2, acidifying the environment. This might lead to undersaturation in sediments bathed in supersaturated bottom water. Hence, by changing the amount of organic carbon arriving at the seafloor, the amount of carbonate dissolution above the saturation horizon can change dramatically, shoaling the lysocline relative to the saturation horizon. This could allow the lysocline to stay fixed at an increased deep water *p*H.

Already in the nineteenth century, *Murray* [1897] mentioned both the depth dependent occurrence of calcareous shells in the marine sediments and the enhancement of carbonate dissolution by the respiration of organic matter. Murray was chief scientist on the ground-breaking 'Challenger' expedition, which, between 1872 and 1875, gave the first globally coherent view on oceanographic, biological and geological data. *Emerson and Bender* [1981] published a first modelling study of carbonate dissolution in seafloor sediments above the saturation horizon, fueled by metabolic processes within the pore waters. Since then, numerous papers dealt with validating this theory in-situ [*Archer et al.*, 1989; *Berelson et al.*, 1990, 1994; *Jahnke et al.*, 1994, 1997; *Hales and Emerson*, 1996, 1997]. The general approach is to measure bottom water fluxes with microelectrodes or benthic flux chambers. Then, numerical models are used to explain the data in terms of carbonate dissolution. Measured dissolved inorganic carbon and alkalinity fluxes yield carbonate dissolution rates. The profiles of O_2, *p*H and pCO_2 are used to reconstruct the carbonate system within the pore waters.

There are two major results. Firstly, estimates were obtained on the amount of calcite or aragonite dissolving in sediments bathed in supersaturated waters, where dissolution is purely driven by remineralization of organic matter. Secondly, the calculations constrain the fraction of carbonate dissolution below the saturation horizon which is biologically mediated. It is therefore possible to differentiate between dissolution driven by physicochemical processes and dissolution driven by remineralization of organic matter. Metabolic processes enhance undersaturation and speed up dissolution. As for the long timescales considered here, the carbonate content in the sediment is in balance with the rain rate of particles and their dissolution rate, the amount of carbonate present may be used – if

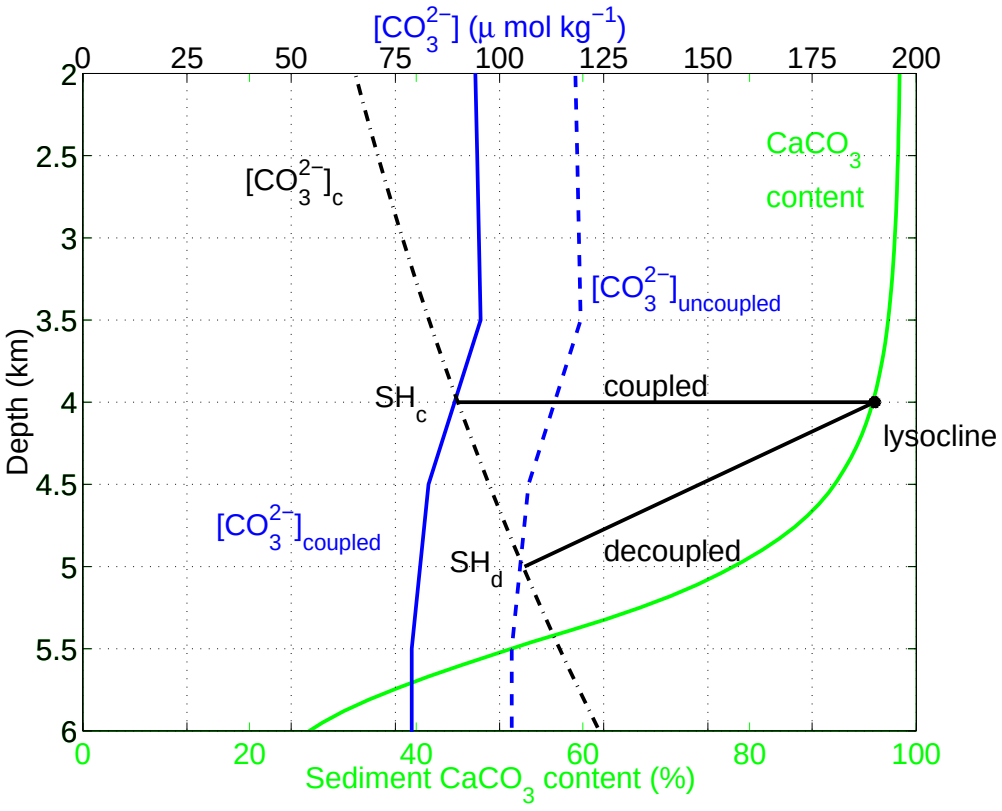

Figure 4.1: Schematic illustration of the effect of decoupling the lysocline from the SH. Dashed dotted: Critical carbonate ion concentration. Solid, light: Sedimentary calcium carbonate content. Solid, dark: Carbonate ion depth profile from GEOSECS data of the equatorial Pacific. Dashed: Carbonate ion depth profile under the assumption of increased *p*H and SH decoupled from the lysocline.

the sedimentation rate is known – to calculate the total dissolution rate. The 'inorganic' dissolution rate can be derived from the bulk saturation state of bottom waters, the metabolic contribution to the total dissolution can then be deduced.

The majority of in-situ observations conclude that the measured carbon and alkalinity fluxes cannot be explained without biologically mediated dissolution, because they find dissolution above the carbonate saturation horizon. Moreover, also sediments in undersaturated waters display metabolically driven dissolution. The quantitative constraints, however, are poor. Some authors have probed undersaturated settings only, others make mere qualitative statements [*Archer et al.*, 1989; *Cai et al.*, 1995]. Quantitative evidence is large in range or is presented as a lower limit. For example, *Hales et al.* [1994] conclude that, at the location they investigate, 35-67% of the calcite rain is dissolving in the sediment, driven only by metabolic addition of CO_2. *Hales and Emerson* [1997] find that more than 20% of the calcite rain is dissolving by biologically mediated dissolution. However, one has to keep in mind that this fact is mainly related to biological variability in different locations and only to a less extent due to measurement precision. The results on the fraction that metabolic processes

contribute to calcite dissolution below the saturation horizon range between 40% and 60%.

There have been several modelling approaches concerning respiration driven calcite dissolution in the sediments during the last decade. *Archer and Maier-Reimer* [1994] coupled a sediment model to an ocean general circulation model, investigating the effect of production changes on the lysocline depth. Their model yields that a 40% decrease in the calcite production decrease the atmospheric CO_2 concentration to the glacial value, if respiration driven dissolution is taken into account. However, they do not indicate how much this depresses the mean depth of the calcite lysocline. More recently, *Sigman et al.* [1998] investigated the effect of changes in the low-latitude export production, using a multibox ocean model [*Keir*, 1988] coupled to a model of calcite dissolution in the sediment. They conclude that any deepening of the SH combined with an increase in respiration driven dissolution leads to a significant deepening of the lysocline as well. Thus, the question whether the lysocline can effectively be decoupled from the SH remains open. In the present thesis, a new approach is followed. A model is developed that focuses on the sediments. For the question of lysocline positioning, the material fluxes to the sediment and the oceanic carbonate chemistry are important. These parameters are considered as boundary conditions or parameters to the model. Thus, no explicit ocean model is needed, reducing computation time significantly. The model concept is explained in detail in the following section. Then, the model's parameterization and equations are introduced. In section 4.2, a modern reference configuration is developed. Various glacial scenarios are calculated in section 4.3.

4.1 The Sediment model

4.1.1 Concept of the model

The model setup is illustrated in Fig. 4.2. It consists of a set of sediment boxes at different depths, following a global bathymetry of the ocean floor. Topographic data are taken from the ETOPO5 dataset [*University of California at San Diego (UCSD)*, 1999]. The topography is discretized into 10 m intervals. Open ocean area is here defined as seafloor depth greater than 2 km and the model is restricted to this part of the seafloor.

The primary production of $CaCO_3$ and C_{org} are parameters of the model. The amount of the primary production exported to depth and how much is remineralized or dissolved in the water column is then calculated (cf. the following section). The remaining flux is reaching the sediments. Each sediment box receives a flux of $CaCO_3$, clay and C_{org} particles in proportion to its surface area. Lateral transport between sediment boxes at different depths is not considered. Each sediment box represents the uppermost 10 cm of ocean floor, which is the depth that is most relevant for respiration processes [*Emerson and Hedges*, 1988]. The saturation with respect to calcite inside the sediment box may be computed from the saturation state of the seawater the box is in contact with and the amount of organic respiration inside the box. Any undersaturation leads to the dissolution of calcite. The sediment box is filled with particulates up to 10 cm in consecutive layers. Each layer represents the amount of $CaCO_3$ and clay that is accumulated in one time step. This is dependent on both the rain rate and the dissolution rate of calcite. The concept is illustrated in Fig. 4.3 for a sediment box

in undersaturation. Here, it takes five layers to fill the sediment box up to 10 cm. The uppermost layer is youngest and hence displays least dissolution. As new layers accumulate, the existing layers progress deeper into the sediment box and the calcite content is more and more dissolved. C_{org} is considered to respire fully in the sediment and is thus not included in the accumulation calculations.

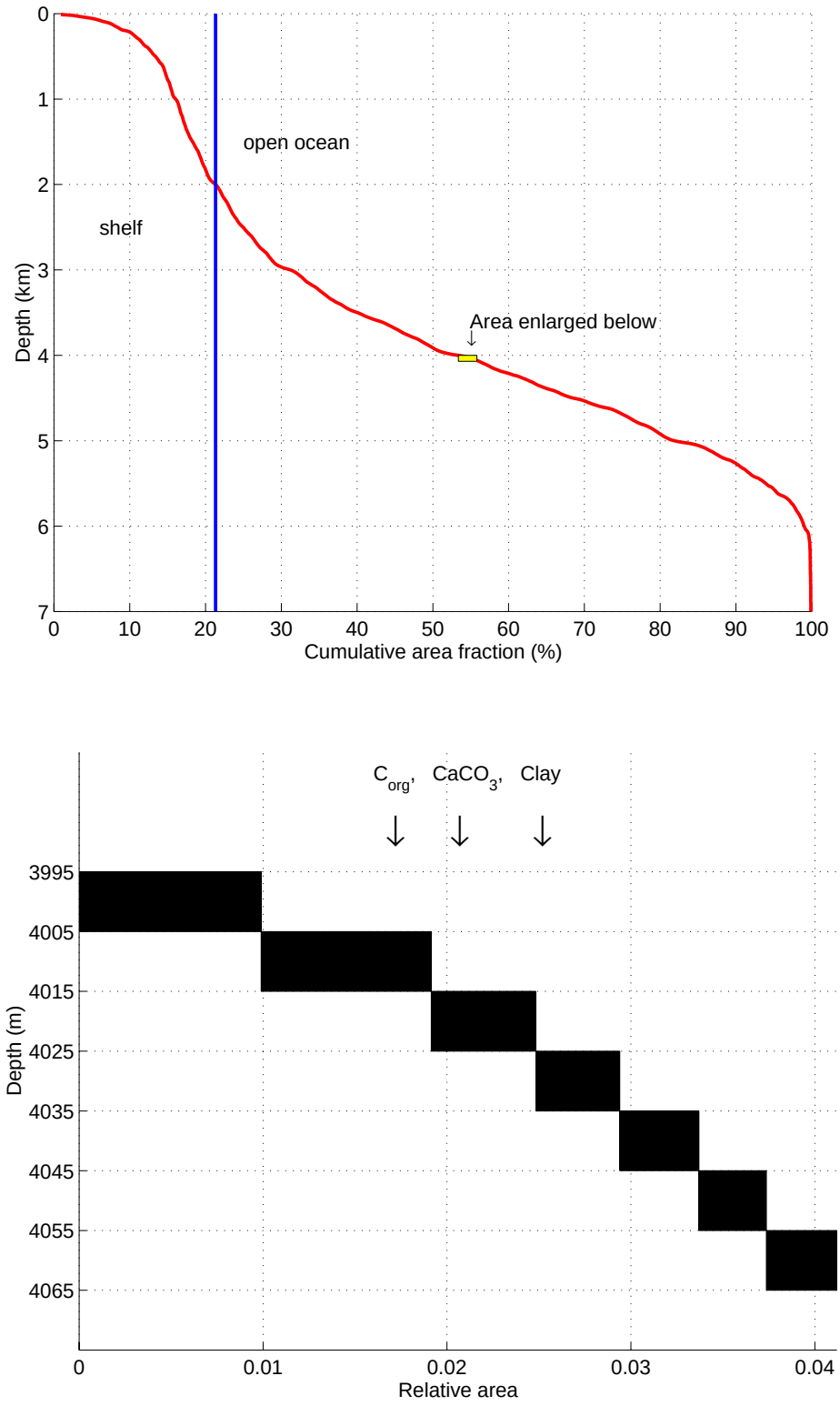

Figure 4.2: Top: Topography derived from the ETOPO5 dataset [*UCSD*, 1999]. Bottom: Sediment boxes from 3995 m to 4065 m depth, covering $\sim 4\%$ of ocean floor. The boxes receive organic carbon, calcite and clay rain in proportion to their surface area.

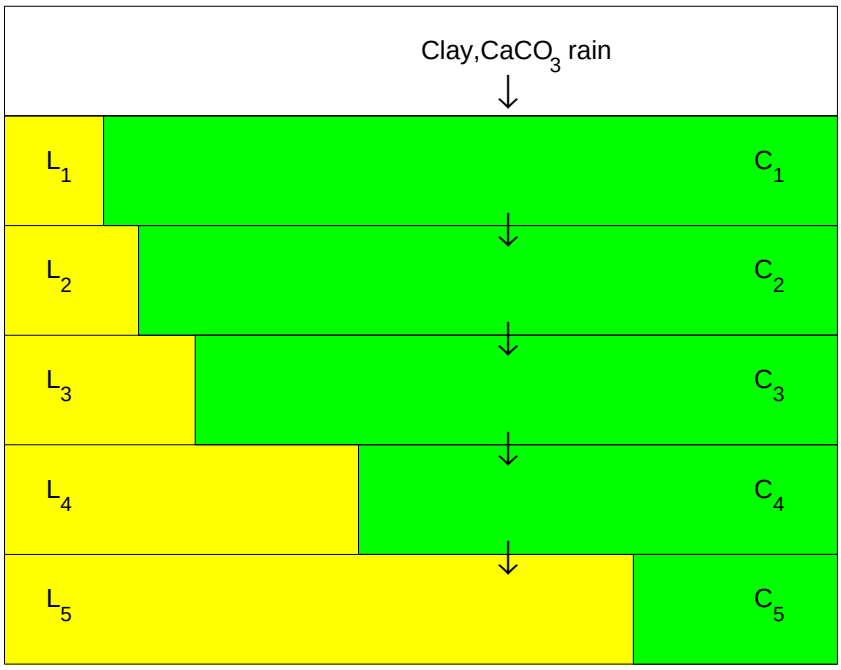

Figure 4.3: Schematic illustration of the sediment box concept with 5 layers in an undersaturated environment. The calcite and clay content of a layer are denoted by C_i, L_i, respectively, where i is the index of the layer.

Summing the contents of all layers gives the calcite content of the sediment box. Doing this for all boxes yields a depth profile of calcite in the sediments at all water depths from 2 km to 7 km. The position of the lysocline and the carbonate compensation depth (CCD) can then be derived, as is illustrated in Fig. 4.4.

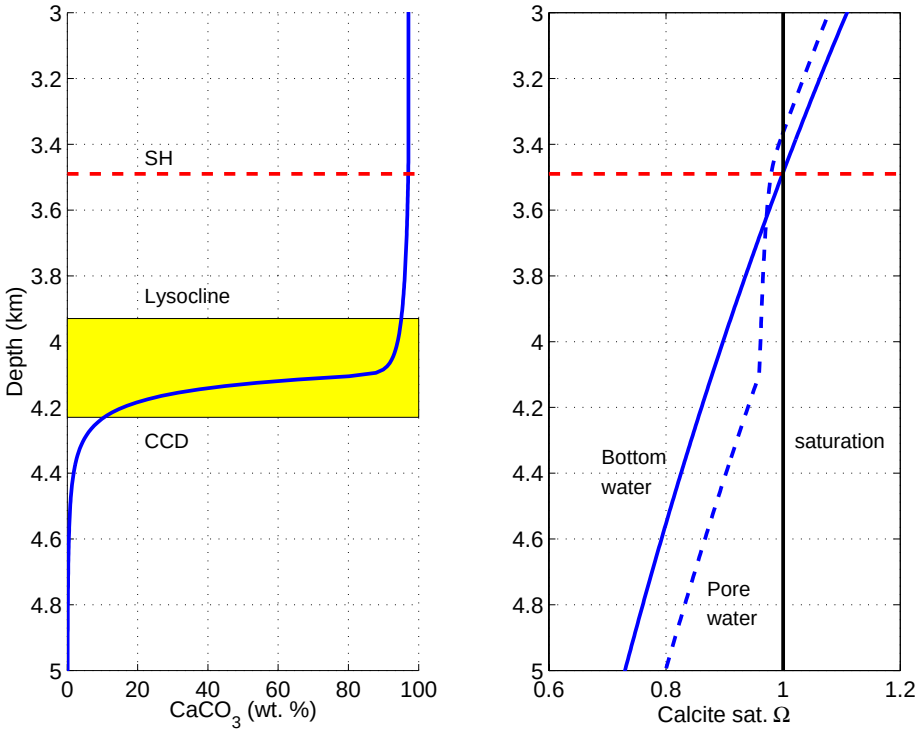

Figure 4.4: Calcium carbonate in sediment profile (left) and calcite saturation (right). The lysocline and the CCD are defined here to be at the depth where the sediment calcite content drops below 95% and 10%, respectively. The saturation horizon is set by the prescribed $[CO_3^{2-}]$ and lies above the lysocline as near to the saturation horizon, the rain rate of $CaCO_3$ exceeds the dissolution rate.

Various assumptions and simplifications are included in the model concept:

- No oceanic circulation model is used because regional aspects are not to be resolved. Rather, the mean response of the lysocline to varied production of $CaCO_3$ and C_{org} and a depression of the SH are investigated. Hence, it is sufficient to incorporate the ocean's role of providing the material fluxes and the carbonate chemistry state as boundary conditions and parameterizations.

- The production values of organic carbon and calcium carbonate are used as globally averaged values, since it is not intended to resolve locally changes in lysocline position, but to investigate the global mean decoupling of the lysocline from the SH.

- The flux of clay is tied to the carbonate production to yield $\sim$ 97% calcite content in shallow

sediments [*Broecker and Peng*, 1982]. In reality, the clay flux is expected to be higher the closer a particulate point in the ocean is to the coast, as clay is of terrigenous origin.

- The model considers the calcite fraction of the carbonate rain only. Estimates on the fraction of calcium carbonate that is produced as aragonite vary considerably, from 10% to 50%. For the present investigation, it is sufficient to look into the connection between calcite lysocline and calcite SH, since the latter sets deep water $[CO_3^{2-}]$ and the aragonite SH strictly follows the location of the calcite SH (cf. Eq. 1.8).

- The model is restricted to depths greater than 2 km. Presently, the calcite lysocline depths are between 3.7 km (Pacific) and 4.45 km (Atlantic) [*Broecker and Takahashi*, 1977], and the SH is located between $\sim \sim 2$ km (North Pacific) and ~ 5.5 km (North Atlantic, cf. Fig. 1.7). Both the SH and the lysocline were located deeper during the LGM. Thus, sediments shallower than 2 km depth are of no interest to the investigations here.

- The carbonate chemistry of the bulk ocean is taken from GEOSECS data [*Takahashi et al.*, 1981]. As deeper than 2 km, the $[CO_3^{2-}]$ displays no significant gradient, DIC and TA are assumed to be constant with depth, i.e. mean deep values are used. The ocean values are not influenced by calcite dissolution in the sediments and resulting fluxes of DIC and TA out of the sediments are very small compared to the amounts of DIC and TA present in the ocean.

The following observations are considered as hard constraints on the model: The glacial position of the calcite lysocline was 600 m deeper than today and the deep water $[CO_3^{2-}]$ was increased in line with the reduced surface ocean pCO_2. On the other hand, the export production of C_{org} and $CaCO_3$, as well as the remineralization depth of organic matter in the water column, are seen as free model parameters that can be tuned in order to produce a model configuration consistent with the hard constraints.

4.1.2 Parameterization of the material fluxes

The model described in the previous section is fueled by the rain of calcium carbonate and organic matter. Estimates on production rates of these biogenic particles are given in Appendix C. However, most of the primary production (PP) is remineralized already in the mixed layer, only a fraction of it leaves the photic zone and sinks to the deep sea. This fraction is called the export production (EP). The ratio of EP to PP is called the export ratio and is denoted by σ. *Laws et al.* [2000] propose a functional relationship between PP, temperature and the export ratio as depicted in Fig. 4.5. PP is expressed in $\mathrm{mg\,N\,m^{-3}\,d^{-1}}$ and has been converted from ^{14}C measurements divided by the Redfield C:N ratio of 5.7. Because the relationship is based on production per volume and production estimates are given per area integrated over the euphotic zone, one has to know the mixed layer depth when applying this parameterization. *Laws et al.* [2000] consider a global PP of $51.2\,\mathrm{Gt\,C\,a^{-1}}$ [*Behrenfeld and Falkowski*, 1997] and derive an export ratio of $\sigma = 0.21$. Thus, EP is $\sim 11\,\mathrm{Gt\,C\,a^{-1}}$, which is in line with the estimate by *Schlitzer* [2000]. This implies a mixed layer depth in the *Laws et al.* [2000] parameterization of 18.25 m, which, for a global mean, is small but reasonable. *von Storch et al.* [1999, page 36] state 10 m – 100 m as a range for the mixed layer depth within the temperate oceans. It generally is deep in the well stratified waters of the high latitudes, whereas the mixed layer depth is shallow at the tropical high-productivity areas. In the present model, global PP of $45.5\,\mathrm{Gt\,C\,a^{-1}}$ (mean 1990-2000 value in Table C.2) and a mean surface temperature of 15.5°C are considered. As the model is restricted to open ocean areas, PP is taken to be 70% of global PP [*Longhurst et al.*, 1995], i.e. $31.8\,\mathrm{Gt\,C\,a^{-1}}$ (cf. Table C.2). The Laws et al. formula then yields $\sigma = 0.11$. This value is within the range reported for oligotrophic regions [*Laws et al.*, 2000]. Thus, EP is $3.4\,\mathrm{Gt\,C\,a^{-1}}$ (Fig. 4.5). The open ocean export ratio is lower than the global export ratio because the shelve areas account for 30% of the global primary production, but cover only 10-20% of sea surface area (depending on where the shelf-break is defined, cf. Fig. 4.2). Hence, on the shelves, relatively more organic matter per area is produced than in the open ocean.

The majority of EP remineralizes in the water column. The fraction that reaches the sediments is calculated via the *Martin et al.* [1987] parameterization:

$$F_{C_{org}}(z) = F_{C_{org}}(100)\left(\frac{z}{100}\right)^{-0.858} \tag{4.1}$$

where $F_{C_{org}}(z)\,(\mathrm{mol\,m^{-2}\,d^{-1}})$ is the flux of organic carbon at depth z (m) and $F_{C_{org}}(100)$ denotes the exported flux. According to (4.1), approximately 8% of the export production (i.e. $\sim 1\%$ of the PP) reaches 2 km depth, while $\sim 2\%$ of it arrives at 7 km depth.

In the case of calcium carbonate, the export production is set equal to the production, i.e. no $CaCO_3$ particles are assumed to dissolve in the mixed layer. If calcite dissolves in the water column, the calcite rain rate is parameterized via [*Archer and Maier-Reimer*, 1994]:

$$F_{CaCO_3}(z) = 0.3\,F_{CaCO_3}(100) + 0.7\,F_{CaCO_3}(100)\,\exp(-z/2000), \tag{4.2}$$

where 30% of the calcite production flux ($F_{Ca}(100)$) sinks without dissolution to the sediment, and the remainder dissolves in the water column with an e-folding depth of 2,000 m. This parameterization

reproduces the dissolution fluxes in the water column estimated by *Milliman and Droxler* [1996]. Alternatively, the model is run with no water column dissolution of calcite.

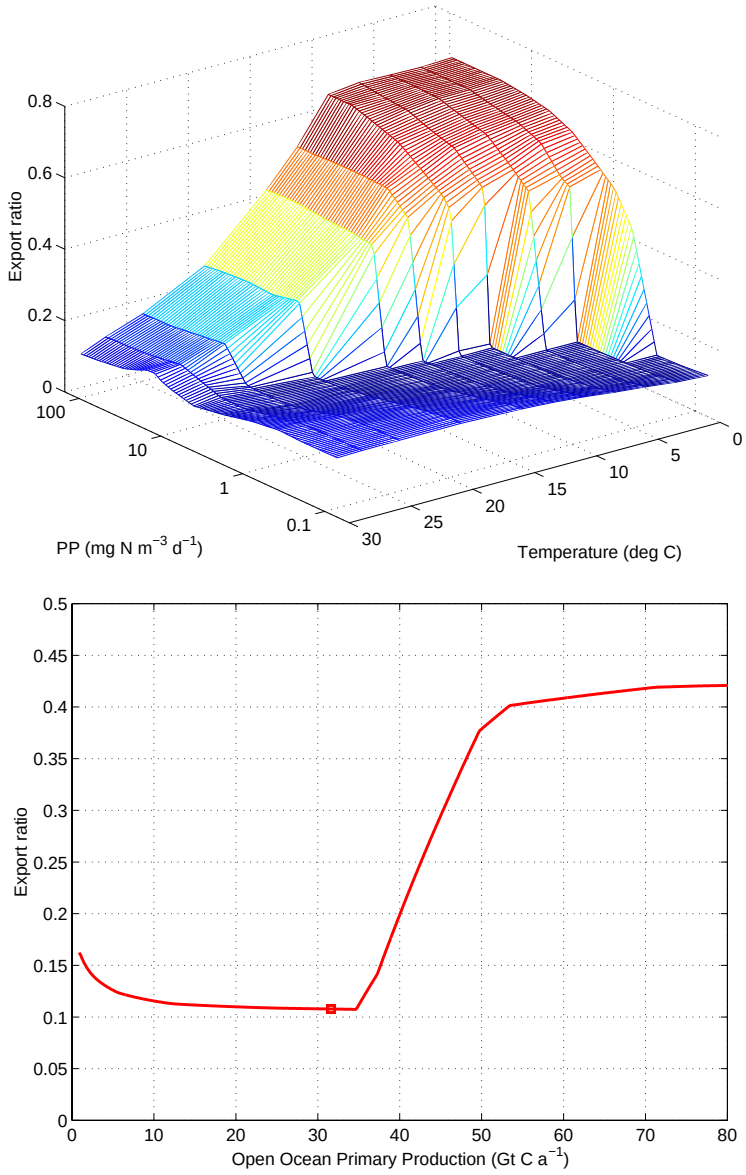

Figure 4.5: Top: Export ratio versus primary production, PP, and temperature, as proposed by *Laws et al.* [2000]. Bottom: Export ratio in the model using a mean mixed layer depth of 18.25 m. The standard modern value is marked with a square.

4.1.3 Equations and parameters of the model

The independent variables of the model are dissolved inorganic carbon (DIC, $\mathrm{mol\,kg^{-1}}$) and total alkalinity (TA, $\mathrm{mol\,kg^{-1}}$). Sources of DIC and TA in the pore water are remineralization of organic carbon (C_{org}) and dissolution of calcium carbonate ($CaCO_3$), as described in Chapter 1.1.2. Thus, the relevant differential equations are

$$\begin{aligned} \frac{dDIC}{dt} &= \frac{\alpha C_s + \beta}{\rho_w \phi V} + \gamma\,(DIC_b - DIC), \\ \frac{dTA}{dt} &= \frac{2\alpha C_s - 0.12\beta}{\rho_w \phi V} + \gamma\,(TA_b - TA), \end{aligned} \tag{4.3}$$

where $C_s\,(\mathrm{mol})$ is the standing stock of calcite in the sediment box of volume V, $\alpha\,(\mathrm{d^{-1}})$ denotes the decay rate coefficient for $CaCO_3$, $\rho_w\,(\mathrm{kg\,m^{-3}})$ is the density of seawater, ϕ (dimensionless) denotes the porosity of the sediment, $V\,(\mathrm{m^3})$ is the box volume, $\beta\,(\mathrm{mol\,d^{-1}})$ is the decay rate for C_{org} and $\gamma\,(\mathrm{d^{-1}})$ is an exchange coefficient parameterizing the diffusion between sediment and bulk seawater. Parameter values are given in Table 4.3. The factor 2 in the equation of TA reflects the fact that dissolution of calcium carbonate increases alkalinity and DIC in a ratio of 2:1; the factor -0.12 is connected to nitrate release proportional to the Redfield ratio of nitrogen to carbon in organic matter (cf. Eq. 1.6 and Table 1.1, value by *Anderson and Sarmiento* [1994] used). DIC_b, $TA_b\,(\mathrm{mol\,kg^{-1}})$ are the bottom water concentrations of DIC and TA, respectively (taken from GEOSECS data). As steady state solutions are sought, the time derivatives in Eq. (4.3) are set to zero and the resulting equations are solved for DIC and TA, yielding

$$\begin{aligned} DIC^* &= DIC_b + \frac{\alpha C_s + \beta}{\rho_w \phi V \gamma}, \\ TA^* &= TA_b + \frac{2\alpha C_s - 0.12\beta}{\rho_w \phi V \gamma}. \end{aligned} \tag{4.4}$$

The dissolution rate α is calculated as [*Archer*, 1996]

$$\alpha = \begin{cases} \kappa(1-\Omega)^\eta & \text{if } \Omega < 1, \\ 0 & \text{else.} \end{cases} \tag{4.5}$$

where $\kappa\,(\mathrm{d^{-1}})$ is the rate constant, η is the rate order and $\Omega = [CO_3^{2-}]/[CO_3^{2-}]_c$ is the saturation with respect to calcite. A discussion on experimentally derived parameterizations of the dissolution kinetic is given in Appendix A. The parameterization proposed by *Keir* [1980] is used here, as it leads to the most realistic carbonate content depth profiles (cf. section 4.2). $[CO_3^{2-}]\,(\mu\mathrm{mol\,kg^{-1}})$ denotes the carbonate ion concentration in the pore water box and is calculated from DIC_b and TA_b. $[CO_3^{2-}]_c\,(\mu\mathrm{mol\,kg^{-1}})$ gives the carbonate ion concentration at saturation. The latter is a function of depth z (km) and is calculated according to *Millero* [1995] (Fig. 1.6).

With the saturation states calculated, the next step is to derive the standing stock of calcite in the pore water box. After one time step, the uppermost layer contains

$$\begin{aligned} C_1 &= (1 - \Delta t\,\alpha)\,(\Delta t\,R), \\ L_1 &= q\,(\Delta t\,R), \end{aligned} \tag{4.6}$$

where C_1,L_1 (g) are the calcite and clay contents, respectively, Δt (d) is the time step and α (d^{-1}) is the fraction of calcite dissolved per day. The rain of calcite is denoted by R(g d^{-1}) and q is the fraction of the rain that is added as clay. As the layers beneath the surface are progressively older, the i^{th} layer contains

$$\begin{aligned} C_i &= (1-\Delta t\,\alpha)^i\,(\Delta t\,R), \\ L_i &= q\,(\Delta t\,R), \end{aligned} \tag{4.7}$$

Summing over all layers, one obtains

$$\begin{aligned} C &= (\Delta t\,R)\sum_{i=1}^{N}(1-\Delta t\,\alpha)^i \\ L &= N\,q\,(\Delta t\,R), \end{aligned} \tag{4.8}$$

where N is the number of time steps (i.e. layers) it takes to fill the box up to 10 cm thickness. Eq. (4.8) contains a geometric series, so C is derived as

$$C = \Delta t\,R\,\frac{(1-\Delta t\,\alpha)-(1-\Delta t\,\alpha)^{N+1}}{\Delta t\,\alpha} \tag{4.9}$$

Thus, the variable N is left to determine the calcite standing stock C. In order to obtain a value for N, one more equation is needed. The volume taken up by the solid particles is given by their weight divided by the specific densities, so the standing stock of the particles has to obey the following equation:

$$\left(\frac{C}{\rho_c}+\frac{L}{\rho_l}\right) = (1-\phi)\,V, \tag{4.10}$$

where ρ_c, ρ_l, (g m^{-3}) are the specific densities of calcite and clay, respectively, ϕ is the porosity of the sediment and V (m^3) is the volume of the box. Substituting Eq. (4.8) and (4.9) into Eq. (4.10) yields

$$\left(\frac{(1-\Delta t\,\alpha)\;-(1-\Delta t\,\alpha)^{N+1}}{\Delta t\,\alpha\,\rho_c}+\frac{q\,N}{\rho_l}\right)\Delta t\,R = (1-\phi)\,V \tag{4.11}$$

Unfortunately, this equation cannot be solved analytically for N. Thus, a Newton-Raphson iteration is used. Having calculated N, the standing stock of calcite is derived from Eq. (4.9). The sedimentary calcite content in weight percent is given by

$$C^{\%} = 100\frac{C}{C+L}. \tag{4.12}$$

Because in Eq. (4.4) the calcite content is required in mol, it is converted by $C_s = C/100$, reflecting the stoichiometry of $CaCO_3$ (1 mol $\hat{=}$ 100 g).

The parameters β (respiration of organic matter) and γ (diffusion with the bulk medium) in Eq. (4.4) remain to be determined. This is done as follows. The amount of organic carbon remineralized in the pore waters depends on the availability of oxygen. Analogous to Eq. (4.3), one can formulate

$$\frac{d[O_2]}{dt} = \frac{-r_{o/c}\,\delta\,R_{org}}{\rho_w\,\phi\,V} + \gamma_{O_2}\,([O_{2,b}]-[O_2]), \tag{4.13}$$

where $[O_2]$ and $[O_{2,b}]\,(\mathrm{mol\,kg^{-1}})$ are the concentrations of oxygen in the pore water and bulk seawater, respectively and $r_{o/c}$ is the Redfield ratio of oxygen to carbon. As a conservative approach, a high value of $r_{o/c} = 1.45$ is considered [*Anderson and Sarmiento*, 1994] (cf. Table 1.1). $R_{org}\,(\mathrm{mol\,d^{-1}})$ is the rain of organic carbon entering the particular pore water box, of which a fraction δ is remineralized. This latter value is determined by assuming Eq. (4.13) to be in steady state and setting $[O_2] = 0$. This gives the fraction of organic matter that may be remineralized using all the available oxygen. In the standard modern (preindustrial) case (discussed in section 4.2), the availability of oxygen does not limit the remineralization of C_{org}, i.e. oxygen is never used up completely. This is attributable to the fact that globally averaged production values and sediments deeper than 2 km are considered. In shallower sediments, organic rain may be larger than the amount that can be remineralized with the oxygen present in the pore waters. In the Arabean Sea, for example, a strong oxygen minimum zone is observed between $\sim$ 150 m and 1200 m water depth [*Hupe and Karstensen*, 2000], resulting in enhanced preservation of organic carbon in the sediment. The bulk seawater oxygen values have been interpolated from GEOSECS data [*Takahashi et al.*, 1981] and are illustrated in Fig. 4.6.

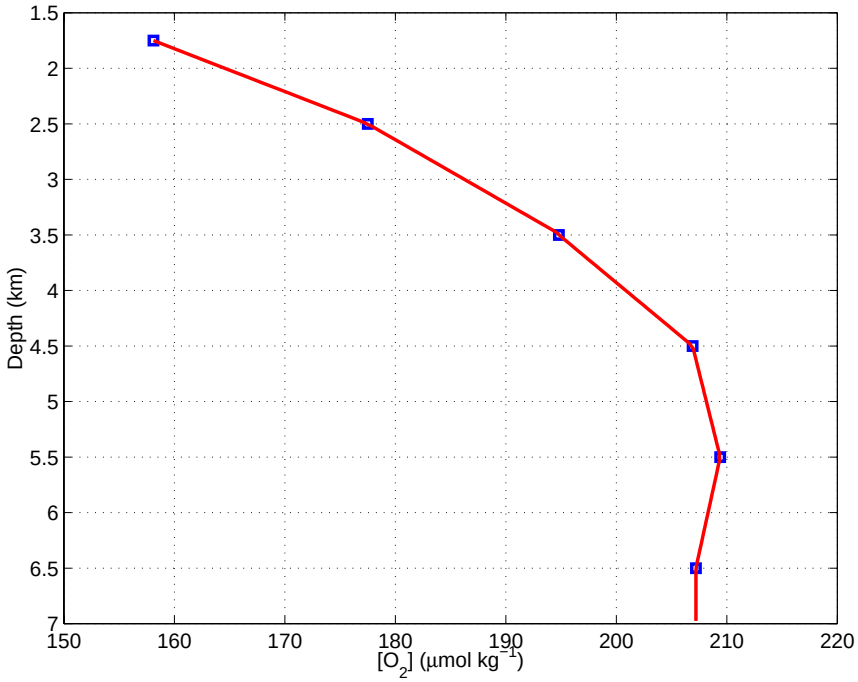

Figure 4.6: GEOSECS mean ocean data (squares) and interpolation (solid line) of seawater oxygen concentration.

The exchange coefficient γ is derived via Fick's first law:

$$F = -D\,\frac{dDIC}{dz} = (DIC_b - DIC)\,\frac{D}{z_b}, \tag{4.14}$$

where $F\,(\mathrm{mol\,m^{-2}\,d^{-1}})$ is the flux of DIC from the bottom water into the pore water box, $D\,(\mathrm{m^2\,d^{-1}})$

is the diffusion coefficient and $z_b\,(\mathrm{m})$ is the thickness of the diffusive boundary layer (DBL). The appropriate diffusion coefficients in pore water are given by [*Schulz*, 1999]:

$$\begin{aligned} D_{HCO_3^-} &= 86400\,\frac{4.81\times10^{-10}+2.54\times10^{-11}\,T}{1-\log(\phi^2)} \\ D_{O_2} &= 86400\,\frac{1\times10^{-9}+4.52\times10^{-11}\,T}{1-\log(\phi^2)}, \end{aligned} \tag{4.15}$$

where $T(^\circ\mathrm{C})$ is the temperature, ϕ is the porosity of the sediment and 86400 the conversion factor from seconds to days. Thus, with $A\ (\mathrm{m}^2)$ denoting the box surface area,

$$\gamma = \frac{D\,A}{\phi\,V\,z_b}, \tag{4.16}$$

giving the fraction of DIC concentration that is lost to or gained from the bottom water per day. The formulation for TA is completely analogous, provided the diffusion coefficient is the same. As DIC and TA are dominated by HCO_3^-, the diffusion coefficient of that ionic species is taken for both DIC and TA. The exchange coefficient γ strongly depends on the DBL, as illustrated in Fig. 4.7. Reasonable gradients between pore water and bottom water concentrations [*Hales and Emerson*, 1996, 1997] are achieved with $z_b = 1\,\mathrm{mm}$, which is in the range of DBL estimations given by *Boudreau and Guinasso* [1980]. The thickness of the boundary layer is primarily controlled by the velocity of the bottom currents and the slope and roughness of the sea floor. The exchange coefficient γ_{O_2} for oxygen is calculated analogously.

The equilibrium values *DIC** and *TA** are calculated according to Eq. (4.4) using the dissolution rate α derived from bottom water saturation values. However, *DIC** and *TA** in turn determine the carbonate ion concentration in the pore water, leading to a saturation state that differs from the bottom water saturation state. Actually, the dissolution rate is itself a function of DIC and TA, as it depends on the carbonate ion concentration: $\alpha = \alpha(\mathrm{DIC}^*, \mathrm{TA}^*)$. Whenever organic carbon remineralization outweighs calcite dissolution, the saturation is decreased in relation to bottom water, while it is higher when calcite dissolution dominates. Thus, the bulk saturation value is taken as a first guess and the solution is iterated with the calculated pore water saturation. The result of this iteration is shown in Fig. 4.8. Obviously, it is not converging to a steady state, except for shallow and deep sediments. It is quite obvious why convergence fails in the intermediate depth: Initially, the bottom water saturation gives rise to considerable calcite dissolution. This raises the saturation state of the pore water to a value greater than unity, i.e. the sediment is supersaturated with respect to calcite in the subsequent step. Hence, the model calculates no dissolution and returns to seawater values, repeatedly adopting the initial state. To avoid this behaviour, an under-relaxation is performed, where in each iteration step only a fraction of the calculated shift in saturation is used for the next iteration step. This yields the following equations, where $n = 1, 2, \ldots$ is the iteration index and ω is the relaxation parameter. Numerical tests result in $\omega \geq 10$ as sufficient for convergence.

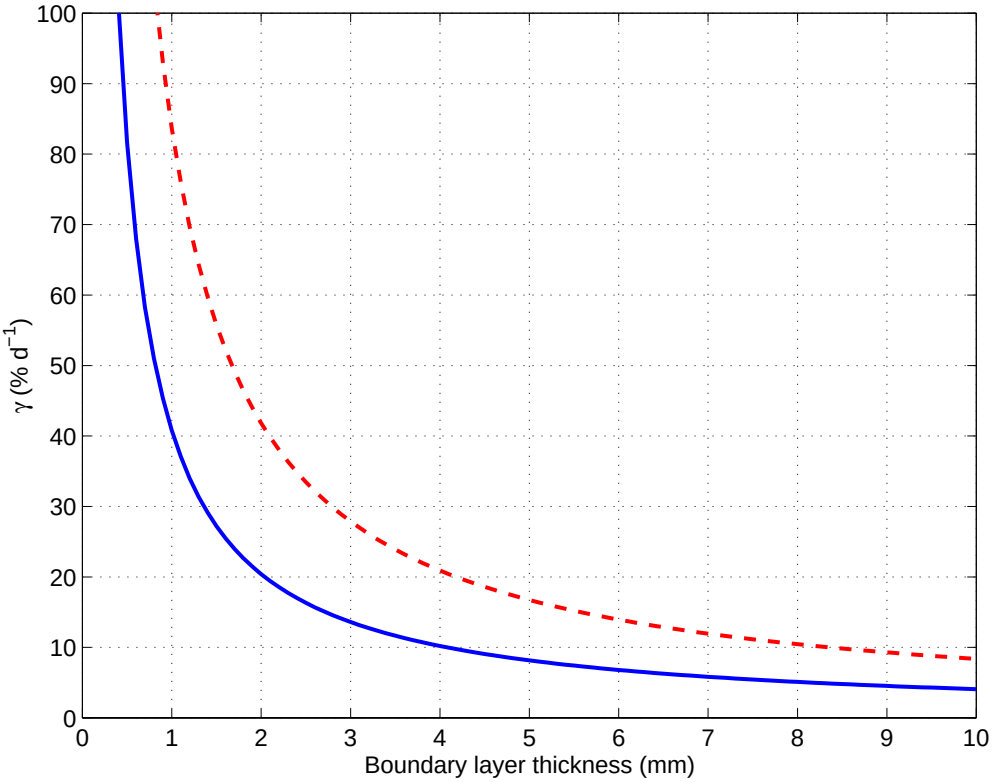

Figure 4.7: Exchange coefficient of DIC and TA (solid) and oxygen (dashed) versus boundary layer thickness.

$$
\begin{aligned}
\mathrm{DIC}^{*} &= \mathrm{DIC}_{b} + \frac{\alpha^{(n)} C_{s}^{(n)} + \beta}{\rho_{w}\,\phi\,V\,\gamma}, \\
\mathrm{TA}^{*} &= \mathrm{TA}_{b} + \frac{2\alpha^{(n)} C_{s}^{(n)} - 0.12\beta}{\rho_{w}\,\phi\,V\,\gamma}, \\
\mathrm{DIC}^{(n+1)} &= \mathrm{DIC}^{(n)} + \frac{1}{\omega}(\mathrm{DIC}^{*} - \mathrm{DIC}^{(n)}) \\
\mathrm{TA}^{(n+1)} &= \mathrm{TA}^{(n)} + \frac{1}{\omega}(\mathrm{TA}^{*} - \mathrm{TA}^{(n)})
\end{aligned}
\tag{4.17}
$$

The complete numerical scheme may be presented as

$$
\begin{array}{ccccccc}
\alpha^{(n)} & \overset{(4.8)-(4.11)}{\longrightarrow} & C^{(n)} & \overset{(4.17)}{\longrightarrow} & (\mathrm{DIC},\mathrm{TA})^{(n+1)} & \longrightarrow & [CO_3^{2-}]^{(n+1)} \quad n = 1,2,\ldots \\
\uparrow & & & \overset{(4.5)}{} & & & \downarrow \\
 & & n+1 & \longleftarrow & n & &
\end{array}
\tag{4.18}
$$

where $\alpha^{(1)}$ is the dissolution rate derived from seawater values of DIC and TA. The iteration (4.18) is repeated for each box until the change in saturation from one step to the next drops below a prescribed limit:

$$
|\Omega_{i}^{(n)} - \Omega_{i}^{(n-1)}| \le \varepsilon_{\Omega}, \quad i = 1,\ldots,N, \tag{4.19}
$$

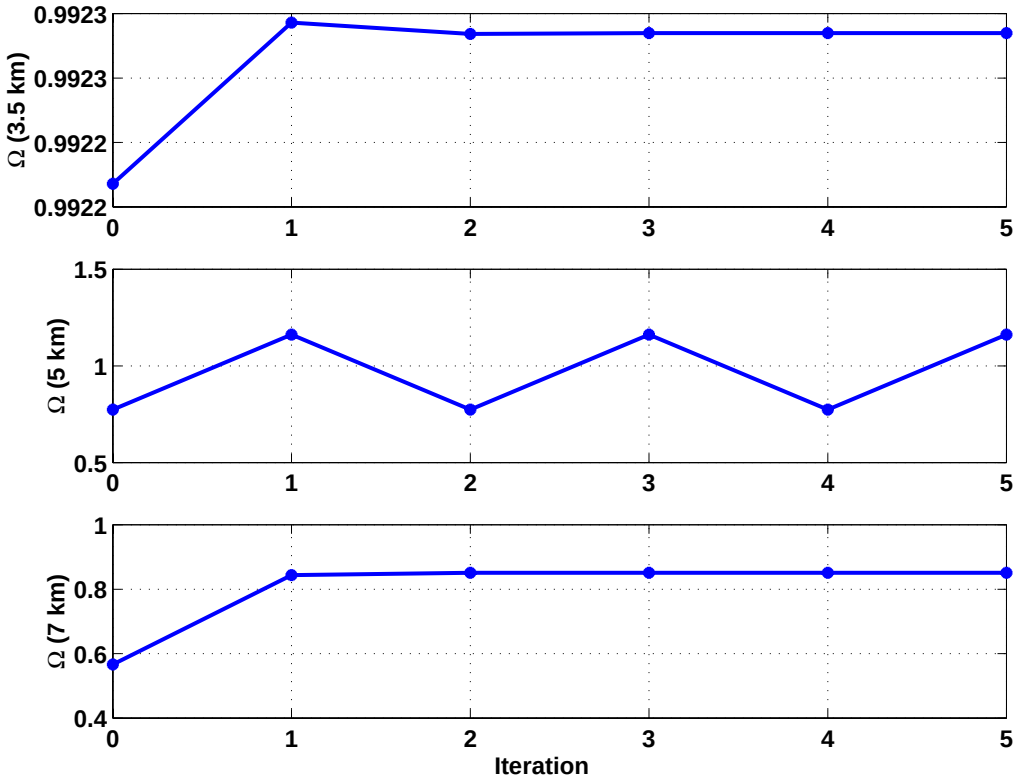

Figure 4.8: Saturation with respect to calcite at different iteration steps.

where the index i loops over all sediment boxes. Table 4.1 gives model results using standard parameter values (Table 4.3) with different values of the convergence limit. Obviously, $\varepsilon_\Omega \leq 10^{-5}$ is sufficient for convergence. The calculated values for the lysocline, CCD and the burial of calcite are discussed in the following section.

4.2 Modern reference configuration

The model is now used to calculate a modern reference configuration. The term 'modern' henceforth refers to the preindustrial state with an atmospheric CO_2 partial pressure of $\sim 280\,\mu$atm, as the thesis focuses on glacial - interglacial variations and does not consider the current, anthropogenically influenced rise of atmospheric pCO_2. Model parameters are given in Table 4.3. Two alternative assumptions are considered:

1. Dissolution of $CaCO_3$ takes place in the sediments only.

2. Some $CaCO_3$ is dissolved in the water column.

Observations [*Milliman et al.*, 1999] hint at water column dissolution of calcite. Although the underlying processes are not yet understood (cf. previous chapters), this feature is included as one scenario.

ε_Ω	Lysocline (km)	CCD (km)	Transition zone (m)	Burial (%)
10^{-2}	3.67	3.81	140	42.86
10^{-3}	3.93	4.18	250	35.52
10^{-4}	3.93	4.23	300	34.06
10^{-5}	3.93	4.23	300	33.90
10^{-6}	3.93	4.23	300	33.89
10^{-7}	3.93	4.23	300	33.89

Table 4.1: Model results for various error limits on the convergence of the saturation state. Relaxation parameter $\omega = 10$. The transition zone is the depth difference between the CCD and the Lysocline. Burial is the fraction of calcite rain that is not dissolved.

The resulting sedimentary carbonate profiles are shown in Fig. 4.9 and 4.10. Key values are given in Table 4.2. The lysocline and the CCD are defined here to be the depth where the calcium carbonate content drops below 95% and 10%, respectively.

Water column diss.	Lysocline (km)	CCD (km)	Transition zone (m)	Burial (%)
No	3.93	4.23	300	33.9
Yes	3.68	3.85	170	12.8

Table 4.2: Preindustrial reference model configuration (cf. Fig. 4.9 and 4.10).

Observational values for the calcite lysocline depth are 4.45 km in the Atlantic, 4 km in the Indian and 3.7 km in the Pacific [*Broecker and Takahashi*, 1977]. Thus, the reference configuration displays reasonable depths of lysocline. Various parameterization of the calcite dissolution kinetics have been tested (cf. Appendix A) and the kinetic parameters given by *Keir* [1980] are seen to yield the most realistic model results for lysocline depth and thickness of the transition zone. Under the assumption of calcite water column dissolution less calcium carbonate enters the sediment, thus the lysocline is located shallower and the transition zone is thinner as without water column dissolution. *Milliman and Droxler* [1996] estimate 60% of $CaCO_3$ production to dissolve in the water column and 18% to be buried in the sediments. In the modern reference configuration shown here, $\sim$ 34% of the production are buried in the sediments when no $CaCO_3$ dissolves in the water column. Taking water column dissolution into account leads to $\sim$ 13% of the carbonate production accumulating in the sediments, while $\sim$ 60% are dissolved in the water column.

Symbol	Parameter	Value	Reference
	Vertical dimension pore water box	10 cm	Emerson and Hedges [1988]
	Resolution of topography	10 m	-
	Open ocean production $CaCO_3$	$60\,\mathrm{Tmol\,a^{-1}}$	Milliman and Droxler [1996]
q	Clay rain as (weight) fraction of $CaCO_3$ rain	3%	Sanyal [pers. comm., 1999]
	Global primary production POC	$3764\,\mathrm{Tmol\,a^{-1}}$	Antoine et al. [1996]
	Open ocean POC production as a fraction of global production	70%	Longhurst et al. [1995]
σ	export ratio	0.11	Laws et al. [2000]
A	Open ocean surface area	$286\times10^6\,\mathrm{km^2}$	ETOPO5 data $>$ 2000m depth
κ	Calcite dissolution rate constant	$3\,\mathrm{d^{-1}}$	Keir [1980]
η	Calcite dissolution rate order	4.5	Keir [1980]
ϕ	Porosity pore water box	0.85	Berner [1980]
ρ_c	Specific weight of calcite	$2.7\,\mathrm{g\,cm^{-3}}$	Young [1994]
ρ_l	Specific weight of clay	$2.65\,\mathrm{g\,cm^{-3}}$	Grim [1962]
z_b	Boundary layer thickness	1 mm	Boudreau and Guinasso [1980]
$r_{C/N}$	Redfield ratio C:N	117:14	Anderson and Sarmiento [1994]

Table 4.3: Modern reference parameter values.

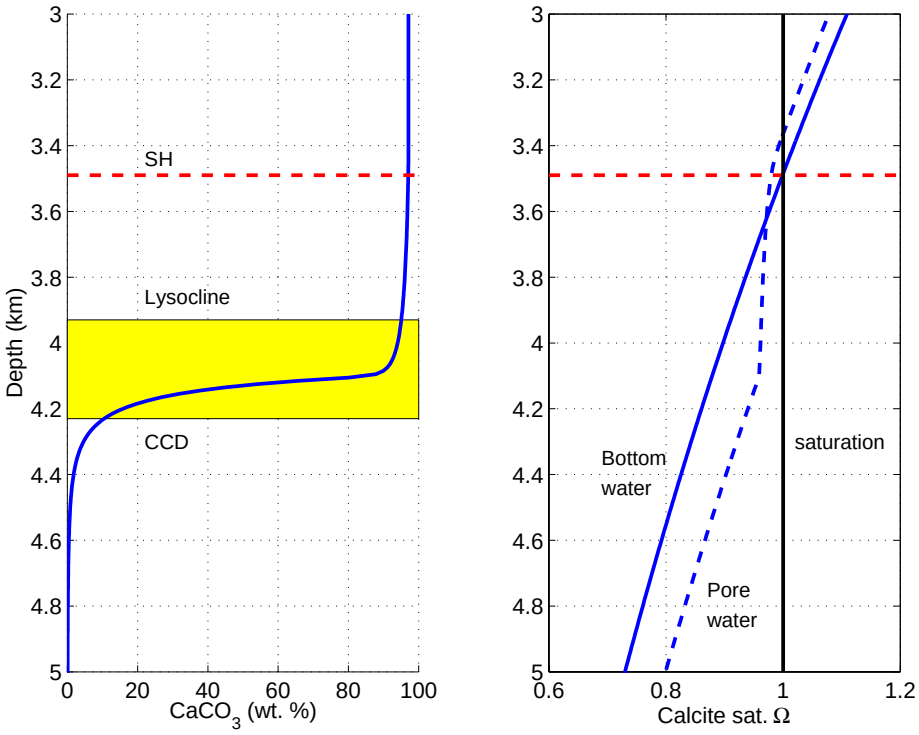

Figure 4.9: Modern reference calcium carbonate in sediment profile (left) and calcite saturation (right). No calcite dissolution in the water column. The saturation horizon is marked with the broken line at 3.49 km depth. The transition zone between the lysocline and the CCD is shaded. In the right graph, the solid line denotes the calcite saturation in bottom water, while the broken line refers to saturation in the pore waters. Note that above ~ 3.6 km, the sediment is more corrosive than the bottom water due to organic carbon remineralization. Below that point, calcite dissolution becomes progressively stronger, resulting in a pore water saturation state that is higher than in bottom waters.

Fig. 4.11 shows the C_{org} : $CaCO_3$ rain ratio in the reference configuration, together with observations of the rain ratio in the ocean. Field data are taken from a compilation by *Emerson and Bender* [1981] (see Table C.4) and from *Tsunogai and Noriki* [1987]. From the latter work, five open ocean stations in the central Pacific and North Atlantic are selected (stations number 18,19,23,24,27,28 and 29 in their notation). The rain ratios in the field data are a bit higher than in the model, reflecting the fact that the model operates on globally averaged data and the field data tends to miss low productivity areas. Furthermore, the model uses mean annual production values, while field data often are taken during the bloom season only.

Fig. 4.12 shows profiles of dissolved inorganic carbon (DIC) and alkalinity (TA) in bottom water and sediment corresponding to the carbonate content profile in Fig. 4.9. The gradients of DIC and TA between bulk sea water and pore water correspond to *p*H gradients of maximal 0.02 *p*H units, which is within the range observed by *Hales and Emerson* [1996, 1997]. Taking the number of time

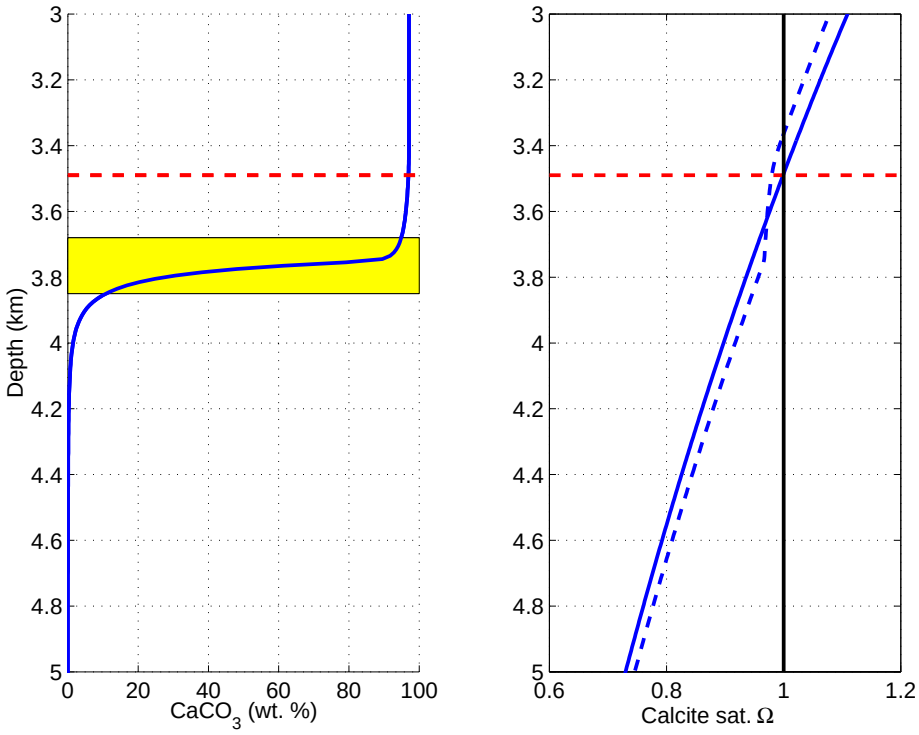

Figure 4.10: Calcium carbonate in sediment profile (left) and calcite saturation (right), where water column dissolution of calcite is considered. The lysocline is situated at 3.68 km, compared to 3.93 km under the assumption of no calcite dissolution in the water column.

steps that are calculated to fill up the boxes, one can derive the sediment growth rate, which is shown in Fig. 4.12. *Jahnke et al.* [1997] observe sedimentation rates of $5 - 20\,\mathrm{cm\,ky^{-1}}$ in a high production area on the Californian continental margin.

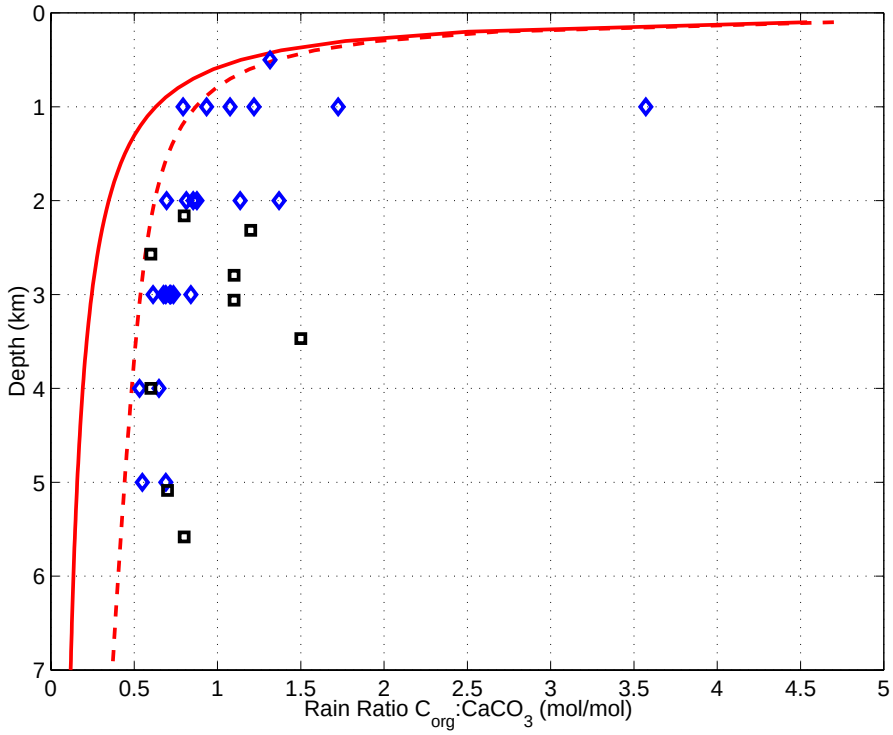

Figure 4.11: Molar C_{org} : $CaCO_3$ rain ratio at the sediment surface versus depth. Solid line: Reference run without carbonate dissolution in the water column. Dashed line: Reference run considering carbonate dissolution in the water column. Field data on rain ratios denoted with squares (Table C.4) and diamonds (data by *Tsunogai and Noriki* [1991]).

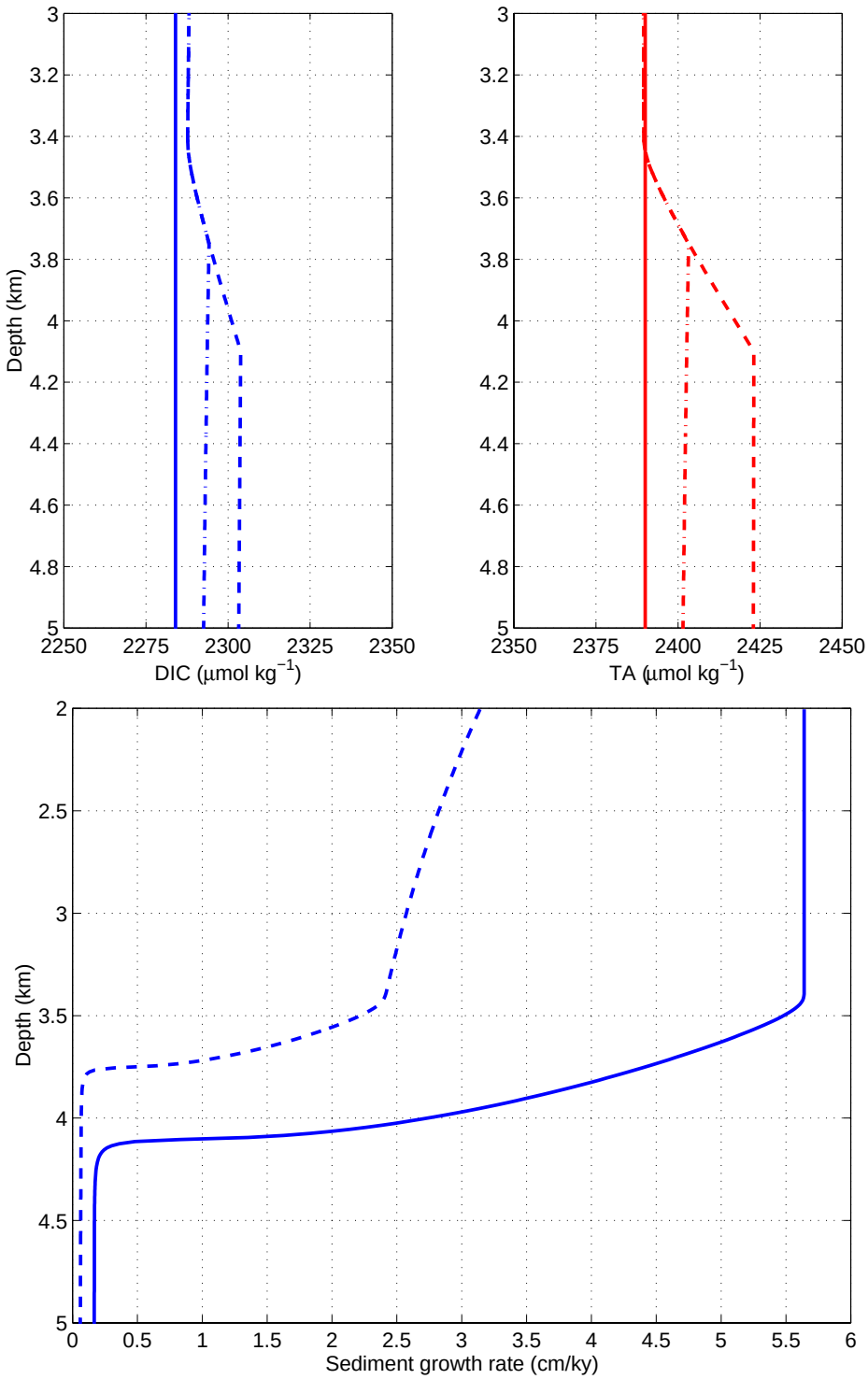

Figure 4.12: Top: DIC and TA in bottom water (solid lines) and sediment pore water (dashed lines without, dotted lines with calcite water column dissolution). Bottom: Sediment growth rate in the modern reference runs with (dashed) and without (solid) water column dissolution of calcite.

4.3 Glacial scenarios

4.3.1 A glacial baseline reference configuration

With modern profiles calculated, glacial scenarios can now be investigated. The lower pCO_2 values in glacial times require higher CO_3^{2-} concentrations compared to modern values. The impact of increased deep water $[CO_3^{2-}]$ is calculated in two steps (Table 4.4). First, modern global mean surface water concentrations of dissolved inorganic carbon ($\sum CO_2$) and alkalinity (TA) [*Takahashi et al.*, 1981, GEOSECS data] are used to calculate the surface oceanic CO_2 concentration. Applying the solubility constants by *Weiss* [1974] and a mean sea surface temperature of 15.5 °C, then yields a pCO_2 of 279 μatm. Reducing the temperature by 2 K and increasing salinity, $\sum CO_2$ and TA by 3% due to the proposed drop in sea level gives a pCO_2 of 266 μatm, denoted as the 'glacial baseline' in Table 4.4. $\sum CO_2$ and TA are then increased in a 1:2 ratio (corresponding to the effect of calcium carbonate dissolution) until the lysocline is located 600 m deeper than in the modern reference profile [*Broecker*, 1992]. This increase is added to surface concentrations as well, leading to a pCO_2 of 254 μatm, denoted by 'glacial lysocline' in Table 4.4. The corresponding sedimentary carbonate profiles are shown in Fig. 4.13. The lysocline is situated 600 m deeper than in the modern reference profile (Fig. 4.9), thus it is located at 4.53 km depth without and at 4.28 km depth with water column dissolution. The saturation horizon is marked with the broken line at 4.1 km depth. The transition zone between the lysocline and the calcium carbonate compensation depth (CCD) is thinner when considering dissolution in the water column, as then less $CaCO_3$ enters the sediments.

In a second step, $\sum CO_2$ and TA are increased in a 1:2 ratio from the 'glacial baseline' situtation to match a certain increase in deep water *p*H. This decreases atmospheric pCO_2 further. For a glacial scenario explaining 1 μatm atmospheric pCO_2 difference (with respect to the pCO_2 level reached by temperature and salinity changes), the CO_3^{2-} concentration has to increase by $\sim 1\ \mu\mathrm{mol\,kg^{-1}}$. Note that for $|\Delta pCO_2| < 60\,\mu$atm, approximately a one to one relationship holds (Fig. 4.14). For larger reductions in pCO_2, a larger increase in $[CO_3^{2-}]$ is required, which is due to the changing buffer capacity of seawater. To obtain the glacial-interglacial $\Delta pCO_2 = 80\,\mu$atm by changes in $[CO_3^{2-}]$, the saturation horizon would be required to deepen $\sim$ 3.7 km relative to its present position of $\sim$ 3.5 km, which would result in the whole oceanic water column to be supersaturated with respect to calcite.

	$\sum CO_2$	TA	S	T	$[CO_3^{2-}]$	pH	pCO_2
				Deep ocean values			
modern	2284	2390	34.76	2.0	82	7.78	
glacial baseline [a]	2353	2462	35.80	1.5	85	7.78	
glacial lysocline [b]	2371	2497			94	7.83	
$+20\,\mu mol\,kg^{-1}$ $[CO_3^{2-}]$	2388	2532			105	7.87	
$+50\,\mu mol\,kg^{-1}$ $[CO_3^{2-}]$	2436	2629			135	7.98	
$+100\,\mu mol\,kg^{-1}$ $[CO_3^{2-}]$	2512	2780			185	8.11	
				Surface ocean values			
modern	2012	2322	34.90	15.5	221	8.18	279
glacial baseline [a]	2072	2392	35.94	13.5	227	8.21	266
glacial lysocline [b]	2089	2426			240	8.23	254
$+20\,\mu mol\,kg^{-1}$ $[CO_3^{2-}]$	2107	2462			253	8.25	242
$+50\,\mu mol\,kg^{-1}$ $[CO_3^{2-}]$	2156	2559			290	8.31	214
$+100\,\mu mol\,kg^{-1}$ $[CO_3^{2-}]$	2232	2710			348	8.39	182

[a] $\sum CO_2$, TA and salinity increased by 3% due to sea level change. Temperature reduced by 0.5 °C in deep waters [*Labeyrie et al.*, 1987] and 2 °C in surface waters [*McIntyre et al.*, 1981].

[b] $\sum CO_2$, TA increased such that lysocline deepens 600 m.

Table 4.4: Calculation of the impact of increased deep water $[CO_3^{2-}]$ ($\mu mol\,kg^{-1}$) on atmospheric pCO_2. $\sum CO_2$, TA ($\mu mol\,kg^{-1}$) and S taken from global mean GEOSECS data [*Takahashi et al.*, 1981]. The maximum deep ocean pH shift is in line with findings of *Sanyal et al.* [1997]. Note that an increase of $100\,\mu mol\,kg^{-1}$ $[CO_3^{2-}]$ in deep water does not increase surface $[CO_3^{2-}]$ by the same amount because the addition is calculated via an increase in $\sum CO_2$ and TA and is thus dependent on the starting point.

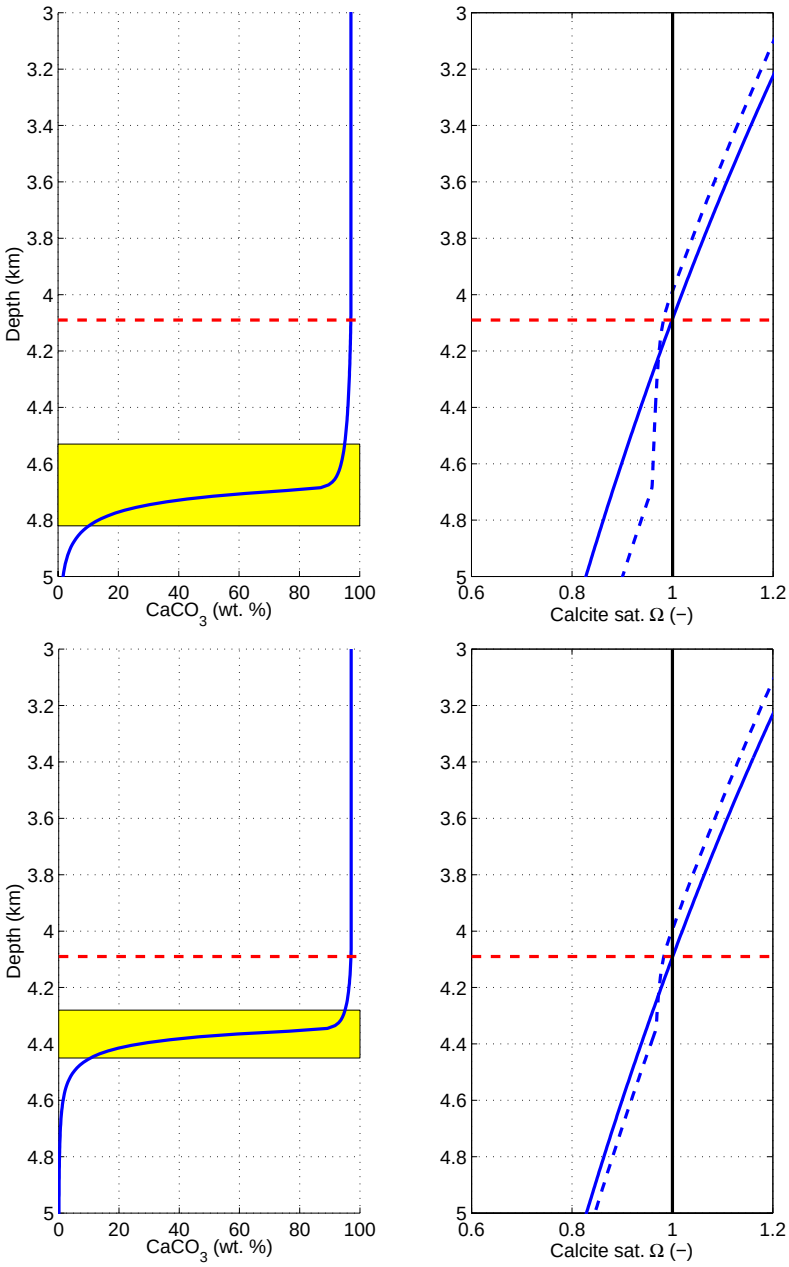

Figure 4.13: Glacial reference profiles of sedimentary calcium carbonate content (left) and calcite saturation (right), both without (top) and with calcite dissolution in the water column (bottom). The saturation horizon is marked with the broken line at 4.1 km depth. The transition zone between the lysocline and the CCD is shaded. In the right graph, the solid line denotes the calcite saturation in bottom water, while the broken line refers to saturation in the pore waters.

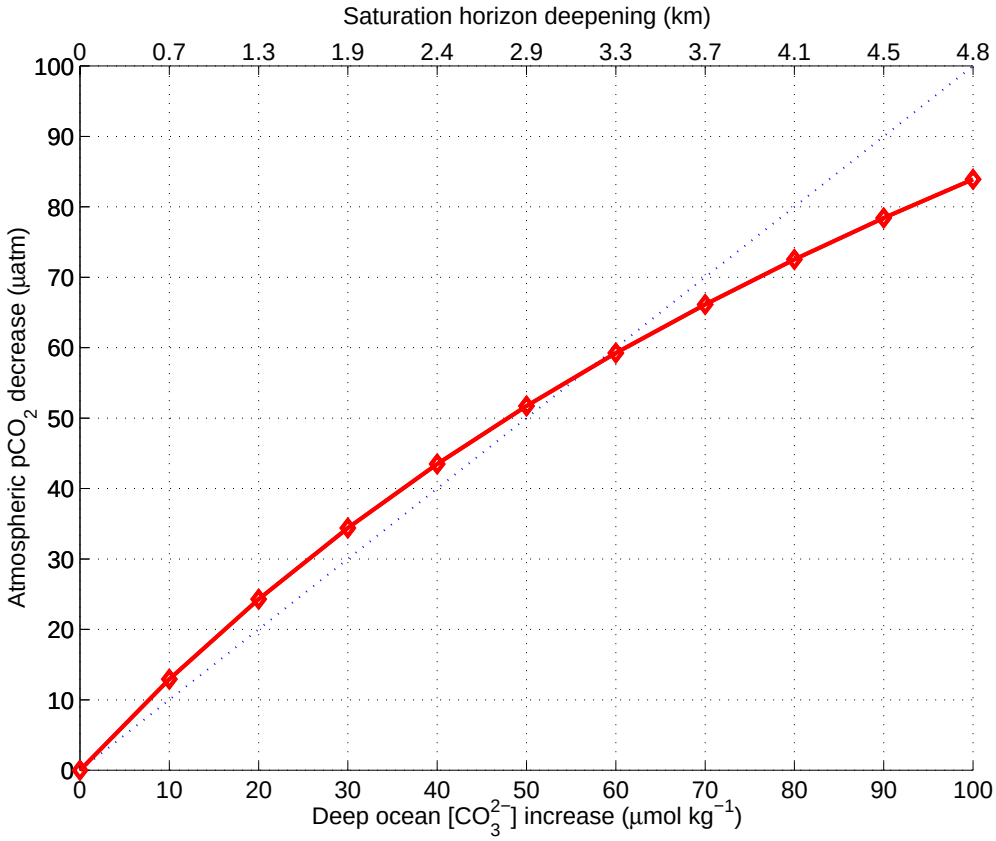

Figure 4.14: Reduction from the glacial baseline $pCO_2 = 266\,\mu$atm level (cf. Table 4.4) by increasing $[CO_3^{2-}]$ (solid line). The dotted line illustrates a 1:1 relationship. The corresponding deepening of the SH is indicated on the top axis.

4.3.2 Selected productivity change scenarios

An increase of the global production of organic carbon during glacial times has been proposed by a number of authors [*Altabet and Curry*, 1989; *Martin*, 1990; *Francois et al.*, 1992; *Marino et al.*, 1992; *Herguera and Berger*, 1994 and *Ganeshram et al.*, 1995] and is associated with higher nutrient availability during glacial times. However, this does not necessarily imply higher calcium carbonate production values during glacial times as well. It has been proposed that the production of $CaCO_3$ was decreased due to an ecological shift from calcareous to siliceous organisms [*Archer and Maier-Reimer*, 1994; *Broecker and Henderson*, 1998; *Harrison*, 2000]. The latter species are supposed to be more successful in areas of high productivity and colder temperatures, both conditions seem to prevail during the last glacial. *Kumar et al.* [1995] state that in the subantarctic zone, a region in the Southern Ocean at present dominated by carbonate-secreting plankton, opal accumulation rates increased several-fold during glacial periods, while carbonate production declined significantly.

Three different scenarios are investigated considering various glacial primary production values. The export production is calculated via the *Laws et al.* [2000] parameterization, as described in section 4.1.2.

- (a) Glacial C_{org} and $CaCO_3$ productivity is kept at modern values.
- (b) $CaCO_3$ and C_{org} production are increased by 50% and 75% over modern values [*Archer et al.*, 2000]
- (c) C_{org} production is increased (+30%) and $CaCO_3$ production is decreased (-30%) compared to modern values.

In this section, all model runs refer to the reference configuration without calcite dissolution in the water column. Scenarios including water column dissolution are investigated in the following section. For each scenario, initial conditions are given as the 'glacial baseline' in Table 4.4. A target pCO_2 value is prescribed and the SH is deepened accordingly by increasing bottom water $[CO_3^{2-}]$. The calcite lysocline is kept fixed 600 m deeper than in the preindustrial reference configurations by increasing the amount of organic carbon reaching the deep sea. This is done by changing the exponent τ in the flux parameterization (4.1):

$$F_{C_{org}}(z) = F_{C_{org}}(100)\left(\frac{z}{100}\right)^{-\tau}, \tag{4.20}$$

where $\tau = 0.858$ corresponds to the *Martin et al.* [1987] parameterization given in Eq. (4.1). By decreasing τ, more organic carbon reaches the deep sea, as is illustrated in Fig. 4.15. Thus, τ is tuned until the resulting lysocline depth is adjusted as required. A justification of deepening the organic carbon remineralization depth is given on page 88.

To illustrate the results, Fig. 4.16 shows the sedimentary carbonate profile in a specific model run. Here, the target pCO_2 value is 240 μatm, 26 μatm below the glacial baseline. This is achieved by increasing $[CO_3^{2-}]$, thus the calcite saturation horizon drops down to $\sim$ 4.75 km. C_{org} production is increased by 30% over modern values, leading to a larger portion of calcite dissolution above the

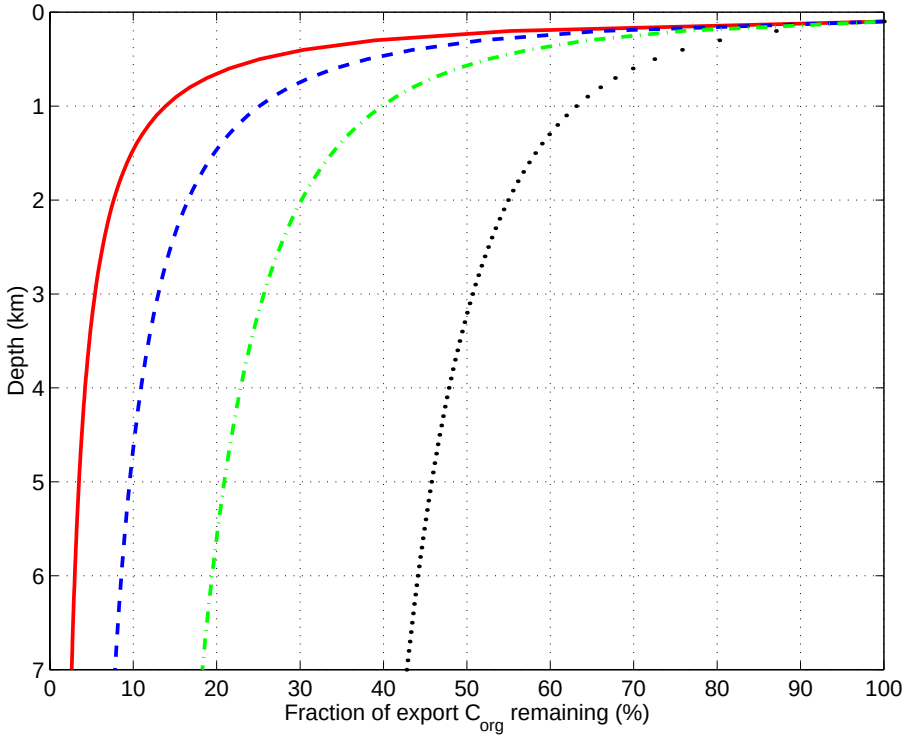

Figure 4.15: POC flux versus depth. Parameterization (4.20) with $\tau = 0.858$ (solid, 'Martin curve'), $\tau = 0.6$ (dashed), $\tau = 0.4$ (dash-dotted) and $\tau = 0.2$ (dotted). The curves are shown here to illustrate the applied mechanism.

saturation horizon. In contrast to the glacial baseline profile (Fig. 4.13), the transition zone has narrowed due to 30% decreased $CaCO_3$ production.

An overview of all model runs is given in Table 4.5. As in scenario (a) $CaCO_3$ and C_{org} production is fixed at modern values, the amount of organic carbon reaching the deep sea has to increase dramatically in order to achieve the glacial target pCO_2 values by decoupling the lysocline from the SH. A pCO_2 reduction of more than 60 μatm is not possible, even if all organic carbon would reach the sediments. In scenario (b), the required deepening of the remineralization depth is lowest, due to the large increase in organic carbon production. Finally, scenario (c) demonstrates that a decoupling of the lysocline from the SH is possible for both an increase and a decrease in $CaCO_3$ production. Results are illustrated in Fig. 4.17. Obviously, organic carbon production is the critical variable. The more organic carbon is produced, the more atmospheric pCO_2 shift may be explained without large reorganizations of the remineralization depth. The observed shift of 80 μatm pCO_2 cannot be explained by scenario (a). The other two scenarios yield the full shift only with unrealistically high amounts of organic carbon reaching the seafloor. In scenario (b), 38% of export production would have to reach the sediments, compared to a modern value of $\sim$ 8%. Accepting 20% of the export production reaching the deep sea as an upper realistic threshold yields a maximum pCO_2 reduction of (a) $\sim$ 30 μatm, (b) $\sim$ 50 μatm and (c) $\sim$ 45 μatm.

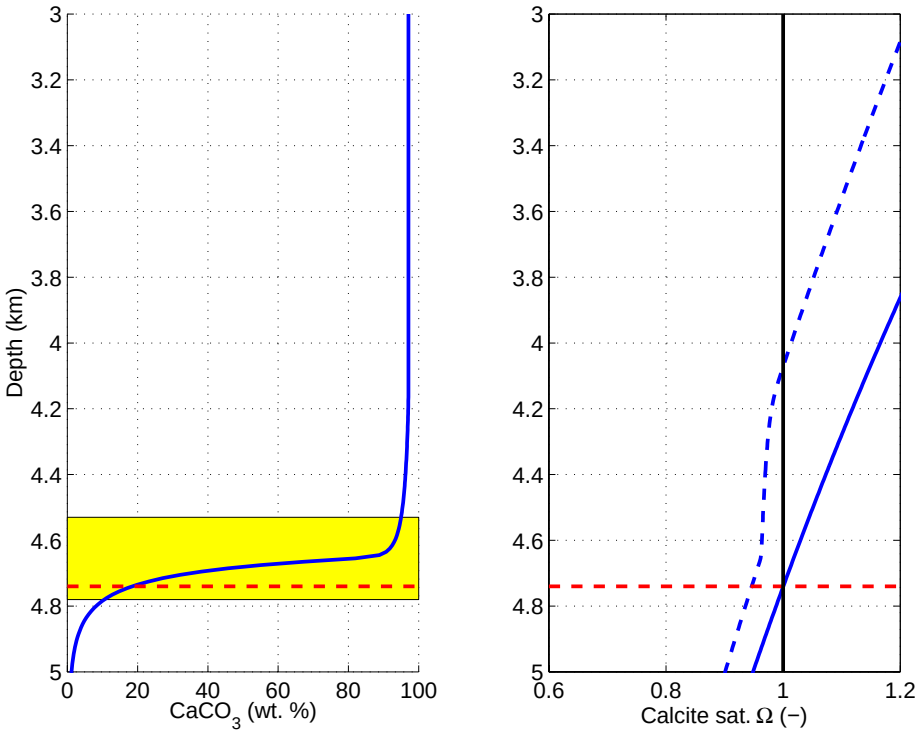

Figure 4.16: Scenario (c): Increased global production of organic carbon and decreased production of calcium carbonate. pCO_2 is 240 μatm, i.e. $\sim$ 40 μatm below the preindustrial level.

The 'glacial lysocline' level (cf. Table 4.4) accounts for 24 μatm reduction, resulting from changes in temperature, salinity, concentration of dissolved substances and lysocline shift. In all scenarios, productivity changes have to be accompanied by an increase of the portion of organic carbon reaching the deep sea in order to obtain a larger reduction in atmospheric pCO_2. A readjustment of the C_{org} remineralization depth has been proposed by *Boyle* [1988 a,b]. The postulated ecological shift towards siliceous organisms [*Archer and Maier-Reimer*, 1994; *Broecker and Henderson*, 1998; *Harrison*, 2000] would lead to deeper remineralization depths as well, since the relatively larger diatoms have a higher sinking velocity than coccolithophorids [*Smetacek*, 1985; *Smetacek*, 2000; *Kemp et al.*, 2000]. Thus, a diatom dominated system transports organic carbon deeper than a system dominated by coccolithophorids does, provided remineralization time constants are similar.

Fig. 4.18 compares modeled $C_{org} : CaCO_3$ rain ratios with literature data. The rain ratios needed to achieve glacial pCO_2 reductions of 30 μatm are amid modern open ocean observations, while the rain ratios calculated for a 50 μatm change are in the range of rain ratios measured in high production areas (taken from *Tsunogai and Noriki* [1991], stations number 5,6,15,16,25,26 in their notation, California upwelling and Central North Pacific). Glacial open ocean rain ratios are likely to be higher considering increased organic carbon production during glacial times. Thus, the rain ratios requested by the model for driving the atmospheric pCO_2 down to 50 μatm are within a reasonable range.

Scenario	ΔpCO_2 (μatm)	C_{org} (%)	τ	$RR_{2\,km}$	$RR_{7\,km}$
Glacial lysocline level	-24.6	7.6	0.858	0.35	0.12
(a) C_{org}, $CaCO_3$	-30	21.0	0.520	0.95	0.50
production constant	-40	41.9	0.290	1.90	1.32
	-50	61.9	0.160	2.81	1.30
	-60	81.6	0.068	3.70	3.40
(b) C_{org}, $CaCO_3$	-30	10.1	0.765	1.27	0.49
production	-40	15.6	0.620	1.97	0.91
increased	-50	21.0	0.521	2.65	1.38
	-60	26.4	0.444	3.33	1.91
	-70	32.1	0.379	4.05	2.52
	-80	38.0	0.323	4.80	3.21
(c) C_{org} production	-30	6.34	0.920	1.15	0.37
increased,	-40	16.30	0.605	2.97	1.39
$CaCO_3$ production	-50	25.33	0.458	4.61	2.60
decreased	-60	34.29	0.357	6.24	4.00
	-70	43.32	0.279	7.89	5.57
	-80	52.80	0.213	9.61	7.37

Table 4.5: Model results showing the required increase in the fraction of C_{org} export production reaching sediments deeper than 2 km to explain the glacial atmospheric pCO_2 shift. The value of τ, the exponent in Eq. (4.20), reflects the remineralization depth of organic carbon. It deepens with decreasing τ. $RR_{2\,km}$ and $RR_{7\,km}$ denote the molar rain ratio $C_{org} : CaCO_3$ at 2 km and 7 km depth, respectively.

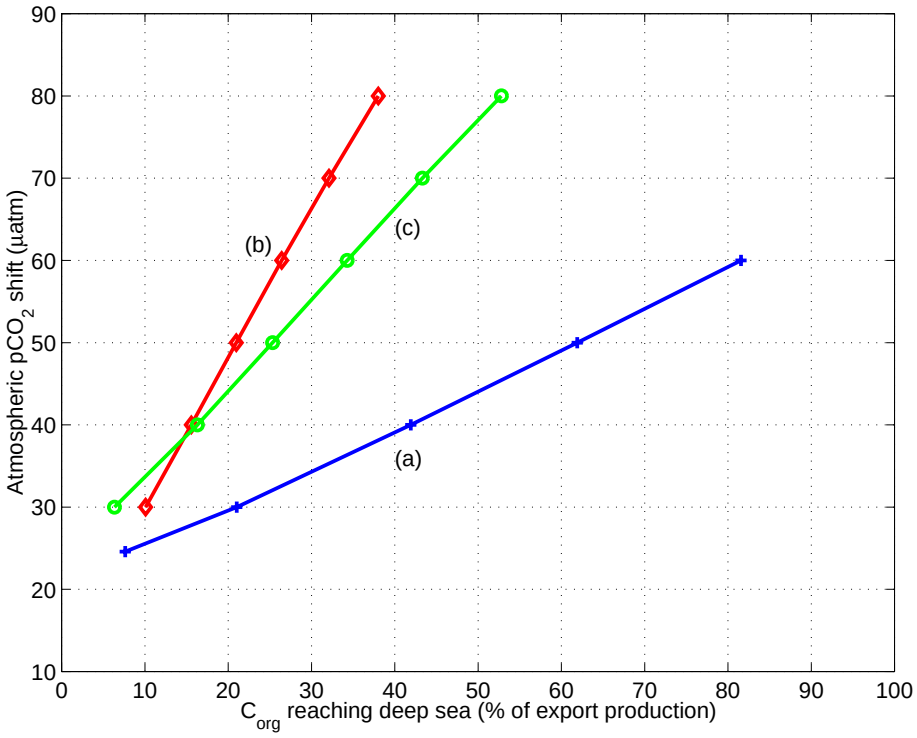

Figure 4.17: Results of model runs for scenarios (a) - (c). (Cf. Table 4.5).

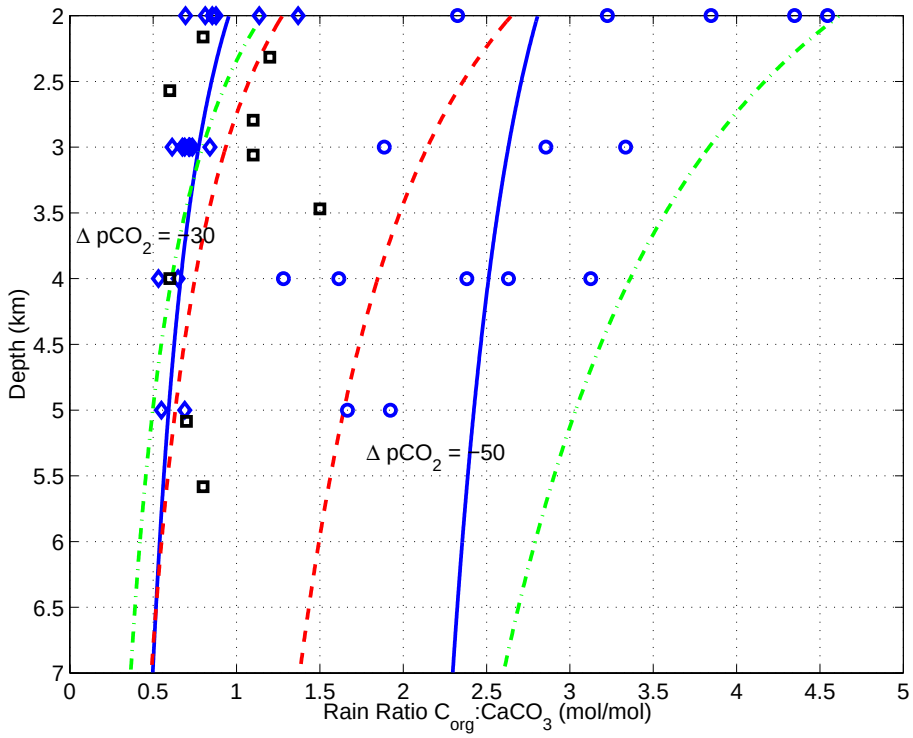

Figure 4.18: Modeled C_{org} : $CaCO_3$ rain ratios compared with literature data. Rain ratio needed to lower atmospheric pCO_2 by 30 and 50 μatm, respectively. Solid line: Scenario (a), no production change. Broken line: Scenario (b), production increased. Dashed-dotted line: Scenario (c), C_{org} production increased, $CaCO_3$ production decreased (Table 4.5). Field data on rain ratios denoted with squares (Table C.4) and diamonds (data by *Tsunogai and Noriki* [1991]). The circles represent data from high productivity areas [*Tsunogai and Noriki*, 1991].

4.3.3 Investigating the full range of productivity change

In this section, a wide range of changes in $CaCO_3$ production (-60% up to +60% compared to present day values) and C_{org} production (up to 100% increase from the modern value) are investigated with respect to their effect on glacial atmospheric CO_2 concentration. Model runs are performed under various assumptions (cf. Table 4.6). In all scenarios, 10% of the export production are allowed to reach the deep sea below 2 km. Thus, it is assumed that remineralization of organic carbon has not deepened significantly in glacial times. The scenarios tested in the previous section explain at most 30 μatm pCO_2 reduction in this case (Fig. 4.17).

The modelling approach is a bit different from the one followed in the previous section: Here, productivity changes as well as the shape of the organic carbon flux curve (cf. Eq. (4.1)) are prescribed. By increasing deep water $[CO_3^{2-}]$, the saturation horizon is adjusted until the lysocline depth matches the observed 600 m shift between glacial and modern times. Surface $\sum CO_2$ and TA are then changed analogous and the resulting glacial pCO_2 value is calculated.

In the real world, biological production is not spatially homogeneous but rather patchy with local blooms. Thus, the expected increase in production during glacial times must have led to locally increased export ratios, but across large areas the export ratio has not changed with respect to the present value. Using globally averaged values as in the presented model might overestimate the influence of export ratios that depend on primary production. Thus, scenarios are included that consider no change in export ratio, representing a conservative view.

	No water column dissolution of $CaCO_3$	Water column dissolution of $CaCO_3$
Export ratio of C_{org} changes with primary production	Scenario 1	Scenario 3
Export ratio fixed to modern value	Scenario 2	Scenario 4

Table 4.6: Assumptions of considered scenarios.

Fig. 4.19 shows resulting glacial pCO_2 values for scenarios 1 and 2. In scenario 1, the calculated atmospheric pCO_2 concentrations range from 231 to 257 μatm, i.e. 22-48 μatm below the preindustrial value. Glacial pCO_2 is seen to be more sensitive to changes in the production of organic carbon than to variations in calcium carbonate rain. $CaCO_3$ production correlates positive with pCO_2, while C_{org} production correlates negative with pCO_2, as is expected from the carbon pumps (cf. Section 1.1.2).

The picture is much more regular in scenario 2. Fixing the export ratio at the present day value

of $\sigma = 0.11$ decreases the range of glacial pCO_2 values to 245 to 258 μatm, i.e. $21 - 34\,\mu$atm below the preindustrial value. Unlike the situation in scenario 1, here the contour lines are straight and equidistant. Thus, pCO_2 changes linearly with production of C_{org} and $CaCO_3$. Given a fixed $CaCO_3$ production, the investigated change in C_{org} production attributes only $\sim 2.5\,\mu\mathrm{atm}$ change in pCO_2. This limited influence of organic carbon production on the atmospheric pCO_2 is attributable to the fact that the model is parameterized such that only 10% of the organic carbon export production (i.e. a mere 1% of primary production, PP) reaches depths below 2 km. Larger changes in the atmospheric pCO_2 are possible only with a larger deepening of the organic matter remineralization depth.

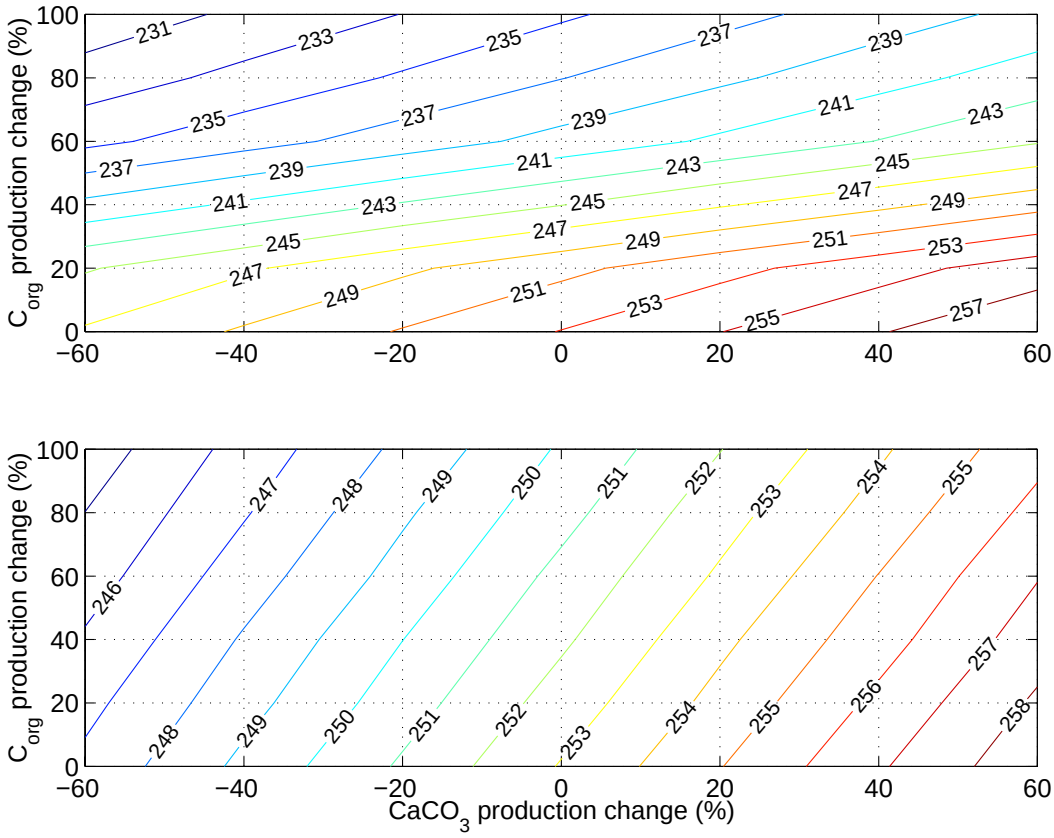

Figure 4.19: Modeled glacial pCO_2 for various $CaCO_3$ and C_{org} production changes. It is assumed that 10% of the export production of organic carbon reaches depths below 2 km (modern value: $\sim 8\%$). Top: Scenario 1, export ratio σ depends on PP, i.e. $\sigma \geq 0.11$. Bottom: Scenario 2, export ratio fixed to $\sigma = 0.11$.

Fig. 4.20 shows the range of rain ratios calculated in scenario 1. To reach a glacial target pCO_2 of 240 μatm, for example, a rain ratio of 2-3 at 2 km depth is needed, while at 4 km depth, the model requires a rain ratio of 1-1.5. Given the range of present-day rain ratios indicated by the shaded areas [*Tsunogai and Noriki*, 1991], a glacial pCO_2 of $230 - 240\,\mu$atm is achievable when rain ratios

observed in present-day high productive areas prevail during glacial times.

Fig. 4.21 shows calculated rain ratios in scenario 2, i.e. the same as in Fig. 4.20 but with the export ratio fixed to the modern value. In this case, atmospheric pCO_2 values less than 245 μatm are not reached. The rain ratio plots show less scatter than in Fig. 4.20 since the export ratio does not scale with PP in this case, hence, less organic carbon variability is seen in the deep sea.

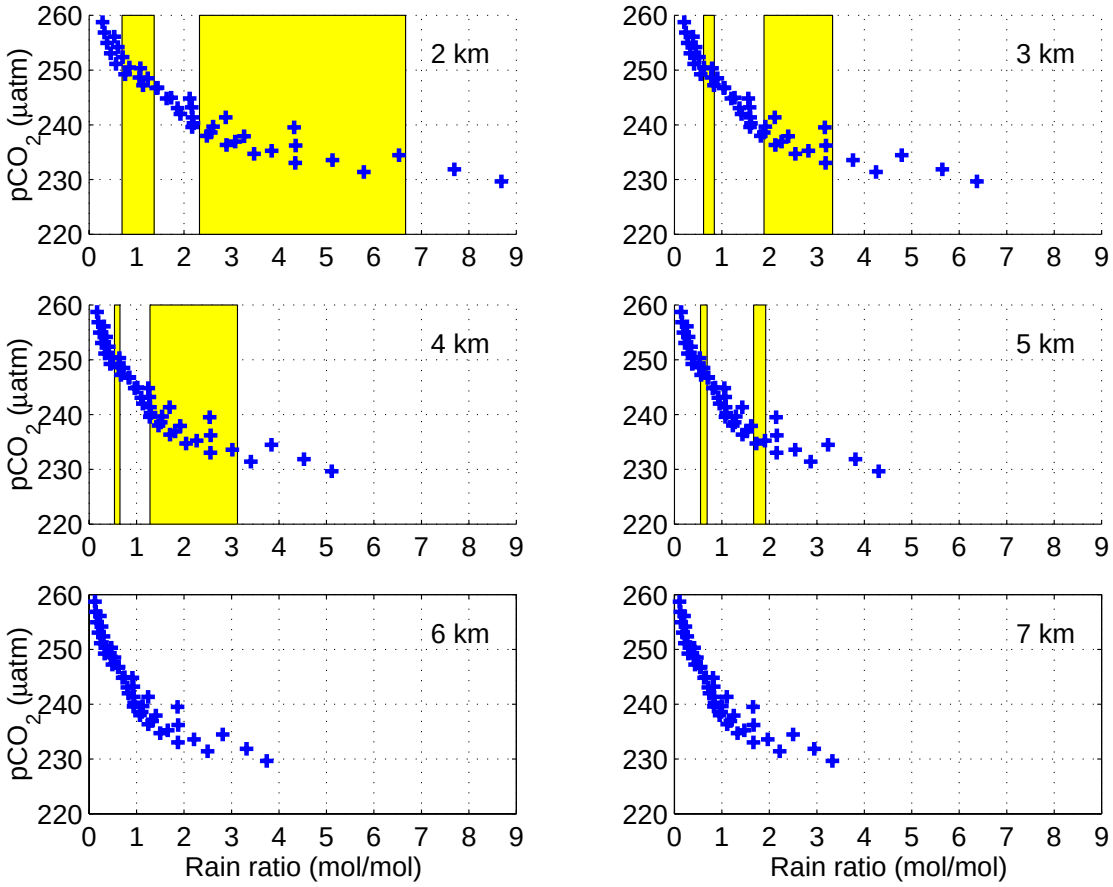

Figure 4.20: Scenario 1 (Variable export ratio, no water column dissolution of calcite): Atmospheric pCO_2 versus $C_{org} : CaCO_3$ rain ratio at 2 km, 3 km, ... 7 km depth. The shaded areas show the range of rain ratios found by *Tsunogai and Noriki* [1991]. Lower values taken from open ocean stations, higher values taken from high productivity areas (cf. Fig. 4.18, no data for 6 km and 7 km depth).

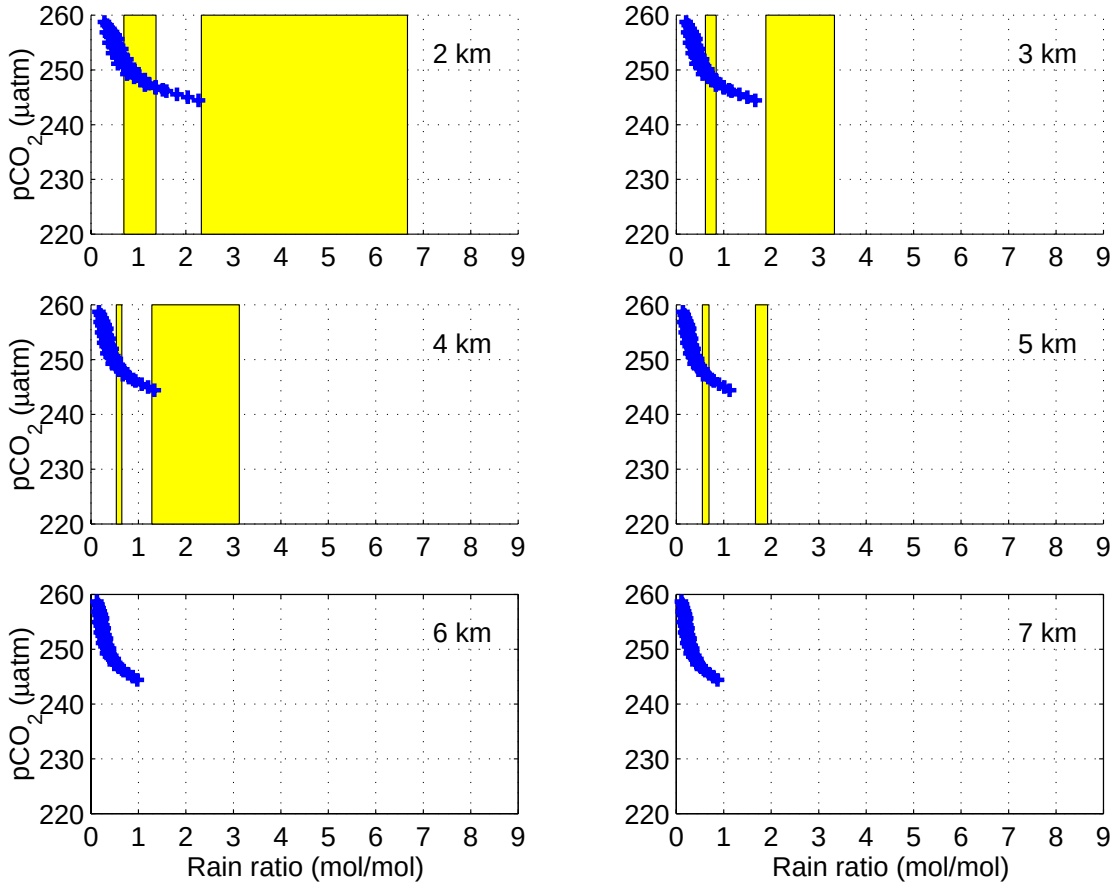

Figure 4.21: Scenario 2 (Fixed export ratio, no water column dissolution of calcite): Atmospheric pCO_2 versus $C_{org} : CaCO_3$ rain ratio at 2 km, 3 km, ... 7 km depth, displayed as in Fig. 4.20.

Fig. 4.22 shows the results of scenario 3 and 4, the model runs with water column dissolution of calcium carbonate. Compared to scenarios 1 and 2, the range of calculated pCO_2 values is slightly reduced, ranging between 233-254 μatm in scenario 3 and from 248 to 255 μatm in scenario 4. Given a fixed change in C_{org} production, the variability in pCO_2 when changing carbonate production is reduced, due to the fact that some carbonate dissolves in the water column and less is reaching the sediments. Considering no C_{org} production change, glacial pCO_2 ranges between 247 and 259 μatm without water column dissolution, while it ranges between 250 and 255 μatm when including water column dissolution.

Fig. 4.23 and 4.24 display modeled rain ratio values and, again, do not differ significantly from the corresponding plots for scenarios 1 and 2. The rain ratios calculated in Scenario 3 scatter less than in scenario 1 due to less variability in calcium carbonate rain.

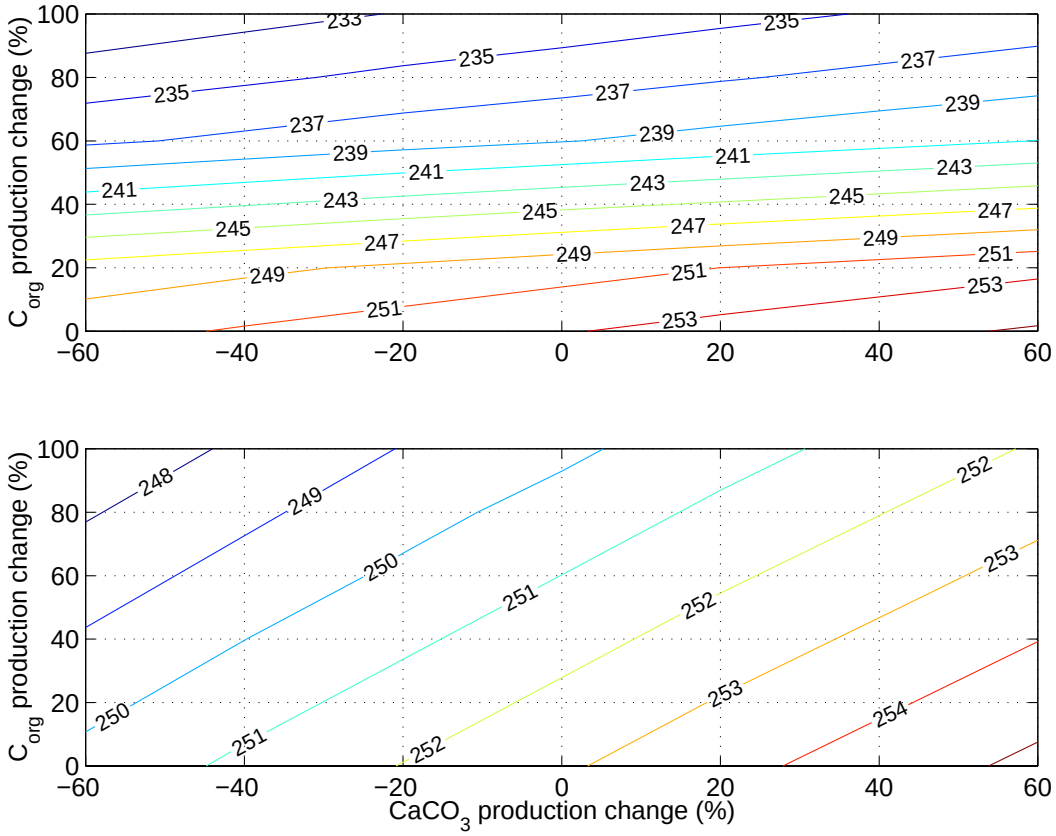

Figure 4.22: Modeled glacial pCO_2 for various $CaCO_3$ and C_{org} production changes. It is assumed that 10% of the export production of organic carbon reaches depths below 2 km (modern value: $\sim$ 8%). Some of the carbonate dissolves in the water column. Top: Scenario 3, export ratio σ depends on PP, i.e. $\sigma \geq 0.11$. Bottom: Scenario 4, export ratio fixed to $\sigma = 0.11$.

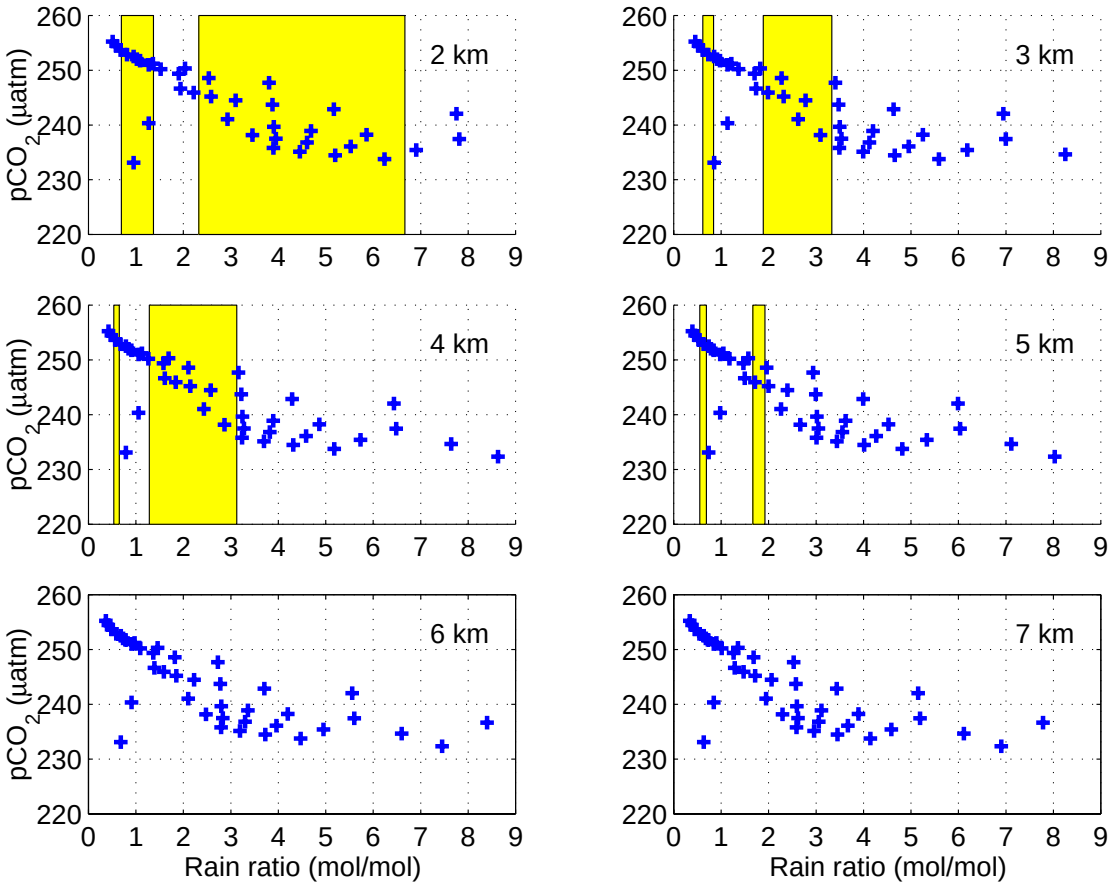

Figure 4.23: Scenario 3 (Variable export ratio, water column dissolution of calcite): Atmospheric pCO_2 versus rain ratio at 2 km, 3 km, ... 7 km depth, displayed as in Fig. 4.20.

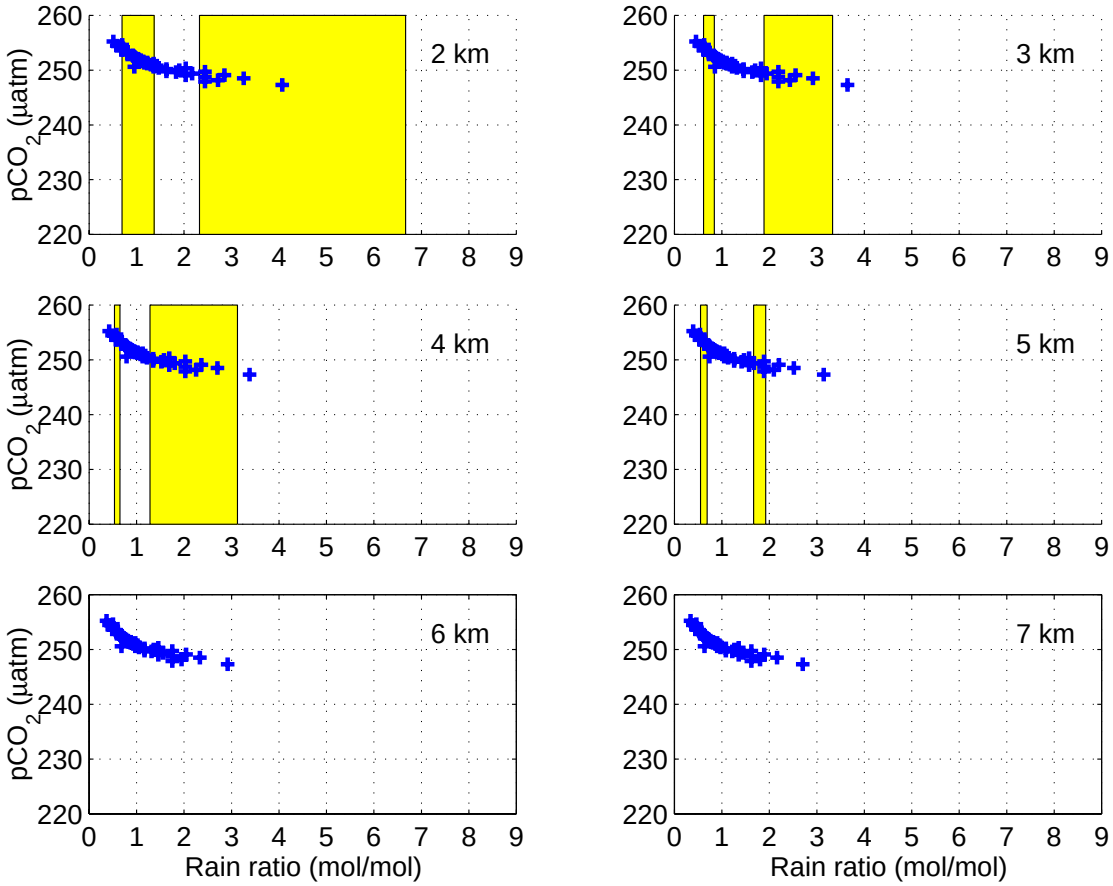

Figure 4.24: Scenario 4 (Fixed export ratio, water column dissolution of calcite): Atmospheric pCO_2 versus rain ratio at 2 km, 3 km, ... 7 km depth, displayed as in Fig. 4.20.

In summary, the model runs show that respiration driven dissolution can significantly influence the atmospheric pCO_2 only when the export ratio is dependent on the primary production. Otherwise, the amount of organic carbon reaching the deep sea sediments is simply too small. With fixed export ratios, variability in $CaCO_3$ production has a greater influence on atmospheric pCO_2 than variability in organic carbon production has.

The results do not differ much whether calcium carbonate is dissolved in the water column or not. This shows that not the fact of water column dissolution is decisive, but the change of material fluxes relative to today. That is, as long as the fraction of exported calcite dissolving in the water column does not change over time, the amount of calcite dissolving in the water column is not influencing the variability of pCO_2 with variable C_{org} and $CaCO_3$ production.

Assuming increased organic carbon productivity during the LGM yields C_{org}:$CaCO_3$ rain ratios that are comparable to modern rain ratios in high productivity areas, as marked in Fig. 4.20,4.21,4.23 and 4.24. Thus, glacial pCO_2 levels of $\sim 230 - 240\,pCO_2$ can be achieved within reasonable rain ratio ranges.

Chapter 5

Summary and conclusions

In this work, four models have been developed to investigate open questions concerning the marine carbonate cycle, as mentioned in the Introduction:

- Can the estimated dissolution of calcium carbonate in the water column be explained by biologically mediated mechanisms ?
- How much of the observed glacial to interglacial shift in atmospheric pCO_2 is attributable to changes in the marine carbonate pump ?
- Can the observations of increased glacial *p*H and lysocline depth be reconciled by a decoupling of the lysocline from the saturation horizon ?

First, a short summary is given of the answers. Then the conclusions that can be drawn from the models are discussed in more detail.

The observed dissolution of calcium carbonate in the water column can partially be explained by the mechanisms tested in this work. A significant portion may be attributed to dissolution in zooplankton guts. Direct physico-chemical dissolution of individually settling particles is seen to be significant in the undersaturated waters of the North Pacific only. Dissolution facilitated by respiration processes in marine snow aggregates does not contribute to the observed loss of calcite in the water column. The corresponding model simulations reveal that the size and settling velocities of macroaggregates are unfavourable to sustain an undersaturated microenvironment against an oversaturated bulk medium.

Turning to the second key question, it is concluded that a glacial to interglacial pCO_2 shift of $\sim 40\,\mu$atm can be explained by changes in the marine carbonate pump. This is approximately two-fold the amount of conventional estimates (which take into account changes in temperature, salinity and sea level only) and half of the total shift ($\sim 80\,\mu$atm) in atmospheric CO_2 concentration derived from ice cores.

Finally, the observations of increased glacial *p*H and lysocline depth cannot be reconciled. It is seen that the lysocline can be, and most probably was, decoupled from the saturation horizon. However, the decoupling needed to be in line with an increased *p*H of 0.3 units is not possible within current estimates on glacial to interglacial production changes.

5.1 Carbonate dissolution in the water column

Two models of dissolution of settling $CaCO_3$ particles in the water column have been developed. The derived physical constraints in the model considering physico-chemical dissolution of individually settling particles reveal that carbonate dissolution in the water column is feasible. As far as calcite is concerned, comparison with the literature reveals that only coccolithophorids and coccoliths sink at rates that make dissolution in the water column possible. Foraminifera sink so fast that virtually no dissolution takes place before reaching the seafloor. On the other hand, the sinking rates given in the appendix all apply to empty (senescent) foraminifera shells. Living organisms are likely to settle much slower [*Jelle Bijma*, pers. comm., 1999]. There is very limited work on pteropod settling rates, they are expected to sink at least as fast as foraminifera. Only due to the better solubility of aragonite compared to calcite, water column dissolution of pteropods can be expected, ranging up to 90% in the model applied to the North Pacific at 5 km depth (Fig. 2.7, 2.8). Thus, the alkalinity maximum in intermediate waters of the Pacific Ocean might be explained in part by water column dissolution of pteropods.

Respiration driven dissolution of calcite in the water column seems to be unlikely, considering the results of the model presented here. The size, settling velocity and porosity of marine snow aggregates is unfavourable for creating a microenvironment with sufficient gradient to convert an oversaturated bulk environment into a locally undersaturated state. However, the amount of modelled calcite dissolution is also dependent on the kinetic parameters, which are still subject of debate. The parameters proposed by *Keir* [1980] lead to slow dissolution kinetics, so the standard model runs presented here give a conservative view. Even with these slow dissolution kinetics, significant respiratory driven dissolution is calculated for porosities less than 0.4. There is no evidence in the literature for marine snow aggregates having porosities smaller than 0.9. However, small aggregates may well exhibit decreased porosities [*Ploug et al.*, 1999]. The porosity of marine snow aggregates increases with increasing aggregate size, because they are fractal objects, with fractal dimensions of around 1.4 to 1.5 [*Logan and Wilkinson*, 1990; *Alldredge*, 1998]. Thus, small and less porous aggregates, which are more favourable for respiration driven dissolution, cannot be ruled out. The model may be improved by adopting a less idealized geometry. The heterogeneous nature of marine snow aggregates may lead to chemical environments inside the aggregate that are not homogeneous as modelled here, altering shape and magnitude of the microenvironment around the aggregate.

The proposed model of carbonate dissolution in zooplankton guts demonstrates that this mechanism contributes to the observed loss of calcium carbonate in the water column. When grazing is continuous, model results yield no significant dissolution. Thus, the high amounts of dissolution (up to 73%) observed by *Harris* [1994] cannot be reproduced under the assumption of constant grazing. The most likely scenario, however, involves alternating grazing and non-grazing periods. This approach yields dissolution fractions up to $\sim 25\%$, with or without feeding restricted to the nighttime period. The potential for calcite dissolution increases with longer non-grazing cycles. The most critical parameter is the gut *p*H, as only *p*H values lower than 6.5 lead to significant dissolution. Since

*p*H data to date are very limited, it may well be that gut *p*H is much lower than measured by *Pond et al.* [1995]. The parameters of calcite dissolution kinetics are taken from experiments of *Keir* [1980] with complete coccoliths. As it is likely that liths are broken during ingestion or mechanical action inside the gut, dissolution should be a bit more effective. Hence, a conservative view is presented here. In bloom situations, community grazing pressure of copepods seems to be too low to significantly contribute to water column calcite dissolution. However, in pre- or post-bloom situations, grazing pressure is assumed to be higher, including grazing on microzooplankton and consumption of faecal pellets, giving rise to $\sim 15\%$ of standing stock calcite dissolved in copepod guts. Compared to $CaCO_3$ dissolution in the upper water column on the order of 60% as reported by *Milliman et al.* [1999], it is concluded that dissolution of calcite in copepod guts does not account for the majority of observed carbonate loss in the water column but may contribute a significant portion. However, further measurements on gut *p*H, ingestion rates and grazing pressure in the field are needed to better constrain the numerical results of the model presented here, as well as to extend the model to include other zooplankton (e.g. pelagic tunicates: *Urban et al.* [1992; 1993]) known to feed on coccolithophorids.

5.2 Sedimentary carbonate dissolution

A conceptual model of calcite accumulation and dissolution in the oceanic sediments has been developed that simulates modern conditions reasonably well. A number of model runs testing different assumptions on changed biological productivity during glacial times have been performed. Results show that a decoupling of the glacial calcite lysocline from the saturation horizon is very likely to have taken place (as suggested by boron isotope based *p*H-reconstructions). In contrast to the results of *Sigman et al.* [1998], it is found that even an increase in both organic carbon production and calcium carbonate production (the latter increasing surface ocean pCO_2) is in line with reduced atmospheric pCO_2. The increased organic carbon flux can compensate the carbonate production by respiration driven dissolution in the sediment. *Sigman et al.* [1998] focused on low latitude production changes and concluded that a decoupling of the lysocline from the saturation horizon is not possible. *Broecker et al.* [1999], however, recently showed that the role of low and mid latitude changes in the reorganization of the glacial carbonate pump has been underestimated hitherto. As high productivity prevails in low latitudes, the impact of organic carbon production on the marine carbonate pump is a relevant factor in regulating atmospheric pCO_2 shifts.

Glacial simulations reveal that, considering respiration driven dissolution in the marine sediments, a greater atmospheric pCO_2 shift than the conventional estimate of $20\,\mu$atm is connected with the carbonate pump. The glacial pCO_2 decrease attributable to changes in the marine carbonate pump is more likely to be on the order of $30 - 50\,\mu$atm. However, in contrast to both the boron isotope reconstructions and the results of *Archer and Maier-Reimer* [1994], the full glacial shift of $80\,\mu$atm cannot be explained by productivity change mechanisms. A deep water *p*H change of 0.3 units cannot be simulated with the proposed model within realistic ranges of productivity and organic

carbon remineralization depth changes. If the glacial lysocline was not located 600 m deeper than today, but has changed its position to a less degree, results would not change principally. The quantitative estimates on the contribution of carbonate pump to the observed pCO_2 shift would be decreased, however. A reduced deepening of the lysocline would simply increase the need of production change and deepening of the remineralization depth to explain the same amount of pCO_2 changes by the mechanisms investigated here. Quantitative estimates have to be constrained better in a model resolving regional and seasonal variability, for which the model developed here can serve as a base. Furthermore, the proposed model can be applied to proxies other than calcium carbonate. For example, it may be developed further to simulate the accumulation and dissolution of silicate in the marine sediments.

Acknowledgements

A lot of people have contributed in some way or other to the present thesis. First of all, I would like to thank Dieter Wolf-Gladrow for advising me throughout the thesis and encouraging me in difficult times. I thank Dirk Olbers for writing a review.

I want to thank Abhijit Sanyal for guiding me into the carbonate world. With Jelle Bijma, Dieter Wolf-Gladrow, Richard Zeebe, Christoph Völker and Guy Munhoven I had many fruitful discussions. Ingrid Zondervan, Ulf Riebesell and Uli Bathmann have always been open to my biological ignorance.

The present thesis was written in the carbon project group at the Alfred Wegener Institute for Polar and Marine Research. All colleagues in the group provided a very comfortable and encouraging working atmosphere.

Last but not least, I want to thank Thies, Bror and my friend Stef Wildung as well as her and my parents for their support.

Appendix A

Carbonate dissolution kinetics

The dissolution rate of calcite or aragonite dissolution may be described as $R = \kappa\,(1-\Omega)^{\eta}$, where $\Omega = [CO_3^{2-}]_{\mathrm{in-situ}}/[CO_3^{2-}]_c$ is the saturation with respect to calcite or aragonite, calculated as the quotient of in-situ carbonate concentration and critical carbonate concentration, $\kappa\,(\mathrm{d}^{-1})$ is the rate constant and η the order of the reaction [*Keir*, 1980; *Walter and Morse*, 1985]. The dissolution rate constant is usually attributed to specific properties of the particle such as geometry and particle size of the calcium carbonate in question [*Keir*, 1980]. The order of the reaction is thought to reflect the pure kinetics of the chemical reaction, and thus should be universal. However, the rate order is not well constrained (cf. Table A.1), as values cited in the literature range between 1 [*Hales and Emerson*, 1997] to more than 5 [*Keir*, 1980] . The latter finds a value of 4.5 ± 0.7 in dissolution experiments with a wide range of species as well as mixed sediment probes. *Hales and Emerson* [1997] fit n=1 to data obtained from in-situ pore water measurements. *Svensson and Dreybrodt* [1992] find the rate order to be dependent on the distance from equilibrium. For saturation values smaller than 0.8, they measure a rate order of 1.5-2.2, whereas the dissolution slows down to a rate order of 4 when the medium is closer to equilibrium. *Burton et al.* [1951], considering the precipitation of calcite, calculate from theory a rate order that changes with distance from equilibrium. *Dreybrodt* [1988] states that precipitation and dissolution principally may be described by the same equation type. The kinetics of aragonite dissolution are not as thoroughly investigated. However, it is generally assumed that the rate order of aragonite dissolution is a little less than that of calcite dissolution, i.e. when undersaturation is the same, aragonite dissolves more quickly [*Keir*, 1980; *Morse and Berner*, 1979].

Dissolution kinetics are influenced by a number of inhibitors, such as organic matter, the contribution of Mg-calcite or the presence of phosphate [*Morse*, 1974b; *Walter and Hanor*, 1979]. Varying $[PO_4^{3-}]$ between 0.1 to 10 $\mu\mathrm{mol\,kg^{-1}}$, *Morse and Berner* [1979] find that the rate order increases from 3 to 17.

Morse [1974a] has introduced the so-called *p*H-*stat* technique to study dissolution kinetics of $CaCO_3$, where the degree of undersaturation during an experimental run is kept fixed by adding acid or base to maintain a constant *p*H. Earlier work by other researchers adopts the *free drift* technique, in which the system is started at undersaturation and allowed to react towards equilibrium. *Morse and Berner* [1979] state an accuracy in determination of the dissolution rate of $\pm 2\%$ for the *p*H-

stat technique. The free-drift technique is generally considered to be less accurate, especially near equilibrium [*Morse*, 1983]. *Sjöberg and Rickard* [1983] have employed both techniques to obtain insight to the influence of experimental design on the measured rates. They observe that the stirring rate, $\omega\,(\text{revolutions}\,\text{s}^{-1})$, is an important parameter, as the dissolution rate behaves like $R \propto \omega^u$, where u is the stirring coefficient, which they find for crystals at pH 8.3 to range between 0.63 and 0.85. In this context it is important to note that some experimental work has been done without significantly stirring the medium. *Keir* [1980], for example, merely excites the medium to maintain the particles in suspension. Hence, any microenvironment that is created during the dissolution process being higher saturated than the bulk water due to the increase of CO_3^{2-} concentration is not destroyed by advection and thus dissolution rates are likely to be underestimated, leading to an overestimation of the rate order.

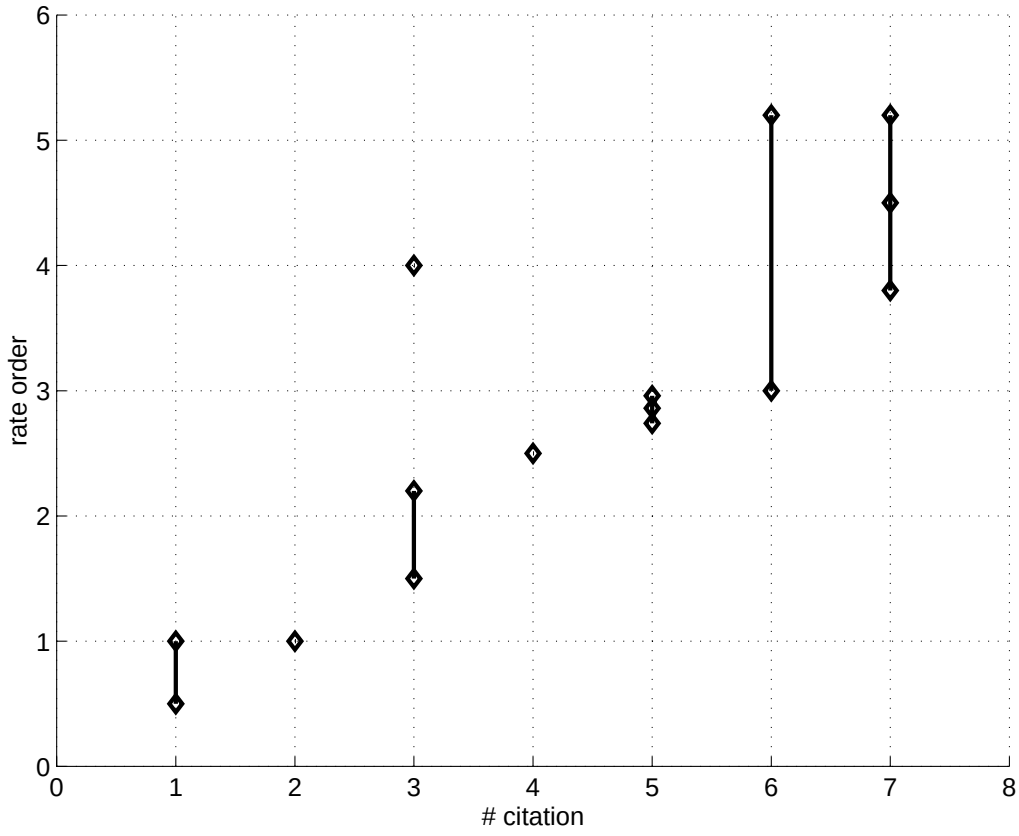

Figure A.1: Rate order of calcite dissolution kinetics as proposed by experimental work. Nr 1: Sjoeberg 1976, Nr 2: Hales & Emerson 1997, Nr 3: Svensson & Dreybrodt 1992, Nr 4: Sjöberg 1978, Nr 5: Walter & Morse 1985, Nr 6: Morse 1978, Nr 7: Keir 1980. Confer to Table A.1 for details.

Reference	η (range)	η (mean)	PO_4^{3-} (μM)	T (°C)	Stirring rate (rev. s^{-1})	Method	Remarks
Hales and Emerson [1997]	1.0	1.0	?	?	?	fit	fit to observational pore water data
Keir [1980]	3.8-5.2	4.5	< 1.3	20	suspension	free-drift	various coccolith and foraminifera species
Morse [1978]	3.0-5.2	-	2.6	?	?	*p*H-stat	sea water, sediment from the Indian, Pacific and Atlantic near saturation
Sjöberg [1976]	0.5-1.0	-	?	20 ± 1	4.6	free-drift	fresh water, η increasing from 0.5 at $\Omega = 0$ up to 1 at saturation
Sjöberg [1978]	2.5	2.5	?	?	?	?	fresh water
Svensson and Dreybrodt [1992]	1.5-2.2, 4.0	-	?	?	suspension, turbulent stirring	free-drift	fresh water, fast reaction far away from equilibrium, slow reaction near saturation
Walter and Morse [1985]	-	2.9	< 0.1	25 ± 0.5	suspension	*p*H-stat	sea water, low-Mg synthetic calcite

Table A.1: Details on calcite dissolution experiments.

Appendix B

Settling velocities of biogenic aggregates

In this appendix, literature data on settling velocities of individual cells as well as aggregates of particles are discussed. Young [1994] states that single coccolithophorid cells (and, thus, coccoliths) are small enough to settle according to laminar flow as may be formalized in the Stokes equation. For spherical cells of $4 - 20\,\mu$m diameter, he calculates sinking velocities of 1 to $10\,\mathrm{m\,d^{-1}}$. For solitary coccolithophorids, Smayda [1971] finds settling velocities ranging from 0.25 to $10\,\mathrm{m\,d^{-1}}$. Honjo [1977] remarks that coccolithophorids enclosed in faecal pellets often sink rapidly to great depths, then after being expelled from the pellet reduce to settling speeds ranging from 0.15 to $1.3\,\mathrm{m\,d^{-1}}$ and dissolve quickly.

Settling velocities of foraminifera have been investigated by a number of authors [*Berger and Piper*, 1972; *Honjo*, 1977; *Bijma et al.*, 1994; *Fok-Pun and Komar*, 1983]. Takahashi and Be [1984] state that sinking rates of spinose species are on average 3-fold slower than those of the non-spinose species. Literature data on pteropod sinking rates is very scarce. Details are given in Tables B.1, B.2 and B.3.

Species	Settl. vel. ($m\,d^{-1}$)	Reference	Vital status
Coccolithus huxleyi	1.5	Smayda [1971]	living cells
Cricosphaera elongata	0.25	Smayda [1971]	living cells
Cyclococcolithus fragelis	10	Smayda [1971]	living cells
Cyclococcolithus fragelis	>100	Smayda [1971]	senescent, in aggregates
E. huxleyi	0.15	Honjo [1977]	not specified
Coccolithus neohelis	0.16	Honjo [1977]	not specified
Coccolithus leptopora	1.3	Honjo [1977]	not specified
maximal range	0.15 - > 100		

Table B.1: Settling velocities of single cells of different carbonate producers (coccolithophorids).

Species	Settl. vel. ($m\,d^{-1}$)	Reference	Vital status
Globorotalia hirsuta	1,275 – 1,925	Fok-Pun and Komar [1983]	senescent
Globigerinoides ruber	415 – 1,295	Fok-Pun and Komar [1983]	senescent
Globigerinoides sacculifer	775 - 2,075	Fok-Pun and Komar [1983]	senescent
Globigerinoides sacculifer	500 – 2,250	Bijma et al. [1994]	senescent
Orbulina universa	2,140 – 3,440	Fok-Pun and Komar [1983]	senescent
not specified	170 – 1,300	Honjo [1977]	not specified
various species	260 – 2,000	Berger and Piper [1972]	senescent
various spinose species	40 – 2,350	Takahashi and Be [1984]	not specified
various non-spinose species	100 – 2,820	Takahashi and Be [1984]	not specified
maximal range	40 – 3,440		
Limacina retroversa	80 – 1,080	Noji et al. [1997]	

Table B.2: Settling velocities of single cells of different carbonate producers (foraminifera and pteropods).

Particle type	Settling velocity ($m\,d^{-1}$)		Reference
	range	mean	
marine snow aggregates	43 – 95	68	Shanks and Trent [1980]
marine snow aggregates	–	91	Alldredge [1979]
marine snow aggregates	35 – 113	74	Alldredge and Gotschalk [1988]
marine snow aggregates	1 – 280	12	Diercks and Asper [1997]
pteropod aggregates	80–1080	301	Noji et al. [1997]
aggr. of phytoplankton detritus	100 – 150	–	Lampitt [1985]
miscellaneous particles	67 – 131	92	Lorenzen et al. [1983]
miscellaneous particles (Eq. Pac.)	180 –	–	Honjo et al. [1995]
miscellaneous particles (North Atl.)	–	70	Honjo et al. [1995]

Table B.3: Settling velocities of biogenic aggregates.

Appendix C

Production estimates

This appendix gives literature data on global primary production of C_{org}, and estimates of new production, i.e. the fraction of primary production that is exported to depth. Furthermore, data on global production of $CaCO_3$ are given and a compilation of rain ratio field measurements.

Reference	New Production ($Gt\,C\,yr^{-1}$)	Source
Eppley and Peterson [1979]	3.4-4.7	Field data
Berger et al. [1987]	4.3-5.4	Field data
Martin et al. [1987]	7.4	Field data
Packard et al. [1988]	21.9	Enzyme activity model
Najjar et al. [1992]	12-15	GCM
Chavez and Toggweiler [1995]	7.2	Field data
Six and Maier-Reimer [1996]	11.1	GCM
Popova et al. [2000]	9.9	Box model
Schlitzer [2000]	11.0	Field data
Palmer and Totterdell [2001]	9.4	GCM
mean	9.9	

Table C.1: Global new production estimates.

Reference	Production ($Gt\,C\,yr^{-1}$)	Production ($Tmol\,C\,yr^{-1}$)	OO_P (%)	OO_A (%)
compilation[a] in Sundquist [1985]	21	2525		
Eppley and Peterson [1979]	19	1592	75	89
Walshet al. [1981]	26	2200	77	91
Walsh [1988]	19	1550	71	84
Berger [1989]	30	2500	-	-
Morse and Mackenzie [1990, p.507]	45	3750	-	-
Knauer [1993][b]	51	4250	-	-
Mackenzie et al. [1993]	30	2500	-	-
Smith and Hollibaugh [1993]	48	4000	90	92
Hedges and Keil [1995]	50	4167	-	-
Longhurst et al. [1995]	45-50	3750-4167	71	89
Antoine et al. [1996]	37-46	3042-3800	-	-
Behrenfeld and Falkowski [1997]	44	3625	-	-
Field et al. [1998]	49	4042	-	-
Jenkins [2000] (pers. comm.)	50	4167	-	-
mean	34.2	2849	76.8	89.0
mean 1990 - 2000	45.5	3788		

[a] 18 estimates prior to 1979
[b] as cited in Longhurst et al. [1995]

Table C.2: Global primary production estimates. OO_P denotes the production in the open ocean area, OO_A denotes the relative area of open ocean.

Reference	Production ($Tmol\,C\,yr^{-1}$)	Open Ocean fraction
Morse and Mackenzie [1990]	86	
Shaffer [1993]	83 – 167	
Westbroek [1993]	83 – 108	
Milliman [1993]	53	
Wollast [1994]	94	
Milliman and Droxler [1996]	90	70%
mean	90	

Table C.3: Estimates on global $CaCO_3$ production.

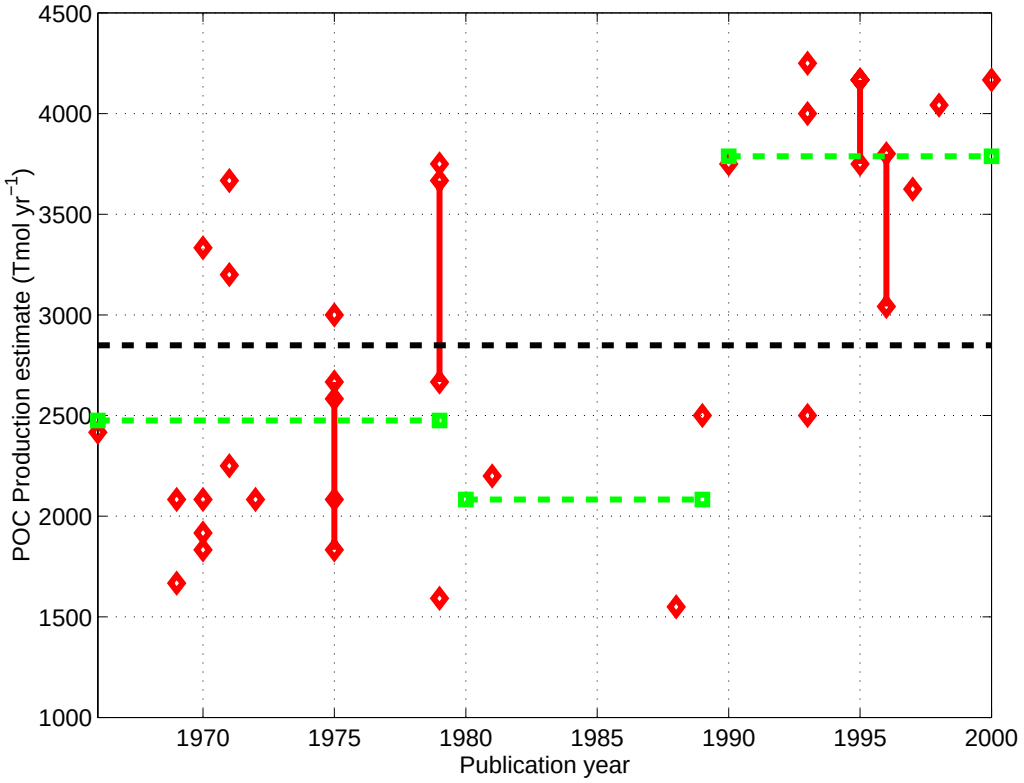

Figure C.1: Estimates on global primary production of organic carbon. A trend towards higher values is visible. However, all measurements exhibit large variabilities.

Depth (m)	$C_{org} : CaCO_3$ (mol/mol)	Location	Reference
4000	0.6	N. Atlantic	Brewer et al. [1980]
5086	0.7	Sub. Trop. Atlantic	Honjo [1980]
5086	0.8	Sub. Trop. Pacific	Honjo [1980]
3470	1.5	N. Atlantic	Hinga et al. [1979]
3059	1.1	N. Atlantic	Rowe and Gardner [1979]
2795	1.1	N. Atlantic	Rowe and Gardner [1979]
2316	1.2	N. Atlantic	Rowe and Gardner [1979]
2162	0.8	N. Atlantic	Rowe and Gardner [1979]
2570	0.6	Eq. Pacific	Cobler and Dymond [1980]

Table C.4: Literature data on the $C_{org} : CaCO_3$ rain ratio. See also Fig. 4.18.

Bibliography

[1] Alldredge, A. The carbon, nitrogen and mass content of marine snow as a function of aggregate size. *Deep-Sea Res. I*, 45:529–541, 1998.

[2] Alldredge, A. L. Discarded appendicularian houses as sources of food, surface habitats, and particulate organic matter in planktonic environments. *Limnol. Oceanogr.*, 21(1):14–23, 1976.

[3] Alldredge, A. L. The chemical composition of macroscopic aggregates in two neritic seas. *Limnol. Oceanogr.*, 24(5):855–866, 1979.

[4] Alldredge, A. L. and C. C. Gotschalk. Direct observations of the mass flocculation of diatom blooms : characteristics, settling velocities and formation of diatom aggregates. *Deep-Sea Res.*, 36(2):159–171, 1989.

[5] Alldredge, A. L. and C. Gotschalk. In situ settling behavior of marine snow. *Limnol. Oceanogr.*, 33(3):339–351, 1988.

[6] Alldredge, A. L. and M. W. Silver. Characteristics, Dynamics and Significance of Marine Snow. *Prog. Oceanog.*, 20:41–82, 1988.

[7] Alldredge, A. L. and Y. Cohen. Can Microscale Chemical Patches Persist in the Sea? Microelectrode Study of Marine Snow, Fecal Pellets. *Science*, 235:689–691, 1987.

[8] Altabet, M. A. and W. B. Curry. Testing models of past ocean chemistry using foraminifera $^{15}N/^{14}N$. *Glob. Biogeochem. Cycles*, 3(2):107–119, 1989.

[9] Anderson, L. A. and J. L. Sarmiento. Redfield ratios of remineralization determined by nutrient data analysis. *Glob. Biogeochem. Cycles*, 8(1):65–80, 1994.

[10] Antoine, D., J.-M. André and A. Morel. Oceanic primary production 2. Estimation at global scale from satellite (coastal zone color scanner) chlorophyll. *Glob. Biogeochem. Cycles*, 10:57–69, 1996.

[11] Archer, D. A data-driven model of the global calcite lysocline. *Glob. Biogeochem. Cycles*, 10(3):511–526, 1996.

[12] Archer, D., A. Winguth, D. Lea and N. Mahowald. What Caused the Glacial/Interglacial Atmospheric pCO_2 Cycles? *Rev. Geophys.*, 38(2):159–189, 2000.

[13] Archer, D. and E. Maier-Reimer. Effect of deep-sea sedimentary calcite preservation on atmospheric CO_2 concentration. *Nature*, 367:260–263, 1994.

[14] Archer, D., S. Emerson and C. Reimers. Dissolution of calcite in deep-sea sediments: *p*H and O_2 microelectrode results.

Geochim. Cosmochim. Acta, 53:2831–2845, 1989.

[15] Arrhenius, G. Rate of production, dissolution and accumulation of biogenic solids in the ocean. *Paleogeography, Paleoclimatology, Paleoecology*, 67:119–146, 1988.

[16] Atkinson, A., P. Ward and E. J. Murphy. Diel periodicity of Subantarctic copepods : relationships between vertical migration, gut fullness and gut evacuation rate. *J. Plankton Res.*, 18(8):1387–1405, 1996.

[17] Balch, W. M., P. M. Holligan, S. G. Ackleson and K. J. Voss. Biological and optical properties of mesoscale coccolithophore blooms in the Gulf of Maine. *Limnol. Oceanogr.*, 36(4):629–643, 1991.

[18] Bard, E. Ice Age Temperatures and Geochemistry. *Science*, 284:1133–1134, 1999.

[19] Barnola, J.-M., D. Raynaud, Y. S. Korotkevich and C. Lorius. Vostok ice core provides 160,000-year record of atmospheric CO_2. *Nature*, 329:408–414, 1987.

[20] Bathmann, U. V., T. T. Noji, M. Voss and R. Peinert. Copepod fecal pellets : abundance, sedimentation and content at a permanent station in the Norwegian Sea in May/June 1986. *Mar. Ecol. Prog. Ser.*, 38:45–51, 1987.

[21] Bautista, B. and R. P. Harris. Copepod gut contents, ingestion rates and grazing impact on phytoplankton in relation to size structure of zooplankton and phytoplankton during a spring bloom. *Mar. Ecol. Prog. Ser.*, 82:41–50, 1992.

[22] Bautista, B., R. P. Harris, P. R. G. Tranter and D. Harbour. *In situ* copepod feeding and grazing rates during a spring bloom dominated by *Phaeocystis* sp. in the English Channel. *J. Plankton Res.*, 14(5):691–703, 1992.

[23] Beers, J. R., J. D. Trent, F. M. H. Reid and A. L. Shanks. Macroaggregates and their phytoplanktonic components in the Southern California Bight. *J. Plankton Res.*, 8:475–487, 1986.

[24] Behrenfeld, M. J. and P. G. Falkowski. A consumer's guide to phytoplankton primary productivity models. *Limnol. Oceanogr.*, 42(7):1479–1491, 1997.

[25] Berelson, W. M., D. E. Hammond and G. A. Cutter. *In situ* measurements of calcium carbonate dissolution rates in deep-sea sediments. *Geochim. Cosmochim. Acta*, 54:3013–3020, 1990.

[26] Berelson, W. M., D. E. Hammond, J. McManus and T. E. Kilgore. Dissolution kinetics of calcium carbonate in equatorial Pacific sediments. *Glob. Biogeochem. Cycles*, 8(2):219–235, 1994.

[27] Berger, W. H. and D. J. W. Piper. Planktonic foraminifera : differential settling, dissolution, and redeposition. *Limnol. Oceanogr.*, 17(2):275–287, 1972.

[28] Berger, W. H., K. Fischer, C. Lai and G. Wu. Ocean productivity and organic carbon flux. Part I. Overview and maps of primary production. Univ. California, San Diego, SIO Reference 87-30, 1987.

[29] Berger, W. H., V. Smetacek and G. Wefer. Ocean productivity and paleoproductivity -

an overview. In W. H. Berger, V. Smetacek, and G. Wefer, editors, *Production of the Ocean: Present and Past*, pages 1–34. Dahlem Konferenzen, John Wiley & Sons Limited, 1989.

[30] Berner, R. A. *Early Diagenesis – A Theoretical Approach*. Princeton University Press, Princeton, 1980.

[31] Bijma, J., C. Hemleben and K. Wellnitz. Lunar-influenced carbonate flux of the planktic foraminifer *Globigerinoides sacculifer* (Brady) from the central Red Sea. *Deep-Sea Research*, 41(3):511–530, 1994.

[32] Boudreau, B. P. and N. L. Guinasso, Jr. The Influence of a Diffusive Sublayer on Accretion, Dissolution, and Diagenesis at the Sea Floor. In D. C. Heath, editor, *The Dynamic Environment of the Ocean Floor*, pages 115–145. 1980.

[33] Boyle, E. A. The role of vertical chemical fractionation in controlling late quaternary atmospheric carbon dioxide. *Journal of Geophysical Research*, 93(C12):15701–15714, 1988a.

[34] Boyle, E. A. Vertical oceanic nutrient fractionation and glacial/interglacial CO_2 cycles. *Nature*, 331:55–56, 1988b.

[35] Båmstedt, U., J. C. Nejstgaard and P. T. Solberg. Utilisation of small-sized food algae by *Calanus finmarchicus* (Copepoda, Calanoida) and the significance of feeding history. *Sarsia*, 84:19–38, 1999.

[36] Brewer, P. G. and J. C. Goldman. Alkalinity changes generated by phytoplankton growth. *Limnol. Oceanogr.*, 21(1):108–117, 1976.

[37] Brewer, P. G., Y. Nozaki, D. W. Spencer and A. P. Fleer. Sediment trap experiments in the deep North Atlantic : isotopic and elemental fluxes. *J. Mar. Res.*, 38:703–728, 1980.

[38] Broecker, W. S. The great ocean conveyor. *Oceanography*, 4:79–89, 1991.

[39] Broecker, W. S. and G. M. Henderson. The Sequence of Events Surrounding Termination II and Their Implications for the Cause of Glacial-Interglacial CO_2 Changes. *Paleoceanography*, 13(4):352–364, 1998.

[40] Broecker, W. S. and T. Peng. *Tracers in the Sea*. LDGO-Press, Palisades, New York, 1982.

[41] Broecker, W. S. and T. Peng. *The Glacial World according to Wally*, chapter What caused the glacial to interglacial CO_2 change? LDGO-Press, Palisades, New York, 1992.

[42] Broecker, W. S. and T. Takahashi. Neutralization of Fossil Fuel CO_2 by Marine Calcium Carbonate. In N. R. Anderson and A. Malankoff, editors, *The Fate of Fossil Fuel* CO_2 *in the Oceans*, volume 6 of *Marine Science*, pages 213–241. Plenum Press, New York, New York, 1977.

[43] Broecker, W. S. and T. Takahashi. The relationship between lysocline depth and *in situ* carbonate ion concentration. *Deep-Sea Research*, 25:65–95, 1978.

[44] Broecker, W. S., J. Lynch-Steglitz, D. Archer, M. Hofmann, E. Maier-Reimer, O. Marchal, T. Stocker and N. Gruber. How strong is the Harvardton-Bear constraint?

Glob. Biogeochem. Cycles, 13(4):817–820, 1999.

[45] Broecker, W. S., M. Klas and E. Clark. The influence of $CaCO_3$ dissolution on core top radiocarbon ages for deep-sea sediments. *Paleoceanography*, 6(5):593–608, 1991.

[46] Burkill, P. H., E. S. Edwards, A. W. G. John and M. A. Sleigh. Microzooplankton and their herbivorous activity in the north-eastern Atlantic Ocean. *Deep-Sea Res. II*, 40(1/2):479–493, 1993.

[47] Burton, W. K., N. Cabrera and F. C. Frank. The growth of crystals and the equilibrium structure of their surfaces. *Phil. Trans. Roy. Soc. London A*, 243(866):299–348, 1951.

[48] Byrne, R. H., J. G. Acker, P. R. Betzer, R. A. Feely and M. H. Cates. Water column dissolution of aragonite in the Pacific Ocean. *Nature*, 312:321–326, 1984.

[49] Cai, W.-J., C. E. Reimers and T. Shaw. Microelectrode studies of organic carbon degradation and calcite dissolution at a California Continental rise site. *Geochim. Cosmochim. Acta*, 59(3):497–511, 1995.

[50] Chappellaz, J., J.-M. Barnola, D. Raynaud, Y. S. Korotkevich and C. Lorius. Ice-core record of atmospheric methane over the past 160,000 years. *Nature*, 345:127–131, 1990.

[51] Chavez, F. P. and J. R. Toggweiler. Physical Estimates of Global New Production : The Upwelling Contribution. In C. P. Summerhayes, K.-C. Emeis, M. V. Angel, R. L. Smith, and B. Zeitzschel, editors, *Upwelling in the Ocean : Modern Processes and Ancient Records*, number 18 in Environmental Sciences Research Report, pages 313–320. John Wiley & Sons, 1995.

[52] Cobler, R. and J. Dymond. Sediment trap experiment on th Galapagos spreading center, Equatorial Pacific. *Science*, 209:801–803, 1980.

[53] Copin-Montegut, C. and G. Copin-Montegut. Stoichiometry of carbon, nitrogen, and phophorus in marine particulate matter. *Deep-Sea Research*, 30(1):31–46, 1983.

[54] Cowles, T. J. and J. R. Strickler. Characterization of feeding activity patterns in the planktonic copepod *Centropages typicus* Kroyer under various food conditions. *Limnol. Oceanogr.*, 28:106–115, 1983.

[55] Crowley, T. J. Calcium-carbonate preservation patterns in the central north Atlantic during the last 150,000 years. *Mar. Geol.*, 51:1–14, 1983.

[56] Crowley, T. J. Late quaternary carbonate changes in the North Atlantic and Atlantic / Pacific comparisons. In E. T. Sundquist and W. S. Broecker, editors, *The Carbon Cycle and Atmospheric* CO_2*: Natural Variations Archean to Present*, number 32 in Geophysical Monographs, pages 271–284. American Geophysical Union, Washington, D. C., 1985.

[57] Culberson, C. and R. M. Pytkowicz. Effect of pressure on carbonic acid, boric acid, and the *p*h in seawater. *Limnol. Oceanogr.*, 13(3):403–417, 1968.

[58] Curry, W. B. and G. P. Lohmann. Late quaternary carbonate sedimentation at the

Sierra Leone Rise (eastern equatorial Atlantic Ocean). *Mar. Geol.*, 70:223–250, 1986.

[59] Dagg, M. J., B. W. Frost and W. E. Walser, Jr. Copepod diel migration, feeding, and the vertical flux of pheopigments. *Limnol. Oceaonogr.*, 34(6):1062–1071, 1989.

[60] Dam, H. G. and W. T. Peterson. The effect of temperature on the gut clearance rate constant of planktonic copepods. *J. Exp. Mar. Biol. Ecol.*, 123:1–14, 1988.

[61] Davis, C. S., S. M. Gallager, M. Marra and W. K. Stewart. Rapid visualization of plankton abundance and taxonomic composition using the Video Plankton Recorder. *Deep-Sea Res. II*, 43(7-8):1947–1970, 1996.

[62] Diercks, A.-R. and V. L. Asper. *In situ* settling speeds of marine snow aggregates below the mixed layer : Black Sea and Gulf of Mexico. *Deep-Sea Res.*, 44(3):385–398, 1997.

[63] DOE (1994). Handbook of methods for the analysis of the various parameters of the carbon dioxide system in sea water. version 2, Dickson, A. G. and C. Goyet, eds., http ://www-mpl.ucsd.edu/people/adickson , 1994.

[64] Dreybrodt, W. *Processes in Karst Systems – Physics, Chemistry, and Geology*. Springer Series in Physical Environment. Springer, Berlin Heidelberg, 1988.

[65] Elderfield, H. and G. Ganssen. Past temperature and δ^{18}O of surface ocean waters inferred from foraminiferal Mg/Ca ratios. *Nature*, 405:442–445, 2000.

[66] Emerson, S. and J. I. Hedges. Processes controlling the organic carbon content of open ocean sediments. *Paleoceanography*, 3(5):621–634, 1988.

[67] Emerson, S. and M. Bender. Carbon fluxes at the sediment-water interface of the deep-sea: calcium carbonate preservation. *J. Mar. Res.*, 39(1):139–162, 1981.

[68] Emiliani, C. Pleistocene temperatures. *J. Geol.*, 63(6):538–578, 1955.

[69] Eppley, R. W. and B. J. Peterson. Particulate organic matter flux and planktonic new production in the deep ocean. *Nature*, 282:677–680, 1979.

[70] Fairbanks, R. G. A 17,000-year glacio-eustatic sea level record : influence of glacial melting rates on Younger Dryas event and deep-ocean circulation. *Nature*, 342:637–642, 1989.

[71] Farrell, J. W. and W. L. Prell. Climatic change and $CaCO_3$ preservation: An 800,000 year bathymetric reconstruction from the central equatorial Pacific Ocean. *Paleoceanography*, 4(4):447–466, 1989.

[72] Fernández, E., P. Boyd, P. M. Holligan and D. S. Harbour. Production of organic and inorganic carbon within a large-scale coccolithophore bloom in the north-east Atlantic Ocean. *Mar. Ecol. Progr. Ser.*, 97:271–285, 1993.

[73] Fiadeiro, M. The alkalinity of the deep Pacific. *Earth Planet. Sci. Letters*, 49:499–505, 1980.

[74] Field, C. B., M. J. Behrenfeld, J. T. Randerson and P. Falkowski. Primary Produc-

tion of the Biosphere: Integrating Terrestrial and Oceanic Components. *Science*, 281:237–240, 1998.

[75] Fok-Pun, L. and P. D. Komar. Settling velocities of planktonic foraminifera: density variations and shape effects. *J. Foraminiferal Res.*, 13(1):60–68, 1983.

[76] Francois, R., M. A. Altabet and L. H. Burckle. Glacial to interglacial changes in surface nitrate utilization in the Indian sector of the Southern Ocean as recorded by sediment δ^{15}N. *Paleoceanography*, 7(5):589–606, 1992.

[77] Frankenberg, D. and L. F. Smith, Jr. Coprophagy in marine animals. *Limnol. Oceanogr.*, 12:443–450, 1967.

[78] Gallager, S. M., C. S. Davis, A. W. Epstein, A. Solow and R. C. Beardsley. High-resolution observations of plankton spatial distributions correlated with hydrography in the Great South Channel, Georges Bank. *Deep-Sea Res. II*, 43(7-8):1627–1663, 1996.

[79] Ganeshram, R. S., T. F. Pedersen, S. E. Calvert and J. W. Murray. Large changes in oceanic nutrient inventories from glacial to interglacial periods. *Nature*, 376:755–758, 1995.

[80] Goldman, J. C. and P. G. Brewer. Effect of nitrogen source and growth rate on phytoplankton-mediated changes in alkalinity. *Limnol. Oceanogr.*, 25(2):352–357, 1980.

[81] Greene, C. H., P. H. Wiebe, C. Pelkie, M. C. Benfield and J. M. Popp. Three-dimensional acoustic visualization of zooplankton patchiness. *Deep-Sea Res. II*, 45:1201–1217, 1998.

[82] Grim, R. E. *Applied Clay Mineralogy*. McGraw-Hill, New York, 1962.

[83] Hales, B. and S. Emerson. Calcite dissolution in sediments of the Ontong-Java Plateau: In situ measurements of pore water O_2 and *p*H. *Glob. Biogeochem. Cycles*, 10(3):527–541, 1996.

[84] Hales, B. and S. Emerson. Evidence in support of first-order dissolution kinetics of calcite in seawater. *Earth Plan. Sci. Lett.*, 148:317–327, 1997.

[85] Hales, B., S. Emerson and D. Archer. Respiration and dissolution in the sediments of the western North Atlantic: estimates from models of *in situ* microelectrode measurements of porewater oxygen and *p*H. *Deep-Sea Research I*, 41(4):695–719, 1994.

[86] Hansen, B. W., B. H. Hygum, M. Brozek, F. Jensen and C. Rey. Food web interactions in a *Calanus finmarchicus* dominated pelagic ecosystem – a mesocosm study. *J. Plankton Res.*, 22(3):569–588, 2000.

[87] Harris, R. P. Zooplankton grazing on the coccolithophore *Emiliania huxleyi* and its role in inorganic carbon flux. *Mar. Biol.*, 119:431–439, 1994.

[88] Harrison, K. G. Role of increased marine silica input on paleo-pCO_2 levels. *Paleoceanography*, 15(3):292–298, 2000.

[89] Head, R. N., D. W. Crawford, J. K. Egge, R. P. Harris, S. Kristiansen, D. J. Lesley, E. Marañón, D. Pond and D. A. Purdie. The hydrography and biology of a bloom

of the coccolithophorid *Emiliania huxleyi* in the northern North Sea. *J. Sea Res.*, 39:255–266, 1998.

[90] Hebel, D. V. W. Concentration and flux of trace metals, carbon-nitrogen, and particulate matter in marine snow. Master's thesis, San Francisco State University, 1983.

[91] Hedges, J. I. and R. G. Keil. Sedimentary organic matter preservation : an assessment and speculative synthesis. *Mar. Chem.*, 49:81–115, 1995.

[92] Hemming, N. G. and G. N. Hanson. Boron isotopic composition and concentration in modern marine carbonates. *Geochim. Cosmochim. Acta*, 56:537–543, 1992.

[93] Hemming, N. G., R. J. Reeder and G. N. Hanson. Mineral-fluid partitioning and isotopic fractionation of boron in synthetic calcium carbonate. *Geochim. Cosmochim. Acta*, 59:371–379, 1995.

[94] Herguera, J. C. and W. H. Berger. Glacial to postglacial drop in productivity in the western equatorial Pacific : Mixing rate vs. nutrient concentrations. *Geology*, 22:629–632, 1994.

[95] Hinga, K. R., J. McN. Sieburth and G. Ross Heath. The supply and use of organic material at the deep-sea floor. *J. Mar. Res.*, 37(3):557–579, 1979.

[96] Holligan, P. M. and J. E. Robertson. Significance of ocean carbonate budgets for the global carbon cycle. *Global Change Biology*, 2:85–95, 1996.

[97] Holmén, K. The Global Carbon Cycle. In *Global Biogeochemical Cycles*, volume 50 of *International Geophysics Series*, chapter 11, pages 239–262. Academic Press, London, 1992.

[98] Honjo, S. Biogenic Carbonate Particles in the Ocean; Do they Dissolve in the Water Column? In N. R. Anderson and A. Malankoff, editors, *The Fate of Fossil Fuel* CO_2 *in the Oceans*, volume 6 of *Marine Science*, pages 269–294, New York, 1977. Plenum Press.

[99] Honjo, S. Material fluxes and modes of sedimentation in the mesopelagic and bathypelagic zones. *Journal of Marine Research*, 38(1):53–97, 1980.

[100] Honjo, S. and M. R. Roman. Marine copepod faecal pellets : production, preservation and sedimentation. *J. Mar. Res.*, 36(1):45–57, 1978.

[101] Honjo, S., J. Dymond, R. Collier and S. J. Manganini. Export production of particles to the interior of the equatorial Pacific Ocean during the 1992 EqPac experiment. *Deep-Sea Res. II*, 42(2/3):831–870, 1995.

[102] Hupe, A. and J. Karstensen. Redfield stoichiometry in Arabian Sea subsurface waters. *Glob. Biogeochem. Cycles*, 14(1):357–372, 2000.

[103] Huskin, I., R. Anadón, F. Álvarez-Marqués and R. P. Harris. Ingestion, faecal pellet and egg production rates of *Calanus helgolandicus* feeding coccolithophorid versus non-coccolithophorid diets. *J. Exp. Mar. Biol. Ecol.*, 248:239–254, 2000.

[104] Irigoien, X. Gut clearance rate constant, temperature and initial gut contents : a

review. *J. Plankton Res.*, 20(5):997–1003, 1998.

[105] Jahnke, R. A., D. B. Craven and J. Gaillard. The influence of organic matter diagenesis on $CaCO_3$ dissolution at the deep-sea floor. *Geochim. Cosmochim. Acta*, 58(13):2799–2809, 1994.

[106] Jahnke, R. A., D. B. Craven, D. C. McCorkle and C. E. Reimers. $CaCO_3$ dissolution in California continental margin sediments : The influence of organic matter remineralization. *Geochim. Cosmochim. Acta*, 61(17):3587–3604, 1997.

[107] Joint, I., A. Pomroy, G. Savidge and P. Boyd. Size-fractionated primary productivity in the northeast Atlantic in May-July 1989. *Deep-Sea Res. II*, 40(1/2):423–440, 1993.

[108] Jouzel, J., C. Lorius, J.-R. Petit, C. Genthon, N. I. Barkov, V. M. Kotlyakov and V. N. Petrov. Vostok ice core : A continuous isotope temperature record over the last climatic cycle (160,000 years). *Nature*, 329:403–408, 1987.

[109] Jumars, P. A. and D. L. Penry. Digestion Theory Applied to Deposit Feeding. In G. Lopez, G. Taghon, and J. Levinton, editors, *Ecology of Marine Deposit Feeders*, volume 31 of *Lecture Notes on Coastal and Estuarine Studies*, pages 114–128. Springer, Berlin Heidelberg, 1984.

[110] Kakihana, H., M. Kotaka, S. Satoh, M. Nomura and M. Okamoto. Fundamental studies on the ion-exchange separation of boron isotopes. *Geochim. Cosmochim. Acta*, 50(1):158–163, 1977.

[111] Karp-Boss, L., E. Boss and P. A. Jumars. Nutrient fluxes to planktonic osmotrophs in the presence of fluid motion. *Oceanogr. Mar. Biol. Ann. Rev.*, 34:71–107, 1996.

[112] Keir, R. S. The dissolution kinetics of biogenic calcium carbonates in seawater. *Geochim. Cosmochim. Acta*, 44:241–252, 1980.

[113] Keir, R. S. On the late pleistocene ocean geochemistry and circulation. *Paleoceanography*, 3(4):413–445, 1988.

[114] Kemp, A. E. S., J. Pike, R. B. Pearce and C. B. Lange. The "Fall Dump" – a new perspective on the role of a "shade flora" in the annual cycle of diatom production and export flux. *Deep-Sea Res. II*, 47:2129–2154, 2000.

[115] Knauer, G. A. Productivity and new production of the oceanic system. In R. Wollast, F. T. Mackenzie, and L. Chou, editors, *Interactions of C, N, P and S Biogeochemical Cycles*, number I(4) in NATO ASI Series, pages 211–231. Springer, Berlin Heidelberg, 1993.

[116] Körtzinger, A., W. Koeve, P. Kähler and L. Mintrop. C :N ratios in the mixed layer during the productive season in the northeast Atlantic Ocean. *Deep-Sea Res. I*, 48:661–688, 2001.

[117] Kumar, N., R. F. Anderson, R. A. Mortlock, P. N. Froelich, P. Kubik, B. Dittrich-Hannen and M. Suter. Increased biological productivity and export production in the glacial Southern Ocean. *Nature*, 378:675–680, 1995.

[118] Lalli, C. M. and T. R. Parsons. *Biological Oceanography: An Introduction*. Pergamon Press, Oxford, 1993.

[119] Lampitt, R. S., T. Noji and B. von Bodungen. What happens to zooplankton faecal pellets? Implications for material flux. *Mar. Biol.*, 104:15–23, 1990.

[120] Laws, E. A., P. G. Falkowski, W. O. Smith, Jr., H. Ducklow and J. J. McCarthy. Temperature Effects on Export Production in the Open Ocean. *Glob. Biogeochem. Cycles*, 14(4):1231 – 1246, 2000.

[121] Li, Y.-H., T. Takahashi and W. S. Broecker. Degree of Saturation of $CaCO_3$ in the Oceans. *J. Geophysic. Res.*, 74(23):5507–5523, 1969.

[122] Logan, B. E. and D. B. Wilkinson. Fractal geometry of marine snow and other biological aggregates. *Limnol. Oceanogr.*, 35:130–136, 1990.

[123] Longhurst, A., S. Sathyendranath, T. Platt and C. Caverhill. An estimate of global primary production in the ocean from satellite radiometer data. *J. Plankton Res.*, 17(6):1245–1271, 1995.

[124] Lorenzen, C. J., N. A. Welschmeyer, A. E. Copping and M. Vernet. Sinking rates of organic particles. *Limnol. Oceanogr.*, 28(4):766–769, 1983.

[125] Mackas, D. L. and K. E. Burns. Post-starvation feeding and swimming activity in *Calanus pacificus* and *Metridia pacifica*. *Limnol. Oceanogr.*, 31(2):383–392, 1986.

[126] Mackenzie, F. T., L. M. Ver, C. Sabine, M. Lane and A. Lerman. C, N, P and S global biogeochemical cycles and modelling of global change. In R. Wollast, F. T. Mackenzie, and L. Chou, editors, *Interactions of C, N, P and S Biogeochemical Cycles and Global Change*, volume 4 of *NATO ASI Series 1 : Global Environmental Change*, pages 1–61. Springer, Berlin Heidelberg, 1993.

[127] Marino, B. D., M. B. McElroy, R. J. Salawitch and W. G. Spalding. Glacial-to-interglacial variations in the carbon isotopic composition of atmospheric CO_2. *Nature*, 357:461–465, 1992.

[128] Marshall, J. and F. Schott. Open-ocean convection : Observations, theory, and models. *Rev. Geophys.*, 37(1):1–64, 1999.

[129] Martin, J. H. Glacial-interglacial CO_2 change : The iron hypothesis. *Paleoceanography*, 5(1):1–13, 1990.

[130] Martin, J. H. and G. A. Knauer and D. M. Karl and W. W. Broenkow. VERTEX: Carbon cycling in the northeast Pacific. *Deep-Sea Research*, 34:267–286, 1987.

[131] Mauchline, J. *The biology of calanoid copepods*. Academic Press, San Diego, 1998.

[132] Mayzaud, P. Digestive enzymes and their relation to nutrients. In E. D. S. Corner and S. C. M. O'Hara, editors, *The Biological Chemistry of Marine Copepods*, pages 226–259. Clarendon Press, Oxford, 1986.

[133] Mayzaud, P. and O. Mayzaud. Kinetic properties of digestive carbohydrases and proteases of zooplankton. *Can. J. Fish. aquat. Sciences*, 38:535–543, 1981.

[134] McIntyre, A. et al. (CLIMAP project members). Seasonal Reconstructions of the Earth's Surface at the Last Glacial Maximum. *Geologic Society of America Map and Chart Series*, (MC-36):1–18, 1981.

[135] Millero, F. J. Thermodynamics of the carbon dioxide system in the oceans. *Geochim. Cosmochim. Acta*, 59(4):661–677, 1995.

[136] Milliman, J. D. Production and accumulation of calcium carbonate in the ocean : budget of a nonsteady state. *Glob. Biogeochem. Cycles*, 7(4):927–957, 1993.

[137] Milliman, J. D. and A. W. Droxler. Neritic and pelagic carbonate sedimentation in the marine environment: Ignorance is not bliss. *Geologische Rundschau*, 85:496–504, 1996.

[138] Milliman, J. D., P. J. Troy, W. M. Balch, A. K. Adams, Y.-H. Li and F. T. Mackenzie. Biologically mediated dissolution of calcium carbonate above the chemical lysocline? *Deep-Sea Res. I*, 46:1653–1669, 1999.

[139] Morse, J. W. Dissolution kinetics of calcium carbonate in sea water. III : A new method for the study of carbonate reaction kinetics. *American Journal of Science*, 274:97–107, 1974a.

[140] Morse, J. W. Dissolution kinetics of calcium carbonate in sea water. V. Effects of natural inhibitors and the position of the chemical lysocline. *American Journal of Science*, 274:638–647, 1974b.

[141] Morse, J. W. Dissolution kinetics of calcium carbonate in sea water : VI. The near-equilibrium dissolution kinetics of calcium carbonate-rich deep sea sediments. *American Journal of Science*, 278:344–353, 1978.

[142] Morse, J. W. The Kinetics of Calcium Carbonate Dissolution and Precipitation. In R. J. Reeder, editor, *Carbonates : Mineralogy and Chemistry*, volume 11 of *Reviews in Mineralogy*, pages 227–264. Mineralogical Society of America, 1983.

[143] Morse, J. W. and F. T. Mackenzie. *Geochemistry of Sedimentary Carbonates*. Number 48 in Developments in Sedimentology. Elsevier, Amsterdam, 1990.

[144] Morse, J. W. and R. C. Berner. Chemistry of Calcium Carbonate in the Deep Oceans. In E. A. Jenne, editor, *Chemical Modeling in Aqueous Systems*, number 93 in AMC Symposium Series, pages 499–535, Washington, D. C., 1979. American Chemical Society.

[145] Munhoven, G. Modelling Glacial-Interglacial Atmospheric CO_2 Variations : The Role of Continental Weathering. PhD thesis, Université de Liège, Liège, 1997.

[146] Murray, J. On the Distribution of the Pelagic Foraminifera at the Surface and on the Floor of the Ocean. *Nat. Sci.* , 17–27, 1897.

[147] Najjar, R. G., J. L. Sarmiento and J. R. Toggweiler. Downward transport and fate of organic matter in the ocean : Simulations with a general circulation model. *Glob. Biogeochem. Cycles*, 6:45–76, 1992.

[148] Neftel, A., H. Oeschger, J. Schwander, B. Stauffer and R. Zumbrunn. Ice core sample measurements give atmospheric CO_2 con-

tent during the past 40,000 yr. *Nature*, 295:220–223, 1982.

[149] Nejstgaard, J. C., H. J. Witte, P. van der Wal and A. Jacobsen. Copepod grazing during a mesocosm study of an *Emiliania huxleyi* (Prymnesiophyceae) bloom. *Sarsia*, 79:369–377, 1994.

[150] Noji, T. T. and K. W. Estep. Image analysis of faecal material grazed upon by three species of Copepods : Evidence for coprorhexy, coprophagy and coprochaly. *J. mar. biol. Ass. U.K.*, 71:465–480, 1991.

[151] Noji, T. T., U. V. Bathmann, B. von Bodungen, M. Voss, A. Antia, M. Krumholz, B. Klein, I. Peeken, C. I.-M. Noji and F. Rey. Clearance of picoplankton-sized particles and formation of rapidly sinking aggregates by the pteropod, *Limacina retroversa*. *J. Plankt. Res.*, 19(7):863–875, 1997.

[152] Norrbin, M. F., C. S. Davis and S. M. Gallager. Differences in fine-scale structure and composition of zooplankton between mixed and stratified regions of Georges Bank. *Deep-Sea Res. II*, 43(7-8):1905–1924, 1996.

[153] Packard, T. T., M. Denis, M. Rodier and P. Garfield. Deep ocean metabolic CO_2 production : calculations from ETS activity. *Deep-Sea Res.*, 35:371–382, 1988.

[154] Palmer, J. R. and I. Totterdell. Production and export in a global ocean ecosystem model. *Deep-Sea Res. I*, 48(5):1169–1198, 2001.

[155] Palmer, M. R., P. N. Pearson and S. J. Cobb. Reconstructing Past Ocean *p*H-Depth Profiles. *Science*, 282:1468–1471, 1998.

[156] Penry, D. L. and B. W. Frost. Re-evaluation of the gut-fullness (gut fluorescence) method for inferring ingestion rates of suspension-feeding copepods. *Limnol. Oceanogr.*, 35(5):1207–1214, 1990.

[157] Penry, D. L. and P. A. Jumars. Chemical reactor analysis and optimal digestion theory. *BioScience*, 36:310–315, 1986.

[158] Petit, J. R., J. Jouzel, D. Raynaud, N. I. Barkov, J. M. Barnola, I. Basile, M. Bender, J. Chappellaz, M. Davis, G. Delaygue, M. Delmotte, V. M. Kotlyakov, M. Legrand, V.Y. Lipenkov, C. Lorius, L. Pepin, C. Ritz, E. Saltzman and M. Stievenard. Climate and atmospheric history of the past 420,000 years from the Vostok ice core, Antarctica. *Nature*, 399:429–436, 1999.

[159] Ploug, H., H.-P. Grossart, F. Azam and B. B. Jørgensen. Photosynthesis, respiration, and carbon turnover in sinking marine snow from surface waters of Southern California Bight : implications for the carbon cycle in the ocean. *Mar. Ecol. Prog. Ser.*, 179:1–11, 1999.

[160] Ploug, H., W. Stolte and B. B. Jørgensen. Diffusive boundary layers of the colony-forming plankton alga *Phaeocystis* sp. – implications for nutrient uptake and cellular growth. *Limnol. Oceanogr.*, 44(8):1959–1967, 1999.

[161] Pond, D. W., R. P. Harris and C. Brownlee. A microinjection technique using a *p*H-sensitive dye to determine the gut *p*H of

Calanus helgolandicus. *Mar. Biol.*, 123:75–79, 1995.

[162] Pond, S., R. M. Pytkowicz and J. E. Hawley. Particle dissolution during settling in the oceans. *Deep-Sea Research*, 18:1135–1139, 1971.

[163] Popova, E. E., V. A. Ryabchenko and M. J. R. Fasham. Biological pump and vertical mixing in the Southern Ocean : Their impact on atmospheric CO_2. *Glob. Biogeochem. Cycles*, 14(1):477–498, 2000.

[164] Prézelin, B. B. and A. L. Alldredge. Primary production of marine snow during and after an upwelling event. *Limnol. Oceanogr.*, 28(6):1156–1167, 1983.

[165] Redfield, A. C., B. H. Ketchum and F. A. Richards. The influence of organisms on the composition of seawater. In M. N. Hill, editor, *The Sea. Vol. 2*, pages 1–34. Interscience, New York, 1963.

[166] Rosenberg, G. G. Filmed observations of filter feeding in the marine planktonic copepod *Acartia clausii*. *Limnol. Oceanogr.*, 25:738–741, 1980.

[167] Rostek, F., G. Ruhland, F. C. Bassinot, P. J. Müller, L. D. Labeyrie, Y. Lancelot and E. Bard. Reconstructing the sea surface temperature and salinity using δ^{18}O and alkenone records. *Nature*, 364:319–321, 1993.

[168] Rowe, G. T. and W. D. Gardner. Sedimentation rates in the slope water of the northern Atlantic Ocean measured directly with sediment traps. *J. Mar. Res.*, 37:581–600, 1979.

[169] Sanyal, A. and J. Bijma. A comparative study of the northwest Africa and eastern equatorial Pacific upwelling zones as sources of CO_2 during glacial periods based on boron isotopes paleo-*p*H estimation. *Paleoceanography*, 14(6):753–759, 1999.

[170] Sanyal, A., M. Nugent, R. J. Reeder and J. Bijma. Seawater *p*H control on the boron isotopic composition of calcite : Evidence from inorganic calcite precipitation experiments. *Geochim. Cosmochim. Acta*, 64(9):1551–1555, 2000.

[171] Sanyal, A., N. G. Hemming, G. N. Hanson and W. S. Broecker. Evidence for a higher *p*H in the glacial ocean from boron isotopes in foraminifera. *Nature*, 373:234–236, 1995.

[172] Sanyal, A., N. G. Hemming, W. S. Broecker and G. N. Hanson. Changes in *p*H in the eastern equatorial Pacific across stage 5-6 boundary based on boron isotopes in foraminifera. *Glob. Biogeochem. Cycles*, 11(1):125–133, 1997.

[173] Sanyal, A., N. G. Hemming, W. S. Broecker, D. W. Lea, H. J. Spero and G. N. Hanson. Oceanic *p*H control on the boron isotopic composition of foraminifera: Evidence from culture experiments. *Paleoceanography*, 11(5):513–517, 1996.

[174] Schlitzer, R. Applying the Adjoint Method for Biogeochemical Modeling : Export of Particulate Organic Matter in the World Ocean. In P. S. Kasibhatla, editor, *Inverse Methods in Global Biogeochemical Cycles*, pages 107–124. American Geophysical Union, Washington, D. C., 2000.

[175] Schmitz Jr., W. J. On the interbasin-scale thermohaline circulation. *Rev. Geophys.*, 33(2):151–173, 1995.

[176] Schulz, H. D. Quantification of Early Diagenesis : Dissolved Constituents in Marine Pore Water. In H. D. Schulz and M. Zabel, editors, *Marine Geochemistry*, pages 85–128. Springer, Berlin Heidelberg, 1999.

[177] Shaffer, G. Effects of the marine biota on global carbon cycling. In M. Heimann, editor, *The Global Carbon Cycle*, volume 15 of *ASI Series*, pages 431–455. NATO, Springer, 1993.

[178] Shaffer, G. Biogeochemical cycling in the global ocean 2. New production, Redfield ratios, and remineralization in the organic pump. *Journal of Geophysical Research*, 101(C2):3723–3745, 1996.

[179] Shanks, A. L. and J. D. Trent. Marine snow : sinking rates and potential role in vertical flux. *Deep-Sea Res.*, 27A:137–143, 1980.

[180] Sherr, E. B., B. F. Sherr and G. A. Paffenhofer. Phagotrophic protozoa as food for metazoans : a 'missing' trophic link in marine food webs. *Mar. Microb. Food Webs*, 1:61–80, 1986.

[181] Sherwood, T. K., R. L. Pigford and C. R. Wilke. *Mass Transfer*. McGraw-Hill, New York, 1975.

[182] Siegenthaler, U. and J. L. Sarmiento. Atmospheric carbon dioxide and the ocean. *Nature*, 365:119–125, 1993.

[183] Sigman, D. M. and D. C. McCorkle and W. R. Martin. The calcite lysocline as a constraint on glacial/interglacial low-latitude production changes. *Glob. Biogeochem. Cycles*, 12(3):409–427, 1998.

[184] Six, K. D. and E. Maier-Reimer. Effects of plankton dynamics on seasonal carbon fluxes in an ocean general circulation model. *Glob. Biogeochem. Cycles*, 10(4):559–583, 1996.

[185] Sjöberg, E. L. A fundamental equation for calcite dissolution kinetics. *Geochim. Cosmochim. Acta*, 40(4):441–447, 1976.

[186] Sjöberg, E. L. Kinetics and mechanisms of calcite dissolution in aqueous solutions at low temperatures. *Stockholm. Contrib. Geol.*, 32:1–92, 1978.

[187] Sjöberg, E. L. and D. Rickard. The influence of experimental design on the rate of calcite dissolution. *Geochim. Cosmochim. Acta*, 47(12):2281–2285, 1983.

[188] Slagstad, D., K. S. Tande and P. Wassmann. Modelled carbon fluxes as validated by field data on the north Norwegian shelf during the productive period in 1994. *Sarsia*, 84:303–317, 1999.

[189] Smayda, T. J. Normal and accelerated sinking of phytoplankton in the sea. *Mar. Geol.*, 11:105–122, 1971.

[190] Smetacek, V. The giant diatom dump. *Nature*, 406:574–575, 2000.

[191] Smetacek, V. S. Role of sinking in diatom life-history cycles : ecological, evolutionary and geological significance. *Mar. Biol.*, 84:239–251, 1985.

[192] Smith, S. V. and J. T. Hollibaugh. Coastal metabolism and the oceanic organic carbon balance. *Rev. Geophys.*, 31(1):75–89, 1993.

[193] Suess, E. Particulate organic carbon flux in the oceans - surface productivity and oxygen utilization. *Nature*, 288:260–263, 1980.

[194] Sundquist, E. T. Geological perspectives on carbon dioxide and the carbon cycle. In E. T. Sundquist and W. S. Broecker, editors, *The Carbon Cycle and Atmospheric* CO_2 *: Natural Variations Archean to Present*, volume 32 of *Geophys. Monogr. Ser.*, pages 5–59. American Geophysical Union, Washington, D. C., 1985.

[195] Svensson, U. and W. Dreybrodt. Dissolution kinetics of natural calcite minerals in CO_2-water systems approaching calcite equilibrium. *Chem. Geol.*, 100:129–145, 1992.

[196] Takahashi, K. and A. W. H. Be. Planktonic foraminifera : factors controlling sinking speeds. *Deep-Sea Res.*, 31(12):1477–1500, 1984.

[197] Takahashi, T., W. S. Broecker and A. E. Bainbridge. Supplement to the alkalinity and total carbon dioxide concentration in the world oceans. In B. Bolin, editor, *Carbon Cycle Modelling*, number 16 in SCOPE Report, pages 159–199, Chichester, 1981. John Wiley & Sons.

[198] Thibault, D., S. Roy, C. S. Wong and J. K. Bishop. The downward flux of biogenic material in the NE subarctic Pacific : importance of algal sinking and mesozooplankton herbivory. *Deep-Sea Res. II*, 46(11-12):2669–2697, 1999.

[199] Trent, J. D. *A study of macroaggregates in the Marine Environment*. PhD thesis, Scripps Institution of Oceanography, University of California, San Diego, 1985.

[200] Tsunogai, S. and S. Noriki. Particulate fluxes of carbonate and organic carbon in the ocean. Is the marine biological activity working as a sink of the atmospheric carbon? *Tellus*, 43B:256–266, 1991.

[201] Tyrrell, T. and A. H. Taylor. A modelling study of *Emiliania huxleyi* in the NE Atlantic. *J. Mar. Syst.*, 9:83–112, 1996.

[202] UCSD. ETOPO5 bathymetric database. http ://nemo.ucsd.edu, 1999.

[203] Urban, J. L., C. H. McKenzie and D. Deibel. Seasonal differences in the content of *Oikopleura vanhoeffeni* and *Calanus finmarchicus* faecal pellets : illustrations of zooplankton food web shifts in coastal Newfoundland waters. *Mar. Ecol. Prog. Ser.*, 84:255–264, 1992.

[204] Urban, J. L., C. H. McKenzie and D. Deibel. Nanoplankton Found in Fecal Pellets of Macrozooplankton in Coastal Newfoundland Waters. *Bot. Mar.*, 36:267–281, 1993.

[205] Van der Wal, P., R. S. Kemper and M. J. W. Veldhuis. Production and downward flux of organic matter and calcite in a North Sea bloom of the coccolithophore *Emiliania huxleyi*. *Mar. Ecol. Prog. Ser.*, 126:247–265, 1995.

[206] von Storch, H., S. Güss and M. Heimann. *Das Klimasystem und seine Modellierung*. Springer, Berlin Heidelberg, 1999.

[207] Walsh, I., J. Dymond and R. Collier. Rates of recycling of biogenic components of settling particles in the ocean derived from

sediment trap experiments. *Deep-Sea Res.*, 35(1):43–58, 1988.

[208] Walsh, J. J. *On the Nature of Continental Shelves*. Academic Press, San Diego, 1988.

[209] Walsh, J. J., G. T. Rowe, R. L. Iverson, C. P. McRoy. Biological export of shelf carbon is a sink of the global carbon cycle. *Nature*, 291:196–201, 1981.

[210] Walter, L. M. and J. S. Hanor. Effect of orthophosphate on the dissolution kinetics of biogenic magnesian calcite. *Geochim. Cosmochim. Acta*, 43(8):1377–1385, 1979.

[211] Walter, L. M. and J. W. Morse. The dissolution kinetics of shallow marine carbonates in seawater : A laboratory study. *Geochim. Cosmochim. Acta*, 49:1503–1513, 1985.

[212] Weiss, R. F. Carbon dioxide in water and seawater : The solubility of a non-ideal gas. *Mar. Chem.*, 2:203–215, 1974.

[213] Westbroek, P. et al. A model system approach to biological climate forcing. The example of *Emiliania huxleyi*. *Glob. Planet. Change*, 8:27–46, 1993.

[214] Westrich, J. T. and R. A. Berner. The role of sedimentary organic matter in bacterial sulfate reduction: The *G* model tested. *Limnol. Oceanogr.*, 29(2):236–249, 1984.

[215] Wollast, R. The relative importance of biomineralization and dissolution of $CaCO_3$ in the global carbon cycle. *Bull. Inst. Oceanog. Monaco spec.*, 13:13–35, 1994.

[216] Wright, J. and A. Colling. *Seawater : Its Composition, Properties and Behaviour*. Pergamon Press, Oxford, 1995.

[217] Young, J. R. Functions of coccoliths. In A. Winter, editor, *Coccolithophores*, pages 63–82. Cambridge University Press, Cambridge, 1994.